Deliverable

2.1. Sectorial drought impacts in the different basins

1. Introduction

Drought is a recurrent and creeping natural hazard, which makes it difficult to quantify its characteristics (Lloyd-Hughes, 2014; Vicente-Serrano, 2016; Wilhite, 2005) or to analyze its possible impacts on both natural and human environments (Mishra and Singh, 2010; Wilhite et al., 2007; Wilhite and Pulwarty, 2017). Drought impacts span a wide spectrum of disciplines, including water resources (e.g. river flow, reservoir storage, groundwater) (Bloomfield and Marchant, 2013; Folland et al., 2015; Van Lanen et al., 2013; Van Loon, 2015), crop yield (Dalla Costa and Gianquinto, 2002; Kim et al., 2019; Webber et al., 2018), forest productivity and tree growth (e.g. Anderegg et al., 2018; Restaino et al., 2016; Sánchez-Salguero et al., 2013), in addition to a variety of environmental systems (e.g. Vicente-Serrano et al., 2020).

Drought is often a climate-driven phenomenon, and assessed using tailored climate indices (Heim, 2002; Mukherjee et al., 2018). In the literature, it is well-recognized that the sensitivity of any socioeconomic sector or environmental system to drought severity can be analyzed by means of drought indices that can be linked directly to sectoral impact data (Bachmair et al., 2016, 2015). This strong association has been evident for streamflow (e.g. Barker et al., 2016; López-Moreno et al., 2013), vegetation activity (e.g. Liu and Kogan, 1996; Vicente-Serrano et al., 2013; Zhang et al., 2016), forest growth (Arzac et al., 2016; Pasho et al., 2011; Skomarkova et al., 2006), and even human health (Sena et al., 2014; Stanke et al., 2013). Hydrological droughts correspond to temporal anomalies in the river flows, characterized by a water deficit regarding to long-term average conditions (Van Loon, 2015), which may be related to different human, climatic and environmental factors. Numerous studies indicate that hydrological droughts can develop differently to climatic droughts, as a function of the dominant physiographic characteristics (López-Moreno et al., 2013; Peña-Gallardo et al., 2019; Tijdeman et al., 2016; Van Lanen et al., 2013) or human management (Rangecroft et al., 2018; Tijdeman et al., 2018). Moreover, numerous studies report a varying response of vegetation dynamics to drought, mainly due to the prevailing vegetation types (e.g. woodland, grassland, steppe, etc.) (Vicente-Serrano et al., 2020b), forest species (Anderegg et al., 2018, 2016; Gazol et al., 2017) and prevailing climate characteristics (Gazol et al., 2018; Pasho et al., 2011). Some of these studies established thresholds to identify drought vulnerability in response to different environmental factors (Slette et al., 2019).

Nevertheless, the majority of studies that assessed the impacts of drought have focused primarily on a specific socioeconomic sector or an environmental system. However, the multi-sectoral response to drought severity is poorly understood. This is probably due to data limitations, which hinders assessment of how multi-sectorial drought impacts can develop and compound in a particular catchment. This assessment is important in many environments to define the extent to which water and land management practices can modulate or accelerate drought impacts on different natural systems and socioeconomic sectors. Specifically, in some natural basins that are not affected by water regulation and human uses, drought impacts may exceed the locations where droughts occur. As such, these negative impacts may propagate downstream (Vicente-Serrano et al., 2017; Xu et al., 2019; Zhang et al., 2014), especially when water supply is essential for the development of different economic activities (e.g. irrigation, domestic use, industry, tourism, etc). Comprehensive assessment of the multi-sectoral drought impacts can also be important when establishing appropriate vulnerability thresholds, especially for ecosystems with complex drought impacts or diverse physiographical or phenological conditions (Allen et al., 2015; Sánchez-Salguero et al., 2013). In these regions, better understanding of multi-sectoral droughts can contribute to more effective monitoring, early-warning (Svoboda et al., 2002) and mitigation of drought risk (Wilhite, 2009, 2002). As such, given that accurate knowledge of the adverse impacts of drought on a variety of economic sectors (Bachmair et al., 2016, 2015) and environmental systems (Vicente-Serrano et al., 2020) is needed for reliable monitoring and management of drought, it is important to

quantify comprehensively the multifaceted impacts of drought that may occur in a single territory.

The overriding objective of this report is to analyze the multisectorial impacts of drought severity in basins of Europe with different characteristics. Specifically, we aim to i) determine the response of water systems to drought variability, and ii) assess the varying response of natural vegetation to drought.

2. Impacts in the German part of the Elbe basin

2.1. Geography of the domain

The German part of the Elbe River basin covers an area of 97,175 km², 65.5 % of the entire basin (Simon et al. 2005). The Elbe River originates from the Czech Republic where practically the complete upstream third of its basin is located, very small parts of the basin belong to Poland and Austria (Figure 1). The Czech–German national boundary stretches along mountain ranges (Bohemian Forest, Fichtel Mountains, Ore Mountains) but does not exactly follow the water divides. Therefore German splinter areas of the Czech upstream part are excluded for this assessment, leaving a contiguous area of 96,864 km² (own GIS analysis) loosely enclosed by the geographical coordinates 8°30'E–15°05'E and 49°45'N–54°30'N. For the sake of simplicity we henceforth refer to this domain as German part of the Elbe basin (GEB).

The Elbe River enters Germany passing the Ore Mountains at Schmilka, approximately 50 km southeast of the city of Dresden. The stream profile at this location is typically 150–200 m wide, and the mean runoff observed during the 20th century was 311 m³/s (Simon et al. 2005). The rivers Schwarze Elster, Mulde, Saale, and Havel constitute the major tributaries along the generally northwestern course of the Elbe River towards the North Sea (see Figure X.1). Some analyses are confined to the Havel subbasin: 23,790 km² of its total area of 23,860 km² are located in Germany (FGG Elbe 2015); to ease readability "Havel area" henceforth only refers to the German part unless stated otherwise. On the final downstream stretch of the Elbe River stream widths increase from approximately 1 km near Hamburg to about 3 km at Brunsbüttel where the transition to the estuary funnel begins. The mean discharge into the sea was estimated at 861 m³/s (Simon et al. 2005); direct runoff measurements are rendered impossible here due to tidal currents.

The highest spot of the GEB has an elevation of 1215 m amsl (Fichtelberg in the Ore Mountains). Also noteworthy are the Harz mountains reaching 1141 m amsl (Brocken) on the western edge of the basin. As most of the GEB is located in the North German Lowlands, the average elevation is only 151 m amsl, and the median is at 81 m amsl; 75.4 % of the area are below 200 m amsl and 93.6 % below 500 m amsl. The Havel area ranges between 23 and 582 m amsl with an average of 69 and a median of 55 m amsl.

With the exception of the the Ore Mountains of late Paleozoic origin surface geology of the GEB domain is characterized by deep sediments ordered by a sequence of glacial series. In the southern and western parts these sediments are topped by loam and loess layers while the central part – including most of the Havel area – is largely characterized by poor, sand dominated soils. Drought is therefore a serious threat for farmers in this region, some of them were facing complete yield losses in 2018 or 2019. Soils with higher water storage capacity can only be found again in the loamy moraine regions of the most recent (Weichsel) glaciation at the north-eastern edge of the GEB or in the silty marshlands around the Elbe estuary.

The land use is dominated by agriculture, pastures and coniferous forests. Such managed ecosystems – which are strongly affected by drought events – cover more than 85 % of the region (Figure 2 and Table 1). Built-up areas account for about 8 % of the land demand, and their share rises slowly but continuosly at the expense of agricultural areas, a trend expected to sustain at least in the vicinity of the big cities (Hoymann et al. 2016, Maretzke et al. 2021).

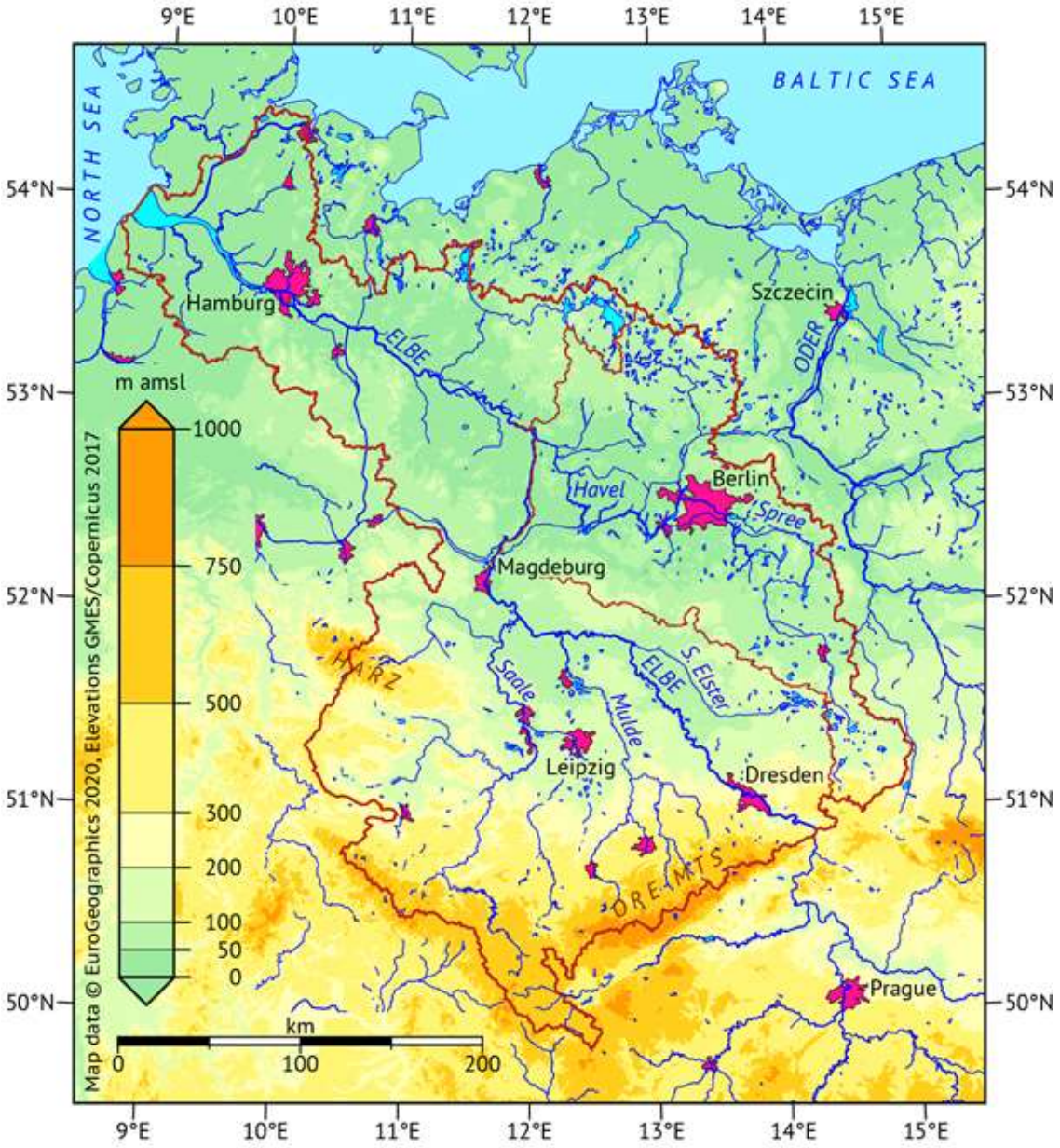

Figure 1: Digital elevation model DGM200 of the German Federal Agency for Cartography and Geodesy, © GeoBasis-DE / BKG 2021. Basin boundaries extracted from geodata provided by the German Federal Institute for Hydrology, © WasserBLIcK/BfG & Zuständige Behörden der Länder, 2020-11-10.

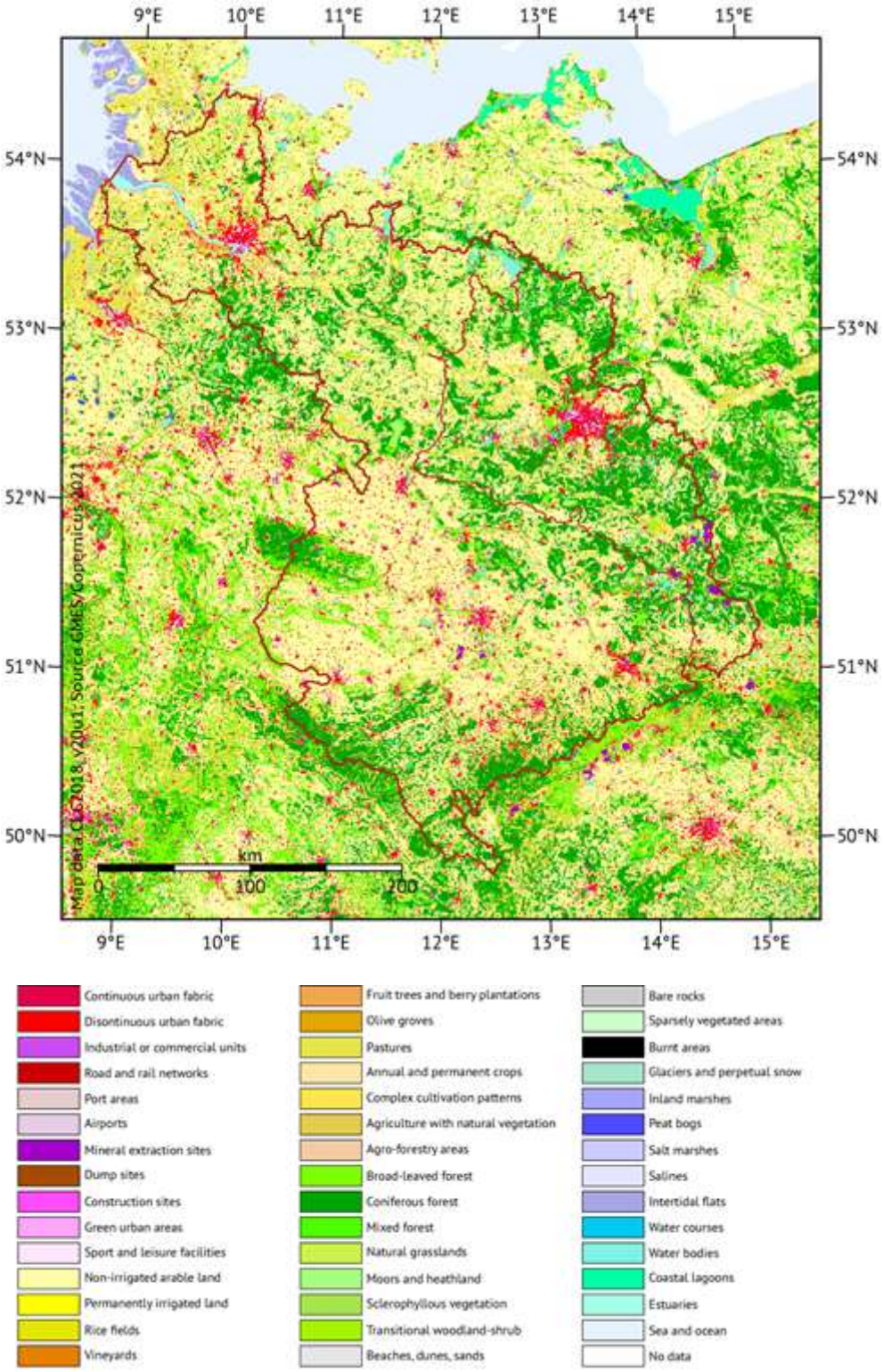

Figure 2: CLC 2018 version v.2020_20u1, downloaded in March 2021. Source: Copernicus Land Monitoring Service, part of the European Earth monitoring programme (GMES).

Table 1: Distribution of land use classes according to CLC 2018 (Copernicus 2020). Included are categories whose coverage exceeds 0.1 percent of the respective basin area. Dominating categories are coloured.

CLC category		GEB		Havel area	
Code	Land use	km²	%	km²	%
111	Continuous urban fabric	155.80	0.16	48.34	0.20
112	Discontinuous urban fabric	6,001.18	6.20	1,535.18	6.46
121	Industrial or commercial units	1,286.06	1.33	345.39	1.45
124	Airports	109.32	0.11	38.85	0.16
131	Mineral extraction sites	379.04	0.39	175.93	0.74
141	Green urban areas	139.00	0.14	53.69	0.23
142	Sport and leisure facilities	547.51	0.57	169.72	0.71
211	Non-irrigated arable land	41,400.68	42.74	7,223.88	30.39
222	Fruit trees and berry plantations	290.18	0.30	26.92	0.11
231	Pastures	14,933.45	15.42	3,526.90	14.83
243	Agriculture with natural vegetation	253.35	0.26	36.41	0.15
311	Broad-leaved forest	5,078.86	5.24	1,013.53	4.26
312	Coniferous forest	20,740.28	21.41	7,829.18	32.93
313	Mixed forest	1,572.77	1.62	480.68	2.02
321	Natural grasslands	290.65	0.30	71.48	0.30
322	Moors and heathland	425.85	0.44	214.59	0.90
324	Transitional woodland-shrub	665.75	0.69	218.19	0.92
411	Inland marshes	114.60	0.12	65.43	0.28
423	Intertidal flats	150.18	0.16	–	–
511	Water courses	213.63	0.22	50.58	0.21
512	Water bodies	1,434.70	1.48	606.02	2.55
522	Estuaries	305.50	0.32	–	–
XXX	Other	375.93	0.39	43.86	0.18
	TOTAL	96,864.27	100.0	23,774.75	100.0

2.2 Administrative divisions

The German Elbe Basin is of course confined to Germany, but Germany consists of 16 federal states (*Bundesländer*) which are further divided into district level units (*Kreise* and *kreisfreie Städte*), henceforth called districts. There are currently 401 or 412 German districts depending on whether Berlin as a whole or its twelve city districts (*Bezirke*) are counted in. Ten federal states and 105 districts have a share in the GEB as shown in Figure 3.

As many data are not available for hydrological basins but for administrative units, we sometimes combine federal state data from Berlin, Brandenburg, Saxony-Anhalt, Saxony, and Thuringia (uniformly yellow tinted in Fig. 3) to characterize the case study area. Each of these states has most of its area inside the GEB, and Berlin and Brandenburg may also serve as data proxy for the Havel basin. Other data are available for East Germany, also including Mecklenburg-Western Pomerania (yellowish stripes in Fig. 3). Notwithstanding minor changes in boundary delineations East Germany resembles the extent of the former German Democratic Republic whose socialist system left many traces still present in the landscape and economy of the domain, more than three decades after the German reunification.

District data are important for regional differentiation. There are currently about 2532 municipalities (*Gemeinden*) as basic administrative units overlapping the GEB, but besides the population analysed in the next section there is not much data published on this level.

Figure 3: Federal states and boundaries of district level units overlapping with the German Elbe Basin. The yellow tints indicate states used for aggegations of statistical data. Hydrography and administrative boundaries © EuroGeographics 2020 and © GeoBasis-DE / BKG 2021. Basin boundaries extracted from geodata provided by the German Federal Institute for Hydrology, © WasserBLIcK/BfG & Zuständige Behörden der Länder, 2020-11-10.

2.2 Climatic conditions and meteorological droughts

2.2.1 Recent climatology

A decade ended in 2020, and a new standard climate normal period (1991–2020) can be analysed since. The German Weather Service (Deutscher Wetterdienst, DWD) provides monthly 1-km raster data of many meteorological variables over Germany (DWD-CDC 2021a–c). The GEB and Havel areas were extracted from these rasters providing the basis for the aggregate figures presented in this subsection.

The 1991–2020 averages of the air temperature at 2 m above ground were 9.4°C in the GEB and 9.7°C in the Havel area. As the upper panel of Fig. 4 illustrates, there were upward trends over the last decades, linear approximations since 1961 estimate a regional warming rate of 0.35 K per decade. Precipitation varied about 656 mm per year (586 mm/a in the Havel area) and did not expose a significant trend, but the drought years 1976, 2003 and 2018 are clearly visible in the middle panel of Fig. 4. Sunshine durations however increased with the temperatures (lower panel of Fig. 4): The trend lines indicate a surplus of 39.3 hours per decade. The 1991–2020 averages amounted to 1682 sunshine hours per year in the GEB and 1738 h/a for the Havel area.

Since the 1970s the average air temperatures increased at about the double rate compared to the global average (Allen et al. 2018). The notable increase in sunshine can at least partly be attributed to anthropogenic brightening (Wild 2014, Wild et al. 2021). The Havel subdomain is a little warmer, drier, and sunnier than the GEB as a whole owing to the lower average elevation (82 m less) and a more continentally located centre of gravity. This effect can also be seen in the isohyetes map in Fig. 5: Besides the mountains, the coastal region near the Elbe estuary receives above-average precipitation. The map also shows the "rain shadow" of the Harz mountains, this area with spots receiving less than 500 mm in an average year is also the driest region of Germany.

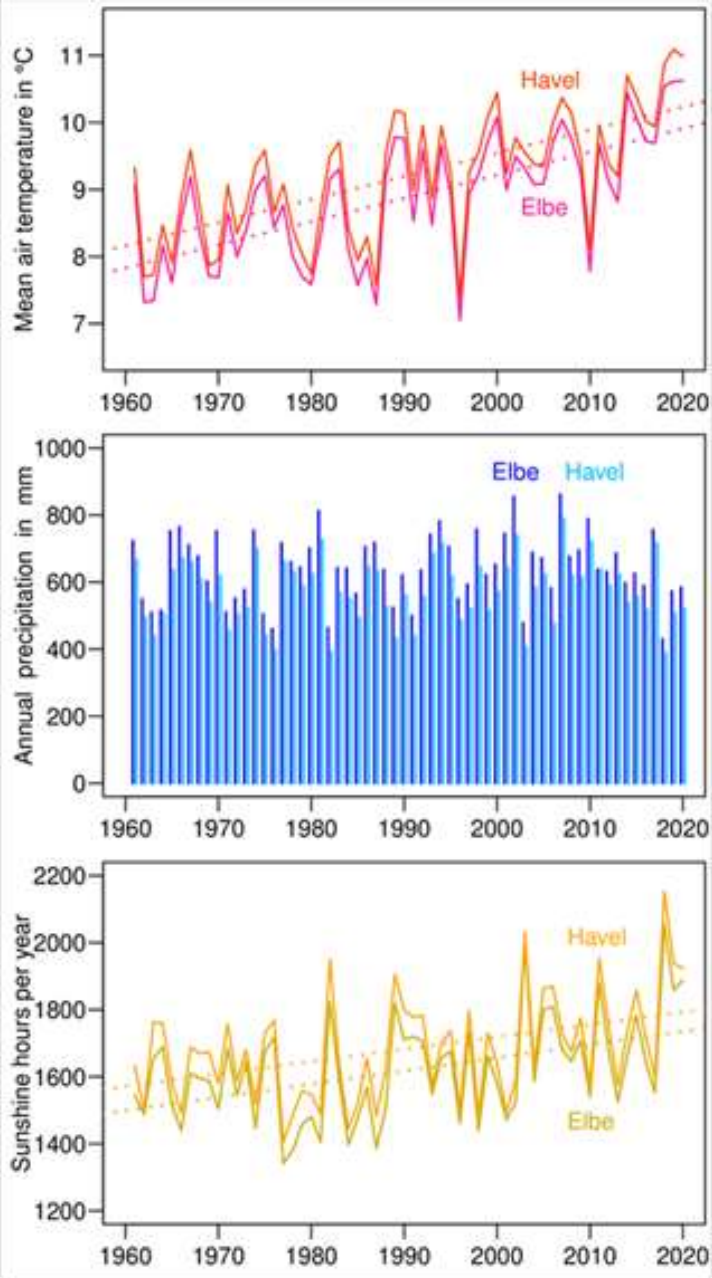

Figure 4: Annual domain averages of air temperature, precipitation, and sunshine hours. Data source: DWD Climate Data Center (CDC): Grids of monthly averaged climate variables, version v1.0. URL: https://opendata.dwd.de/climate_environment/CDC/grids_germany/monthly/ – last accessed in May 2021.

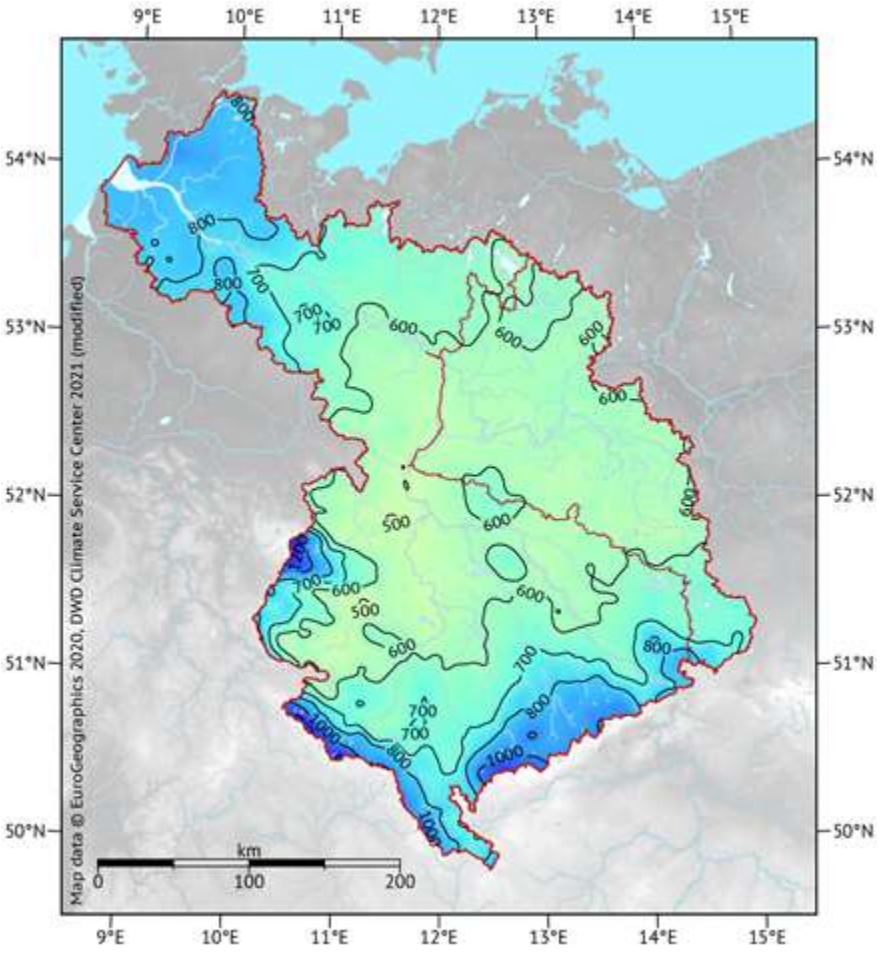

Figure 5: Isohyet map of the German Elbe basin for the climate normal period 1991–2010. Data source: DWD Climate Data Center (CDC): Grids of monthly total precipitation over Germany, version v1.0. URL: https://opendata.dwd.de/climate_environment/CDC/grids_germany/monthly/ – last accessed in May 2021.

The Walter–Lieth climogram in Fig. 6 shows the seasonality of temperature and precipitation in the 1991–2020 climate normal period. The coldest month was January with 0.8°C, the warmest July with 18.7°C, which means an average annual amplitude of 17.9 K. The driest month was April with 35.2 mm of precipitation, and the wettest July with 79.7 mm. A substantial share of the summer precipitation is generated in convective clouds; thunderstorms, hail, and heavy rain events occur most frequently during the hot season.

2.2.2 Meteorological droughts

A meteorological drought is defined as an extended time period with less than average precipitation. There is no generally accepted rule about the duration or deviation thresholds, but drought indices galore (WMO & GWP 2016). Among the most important are SPI and SPEI:

SPI – Standardized Precipitation Index (McKee et al. 1993). It was recommended by the WMO in 2009 as the main meteorological drought index countries should use to monitor and follow drought conditions (Hayes et al. 2011). The only input is a long time series of precipitation (at least 20 years of observations), and normalized negative deviations from period averages, specifically index values below −1, are flagged as drought situations (WMO 2012). The German Weather service (DWD) produces monthly maps with SPI classifications.

SPEI – Standardised Precipitation Evapotranspiration Index (Vicente-Serrano et al. 2010, Beguería et al. 2013). With temperatures rising under climate change, drought frequency and severity may increase over time even if there is no long-term trend in precipitation. The SPEI accounts for that through temperature-derived potential evapotranspiration as additional input. The calculus and interpretation is similar to SEI using a log-logistic probability distribution. SPEI has been widely recognized and is combined with SEI into the GPCC-DI drought index of the Global Precipitation Climatology Centre (GPCC).

The DWD grid products also contain the drought index according to de Martonne (dMI; de Martonne 1926) on annual and monthly basis, a simple indicator based on precipitation and temperature: dMI = P/(T+10). There are also regular updates of dMI anomaly maps for Germany (https://www.dwd.de/EN/ourservices/klimakartendeutschland/klimakartendeutschland.html – last accessed in May 2021; choose "Aridity index" and the desired month from the dropdown menus) allowing for a quick check of the current meteorological drought situation.

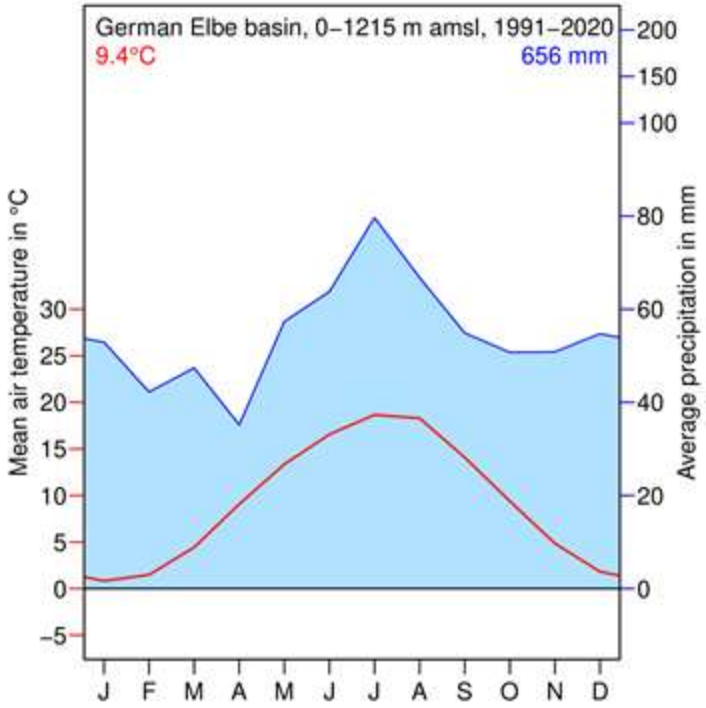

Figure 6: Walter–Lieth climogram for the German Elbe basin, climate normal period 1991–2020. Data source: DWD Climate Data Center (CDC): Grids of monthly averaged climate variables, version v1.0. URL: https://opendata.dwd.de/climate_environment/CDC/grids_germany/monthly/ – last accessed in May 2021.

Figures 7 and 8 show time series of these three drought indices over six decades for the GEB and the Havel area, respectively. They are based on area averages of precipitation and temperatures according to the monthly DWD climate grids; SPI and SPEI have been calculated using the SPEI R package (Beguería & Vicente-Serrano 2017). The upper halves of the figures show the results for three-month moving averages, the lower halves are calculated with twelve-month averaging windows. The first impression is that, as these indices quantify drought always relative to the regional climate normals, there is not much difference between the GEB and its generally drier sub-region. Second, the advantages and disadvantages of the two time windows are obvious: While the three-month analyses better represent the actual occurrence of dry spells (cf. 1976 and 2003: in the twelve-month indices both events extend into the subsequent years) the indices based on the extended time window much better

convey the critical years or time periods given the hysteretic cascading drought effects in other sectors. Third, the graphs of the twelve-month dMI anomalies (dMIa12) look very similar to the SPEI despite their much simpler calculation. However, their values are not distribution-based, and their drought thresholds marked in orange and red are chosen arbitrarily (−2.5 and −5.0 for dMIa3, −1.5 and −3.0 for dMIa12). For SPI and SPEI the orange and red thresholds are at −1.0 and −2.0 indicating “drought” and “extreme drought”, respectively.

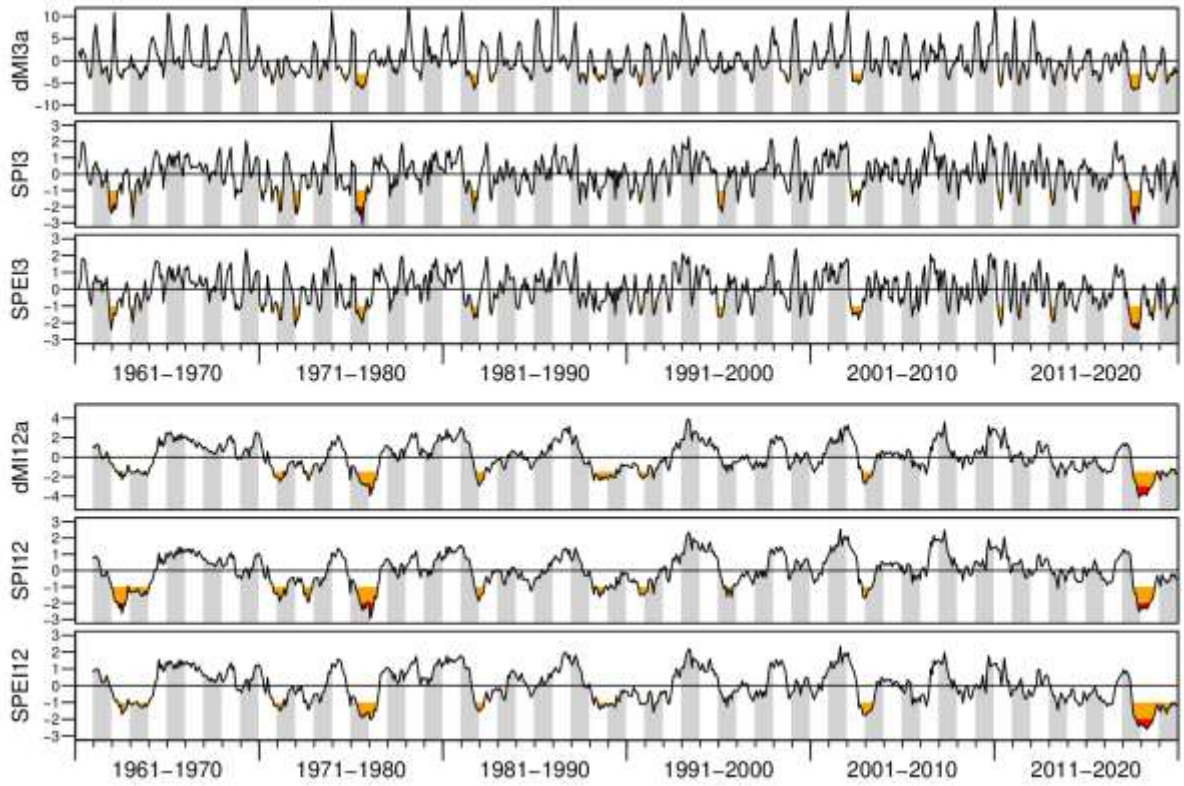

Figure 7: Three meteorological drought indices for the GEB area, calculated for 3- and 12-month running averages. Data source: DWD Climate Data Center (CDC): Grids of monthly total precipitation and monthly average air temperature over Germany, version v1.0. URL: https://opendata.dwd.de/climate_environment/CDC/grids_germany/monthly/ – last accessed in May 2021.

The top event within the six decades occurred just in 2018 and the two following years in which precipitation was still below average and could not compensate the severe loss from soil and groundwater storages. This is correctly captured by the SPEI and even the simple dMI anomalies, only the SPI which does not account for evapotranspiration shows the 1976 event on a comparable level. The 1976 drought is however certainly second in the severity ranking, and the heat wave of 2003 may claim the bronze medal. Notable are also dry starts of two pairs of subsequent years, 1963 and 1964 as well as 1972 and 1973, the dry autumn of 1982, and, especially in the Havel area, an extended below-average precipitation in and around 1989. Owing to data availability and comparability with the present economy sector effects will be studied primarily for the more recent events, the 2003 heat wave and the 2018 drought.

2.3 Drought impacts on natural systems

2.3.1 Soils

The depletion of the soil water storage is one of the immediate effects of meteorological droughts caused by soil evaporation and plant transpiraton, the latter virtually equalling root water uptake. The top soil layers are the first to dry out (and the first whose water storage is

repleted by precipitation); deeper soil layers show a more hysteretic reaction and can sustain an accumulated water deficit over years hampering plant growth and agricultural production.

The agrometeorological model of the DWD, AMBAV (Löpmeier 1993, 1994, n.d.) calculates not only the potential evapotranspiration according to Penman–Monteith but also the actual one for a standard grassland on a sandy loam standard soil. Soil water content is among the modelled variables, and the results can be obtained as monthly gridded data products for Germany since 1991. Figure 9 shows monthly averages for GEB and Havel area as easonal cycles of all years up to 2020 expressed as fraction of the plant available soil water capacity.

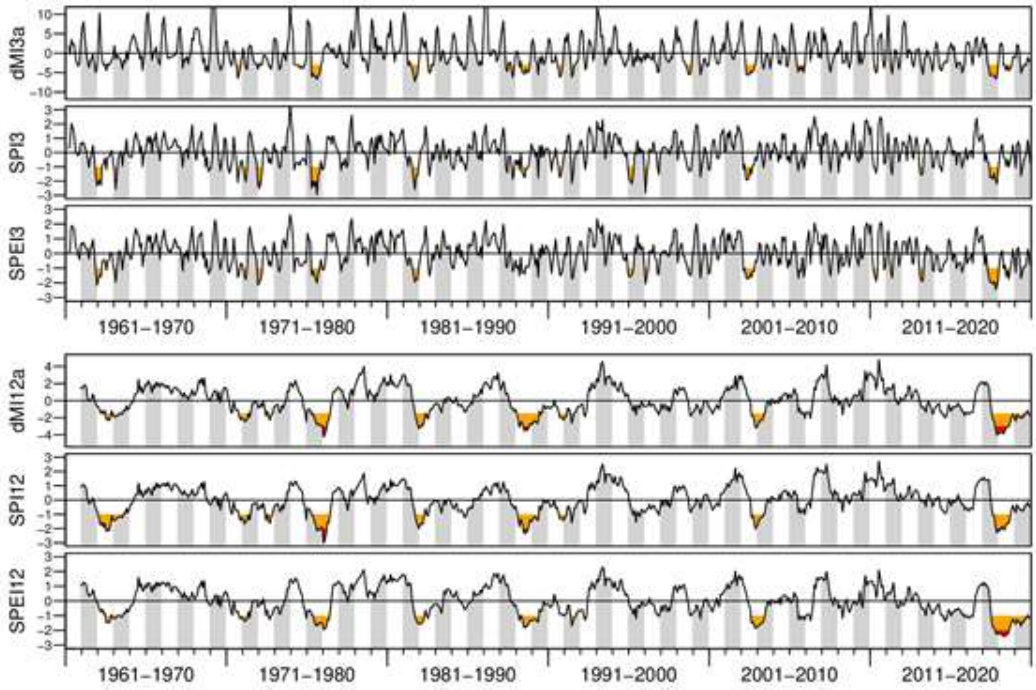

Figure 8: Three meteorological drought indices for the Havel area, calculated for 3- and 12-month running averages. Data source: DWD Climate Data Center (CDC): Grids of monthly total precipitation and monthly average air temperature over Germany, version v1.0. URL: https://opendata.dwd.de/climate_environment/CDC/grids_germany/monthly/ – last accessed in May 2021.

From the colour coding of the individual years in Fig. 9 one can see that there had been clear trend towards drier soils in the most recent years. Especially in May and June the model soil became increasingly dry, and only in two or three years of the last decade a recovery was possible already during summer. After the extreme drought in 2018 soil water contents were on extremely low levels still in November and could not fully recover in the following winter: the lowest February values (red graphs, 89.6 % for the GEB and 85.8 % for the Havel area) are from the year 2019 as well as the record minimum of 35.9 % in the Havel area in September.

More than a third of plant available water left may not sound dramatic. The values are however only averages for larger regions, and smaller sub-areas had been affected more severely. In addition to that, most soils in the real Havel area are sand-dominated and do not provide the storage capacity of the standard soil in the model. Consequently, there have been complete cropping failures for some farmers in 2018 and 2019.

A modelling initiative considering the different hydrological properties of Germany's soil landscape is the Drought Monitor Germany at the Helmholtz Centre for Environmental Research (UFZ) in Leipzig (https://www.ufz.de/index.php?en=37937, last accessed in June 2021). Soil water content is modelled daily and nationwide with the mesoscale hydrological

model (mHM) for profiles of approximately 1.8 m depth and 4 km horizontal grid resolution (Zink et al. 2016).

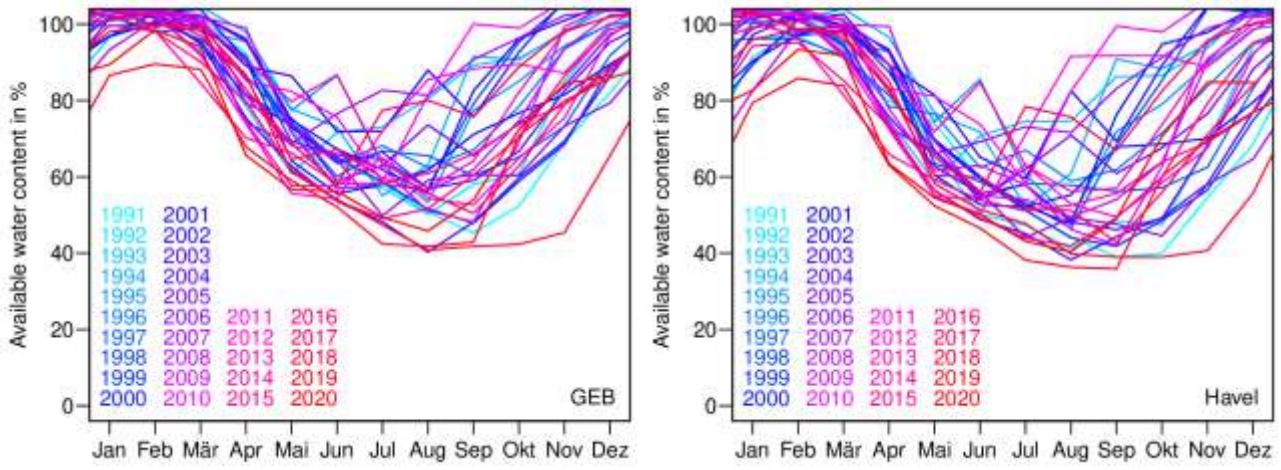

Figure 9: Seasonal cycles of available soil water modelled with AMBAV for a standard soil (sandy loam) of 1 m depth. Regional averages for the GEB (left) and Havel area (right). Data basis: DWD Climate Data Center: Calculated monthly values for different characteristic elements of soil and crops,Version v19.3, 2019. URL: https://opendata.dwd.de/climate_environment/CDC/derived_germany/soil/monthly/historical / – last accessed in June 2021.

Output is given in form of a soil moisture index (SMI) which is however not defined on a standard normal distribution but within a [0,1] interval. Values of 0.3 or less are characterised as “abnormally dry”, 0.2 or less means drought with 0.1 (severe drought), 0.05 (extreme drought), and 0.02 (exceptional drought) being further escalation thresholds which also indicate the long-term occurrence probabilities (e.g. 0.02 = 2% of a multi-decadal time series). Another difference to the other drought indices presented here is the time frame of the underlying statistics, currently the UFZ uses the years 1951–2019.

The end-of-summer situations during the extreme meteorological drought of 2018–2019 is shown in Fig. 10. While the northeastern part of the GEB was still not so much affected in 2018, one year later more or less the entire research domain was struck by exceptional soil drought. Figure 11 shows the end-of-winter counterparts, extended by the years 2020 and 2021. As the SMI adapts to the seasonal cycle of soil moisture similar to other drought indices a certain water content in spring might be flagged with the same drought severity as a much lower level in autumn, but there is no doubt that in early 2018 the soil water storage was still in a normal state that was damaged soon thereafter and did not recover since.

Another interesting observation when comparing Figs 10 and 11 is that the most affected parts of the GEB relocalised first from the south to the northwest, and meanwhile concenrate more or less in the central part, albeit with a high spatial heterogeneity.

The long-term temporal evolution of the SMI in the GEB and the Havel area is shown similarly to the other drought indices in Figure 12. There is no doubt that the recent drought was (and still is) the most severe regarding sustained soil moisture deficits within the observed time period.

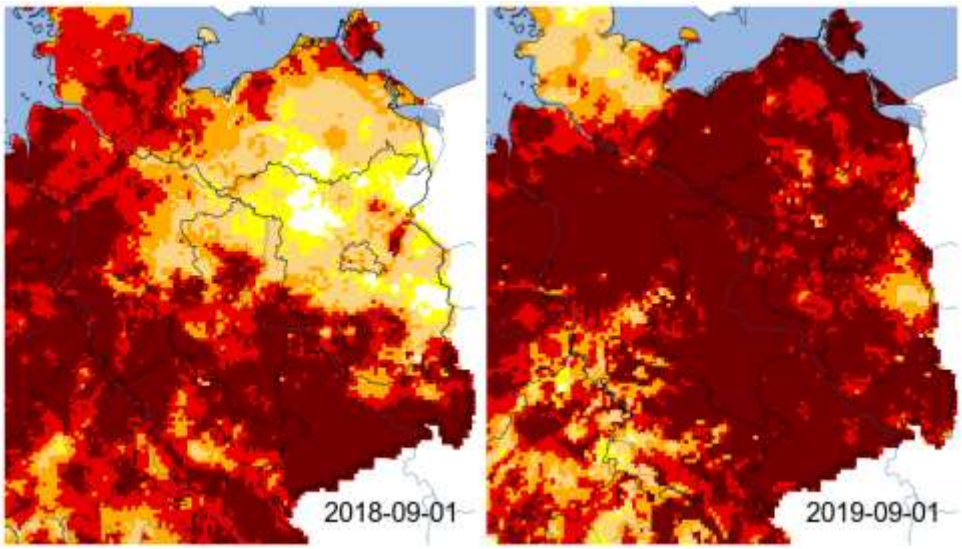

Figure 10: Spatial distribution of full profile (1.8 m) SMI extremes in Northeastern Germany after the summers of 2018 and 2019. Orange colours indicate drought (values of 0.2 or less); scarlet (0.05 or less) and brown red (0.02 or less) show extreme and exceptional drought, respectively. Source: UFZ Drought Monitor / Helmholtz Centre for Environmental Research.

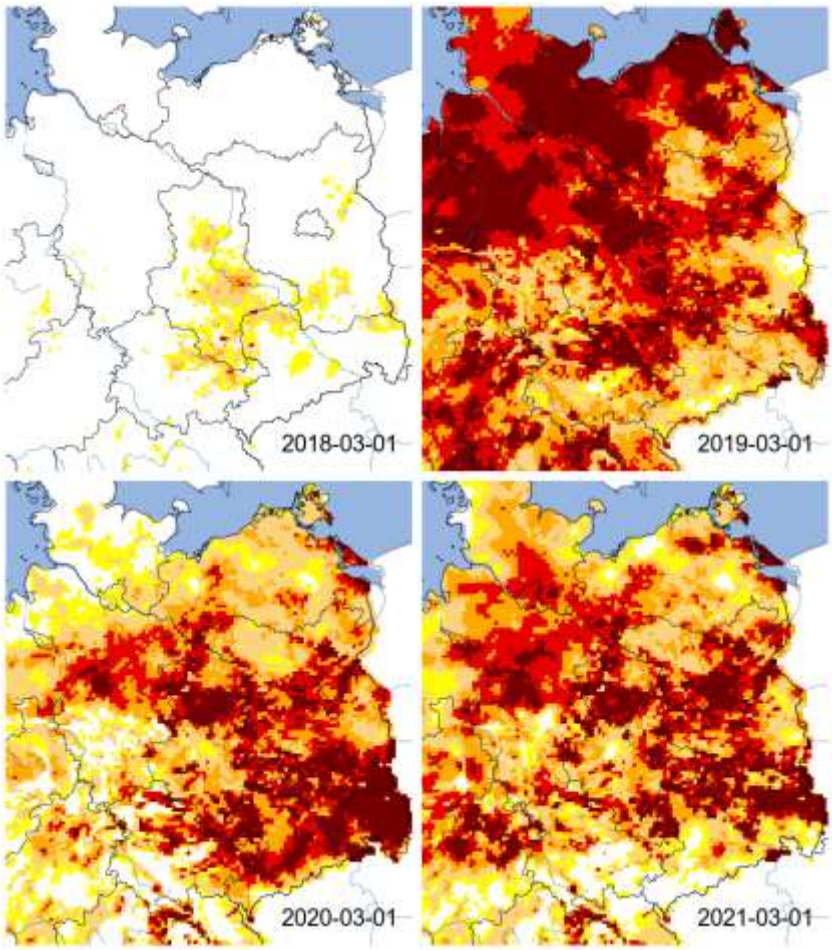

Figure 11: Spatial distribution of full profile (1.8 m) SMI extremes in Northeastern Germany at begin of spring for the years 2018–2021. Orange colours indicate drought (values of 0.2 or less); scarlet (0.05 or less) and brown red (0.02 or less) show extreme and exceptional drought, respectively. Source: UFZ Drought Monitor / Helmholtz Centre for Environmental Research.

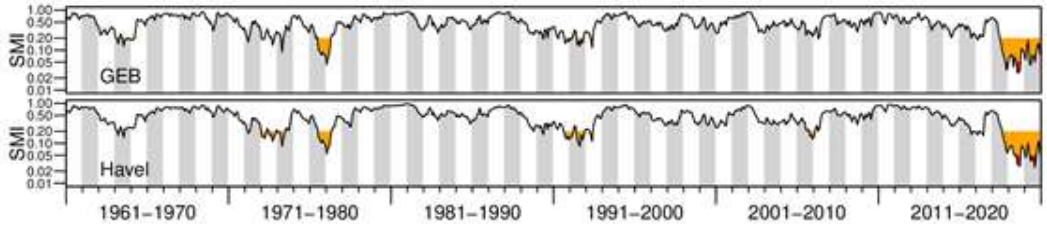

Figure 12: Time series of monthly soil moisture index (SMI) spatial averages for the German Elbe Basin (GEB) and the Havel area. Note the confinement of the index values to the [0,1] interval and the log scale of the y-axis (applied for optical reasons). Data source: UFZ Drought Monitor / Helmholtz Centre for Environmental Research.

2.3.2 Water bodies

Hydrological drought manifests in low or disappearing stream runoff, shrinking water surfaces, and decreasing groundwater levels. As shorelines of lakes and rivers are not frequently surveyed and groundwater level measurements are not easily accessible we concentrate on river discharge for evaluating the hydrological drought situation in the GEB. The map in Fig. X.14 shows the positions of three principal gauges – Dresden and Neu Darchau at the Elbe river and Rathenow at the Havel river – and their catchment areas. For these gauges complete time series of daily runoff data could be obtained for the years 1961–2019 from the Global Runoff Data Centre (GRDC) at Koblenz, Germany; the year 2020 could therefore not be evaluated.

While Rathenow represents 80.8 % of the entire Havel river catchment (19,288 of 23,860 km², including the Czech part), the discharge contribution from the GEB had to be approximated from the difference area of the gauge catchments of Dresden and Neu Darchau (78,854 km²) which includes the Havel catchment; the respective areas are shown in Fig. 13.

River streamflow integrates the hydrological situation of the catchment area very well especially during low runoff phases provided it is not largely controlled by reservoir operations. Then it corresponds more or less to the groundwater discharge which in turn is strongly correlated to the current groundwater storage situation.

Groundwater is principally the most hysteretic storage system in the land part of the hydrological cycle and is locally of the same or even higher importance for plant water uptake than soil water storage. For human needs, groundwater is the most important resource: In the German Elbe area 1,055.788 million m³ water were furthered by public waterworks in 2016, 602.851 million m³ of this volume was furthered from groundwater, a share of 57.1 %. The respective numbers for the Havel area are 326.395 and 163.037 million m³, indicating a groundwater share of 50.0 % (DESTATIS 2019b).

The dynamics of surface water bodies are also largely captured by stream runoff fluctuations, because the close relationship of river water stages and runoff is actually used for runoff measurements via so-called rating curves. It is however not possible to derive important ecological thresholds (disconnection or dryfall of river lakes) from streamflow values alone, and water levels in lakes and reservoirs not directly connected to the river system may react quite differently.

While the runoff time series of Rathenow could be used as is (shown in the upper part of Fig. 14), simple differences between the Dresden and Neu Darchau readings do not equal the actual streamflow contribution of the intermediate catchment area: the travel time and dispersion of flood waves along the main river channel must be considered. The average time lag of a flood wave from Dresden to Neu Darchau is approximately 6.5 days, and the distance

between the gauges along the river course is 480.84 km (which indicates a wave celerity of about 0.9 m/s). Considering the time lag and accomodating the dispersion with a gamma kernel allows for separating the streamflow contribution from the intermediate (Elbe) area; the hydrograph is shown in the upper part of Fig. 15.

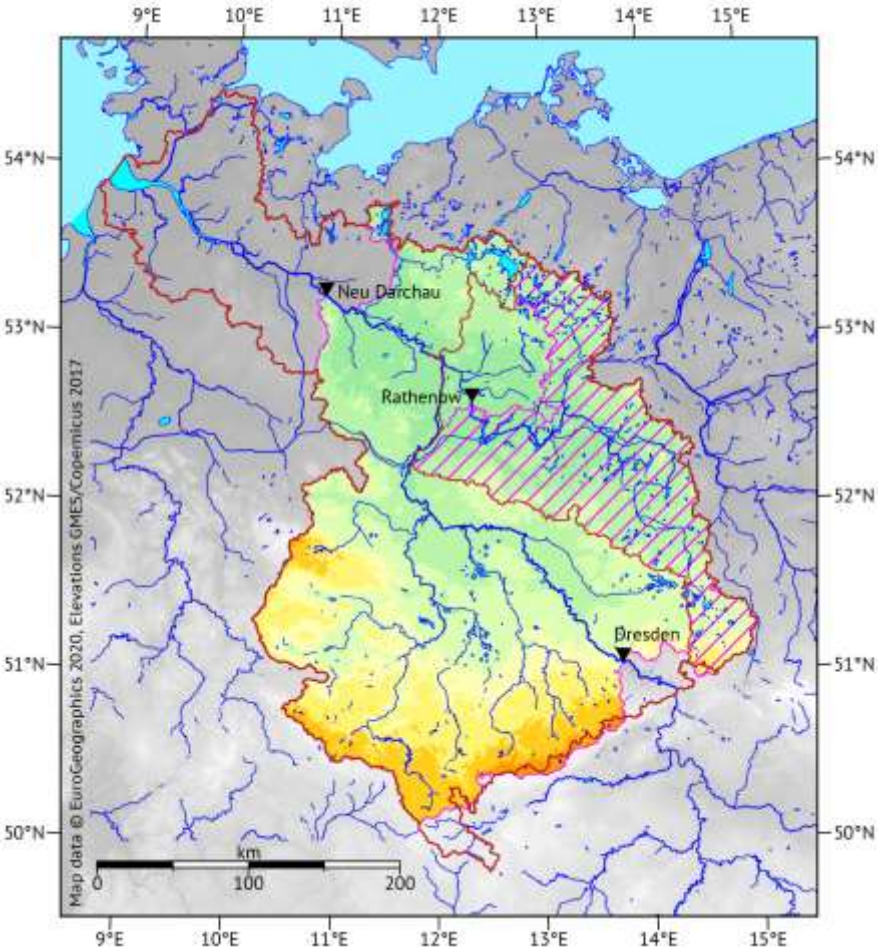

Figure 13: Approximations of GEB and Havel area by stream runoff gauge catchments. GEB is approximated by the Neu Darchau minus the Dresden catchment (area with elevation colours), and the Havel area is represented by the Rathenow catchment (magenta-coloured hachure).

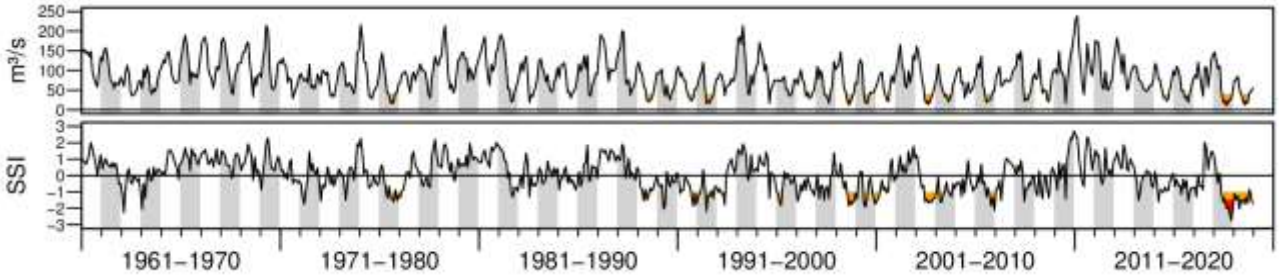

Figure 14: Streamflow Index for the Havel area.

In order to assess drought severity from the river streamflow perspective we calculated the SSI (standardized streamflow index) generally following the Best Monthly Fit (BMF) approach by Vicente-Serrano et al. 2012. Like the meteorological drought indices SPI and SPEI the SSI compares monthly runoff values to distributions of other runoff records of the same month and provides the results in a normalized way as *z*-values. At the core of the BMF method is the

selection of a probability distribution from a candidate set to optimally approximate the data distribution for each calendar month separately. We used the same candidate distributions Vicente-Serrano et al. proposed (GEV, PearsonIII, Generalized Pareto, Lognormal, Log-Logistic, and Weibull), but did not fit the distribution parameters through L-moments but maximum likelihood estimation. The selection of the distribution to apply was based on *p*-values calculated by the Kolmogorov–Smirnov-test. Table 2 lists distributions and *p*-values for catchment areas and calendar months.

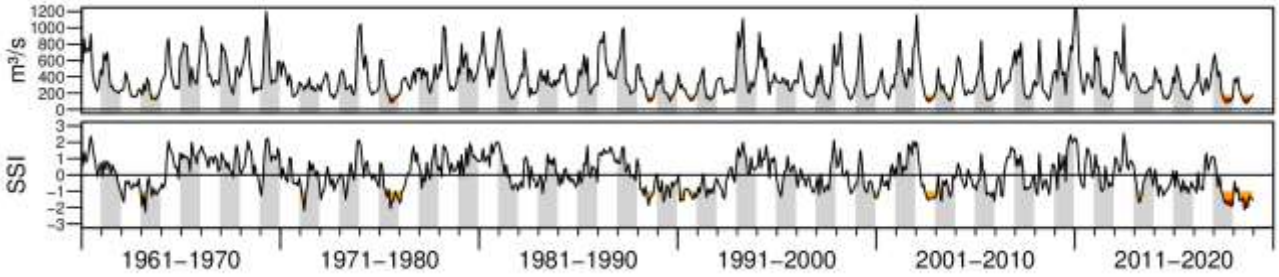

Figure 15: Streamflow Index for the approximated GEB.

Table 2: Probability distributions selected in the Best Monthly Fit method of the SSI calculation and their *p*-Values according to KS-testing.

	Elbe basin (Dresden–Neu Darchau)		Havel catchment, gauge Rathenow	
Month	Prob. distribution	p-Value	Prob. distribution	p-Value
January	Log-Logistic	0.068	PearsonIII	0.077
February	Log-Logistic	0.111	Lognormal	0.068
March	Lognormal	0.085	Lognormal	0.107
April	Lognormal	0.064	Lognormal	0.070
May	Log-Logistic	0.079	Lognormal	0.064
June	Log-Logistic	0.090	PearsonIII	0.053
July	Lognormal	0.055	Weibull	0.069
August	Lognormal	0.072	Lognormal	0.062
September	Lognormal	0.088	PearsonIII	0.067
October	Log-Logistic	0.070	Lognormal	0.045
November	Log-Logistic	0.111	PearsonIII	0.047
December	Log-Logistic	0.062	PearsonIII	0.058

Interestingly, the distribution of the monthly streamflows generated between the Elbe gauges approximating the GEB discharge can be approximated best by either lognormal or log-logistic probability distributions while the Havel streamflow at Rathenow can usually be represented by PearsonIII or Lognormal distributions. The *p*-Values are generally lower for the Havel catchment, probably due to noise in the Elbe data remaining from incomplete filtering of the inflow signal from upstream Dresden. For interpreting the results it should also not be neglected that both streamflow generating areas are to some extent subject to human

interventions: Before the German Reunification in 1990 there were massive lignite mining activities in the southern part of the Havel catchment for which up to 30 m^3/s of groundwater were extracted and released into the Spree river. Meanwhile, most former open-cast mining areas are being flooded and groundwater storage recovers which naturally means less streamflow contribution (Grünewald 2001, 2010; Koch et al. 2005). Consequently the 1976 and 1989 droughts are less pronounced in the Havel SSI (Fig. 15) compared to the time series for the entire contribution area between the Elbe gauges (Fig. 14), while the downward SSI peak of 2018 was more negative for the Havel sub-area. Other upstream areas of the GEB may expose streamflow modifications from reservoir operations, the reservoirs in the Harz and Ore mountains are however small and can neither alter the general runoff seasonality nor provide sustained runoff during drought.

Comparing the drought indices along the cascade of hydrometeorological effects from weather via soil water to streamflow illustrates the temporal hysteresis: The meteorological indices with three month time windows signal the 1976 drought in summer and autumn of that year while the soil water and discharge indices indicate the most extreme negative deviation of this drought not before winter 1976/1977. The 2018 drought was not repeated with the same intensity in 2019 and 2020 according to the meteorological indices, the soil water however still remains on extreme low levels in 2021, and the streamflow was probably also still affected in 2020 (unfortunately missing due to the limitation of the available runoff data).

2.3.3 Vegetation

How meteorological droughts affect different kinds of vegetation in the Elbe River basin strongly depends on the drought characteristics. Timing and duration account for different stressors and types of vegetation affected. Rooting depth of plants is an important for their drought resistance, and the plant-available water distribution in soil profiles is the decisive factor of vegetation status under drought conditions. For instance grasses were the first natural vegetation seen wilting in the drought years 2018–2020; they strongly depend on water availability in shallow soils (Reinermann et al. 2019).

Dry conditions in spring during the onset of the vegetation period are a major threat for plants. In the 2003 drought, this was the case in vast areas of the Elbe-River basin. Enhanced Vegetation Indices (EVI) attest reduced growing rates in the months of March and April whereas in the 2018 drought wet conditions favoured vegetation growth still during those months. However, due to major precipitation deficits during summer the resulting effects on vegetation were of the same magnitude as in the other drought years under investigation (Reinermann et al., 2019).

As drought conditions continued in the subsequent years 2019 and 2020, decreasing water availability also affected deeper rooting kinds of vegetation. The effects are visible in the forests of the Elbe River basin. Forests in the overlapping non-city federal states SN, ST, BB and TH are severely affected. A combination of abiotic and biotic threats accompanied the drought conditions: wind storms and a bark beetle infestation favoured by warm winter weather caused severe forest diebacks in spruce stands in the GEB. Among the survivors, the overall tree condition has decreased.

As shown in Fig. 16 below, after exceeding a new maximum for the share of trees with severe damages in 2019, the situation exacerbated in Saxony in 2020 (SMEKUL 2020). Whereas in Brandenburg the worst condition was reached in 2019 with a slight relief in 2020 (Forst Brandenburg 2020). In Thuringia 55 % of trees were severely damaged in 2020 which is the highest value in the four federal states (TMIL 2020). In Saxony-Anhalt the share of severely damaged trees seems comparably low, but since 2018 it exceeded the 1991–2017 values; with the 2019 value of 12 % tripling the former 2004 maximum (MULE n.d.). Overall, the effects of the 2003 drought on forests were by far exceeded in the 2018–2020 drought period.

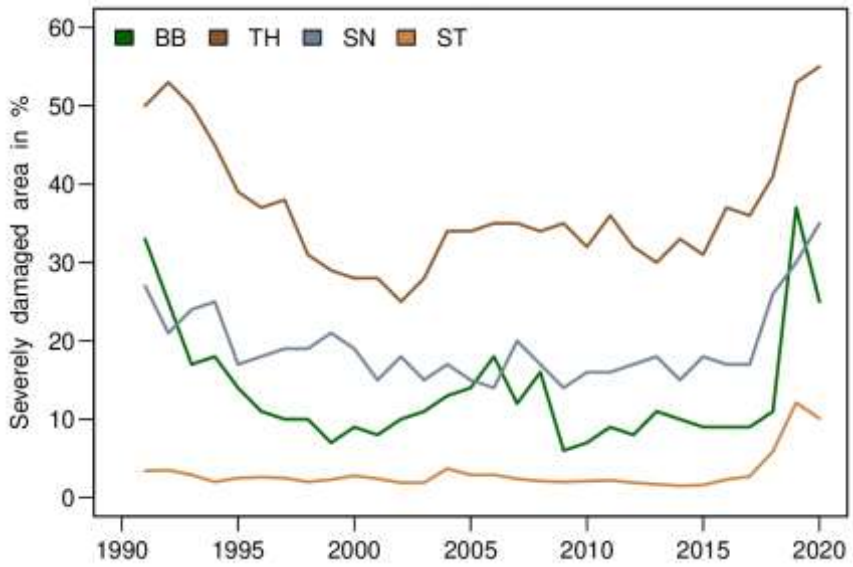

Figure 16: Area of forest with severe damages in the federal states BB, TH, SN and ST. Sources: (TMIL 2020, MULE n.d., SMEKUL 2020, Forst Brandenburg, 2020).

In terms of biodiversity, wetlands are important ecosystems with surplus features as carbon sink and water storage (Maltby and Acreman, 2011). Due to higher evaporation rates and lowering groundwater levels during droughts, Dietrich et al. (2012) suggest stressing conditions for wetlands in the Elbe River basin in a future dryer and warmer climate. In fact, renaturation of wetlands in the Elbe River basin is necessary due to low precipitation rates in recent years (MULE 2021).

Ludewig et al. (2015) found only slight effects on floodplain meadow in a study conducted with artificially reduced summer precipitation in the Elbe River basin. However, the study may not picture a drought period as seen between 2018 and 2020. Heklau et al. (2019) suggest mitigation of drought impacts for floodplain forests by flooding events before or after a drought event at the Saale River. This concludes the amplification of drought impacts on floodplain forests by missing flood events.

The floodplain forest (*Auwald*) was investigated for impacts of the extreme drought years 2018 and 2019. In this investigation Wirth et al. (2021) found moderate drought impacts in 2018 and much amplified impacts in the subsequent year for water flow in oak trees and for growth rates in ash trees. Furthermore, ash-trees showed the worst reaction on the extreme drought event. Already affected by pests before, the number of ash trees with irreversible damages increased from 14 % in 2016 to 47 % in 2020.

The extreme drought and heat conditions during 2018 also affected inner city ecosystems such as parks. There, the most obvious impact on vegetation were local extinctions of grasses and other low-growing vegetation, especially where tree canopy was missing (Kabisch and Kraemer, 2020).

2.3.4 Wildlife

Rivers and standing water bodies are among the most threatened ecosystems under extreme drought conditions. Impacts such as lower oxygen levels, bacteria blooms and elevated contamination levels are stressors for many wildlife species of freshwater ecosystems (Mosley 2015). In extreme cases droughts result in the drying-up of water bodies which eliminates most biota species (Humphries and Baldwin 2003).

In December 2018 and January 2019 vast amounts of fish died in canal systems near the Elbe estuary. The fishes were dying from Aluminium (Al) contamination which damages the gills and inhibits oxygen uptake. The Al contamination was the result of low groundwater levels allowing oxidation processes which then resulted in acidification. Since metals dissolve under acidic conditions, Al was dissolved in high amounts, and precipitation events in December 2018 finally transported the contaminated water into the canal system (Möllers, no date a).

The canal system was investigated for fish species populations in August 2019. The results were no significant differences in fish species diversity and overall population. However, the fish biomass decreased by 87.6 % in principally affected and by 56.5 % in moderately affected sections. The most harmed species were eels whereas sticklebacks were the species most benefitting from the absence of predators (Möllers, no date b). Small numbers of eels might also result from bacterial infections caused by a bacterial bloom in warm water temperatures (Möllers, no date b).

Amphibians are another species strongly depending on wet habitats. The reproduction depends on suitable environments for spawning. In the recent drought most of the spawning sites in BB had dried. This resulted in a decline of 67% in the BB newt population (SVZ 2020). Further effects of drought impacts on amphibia population have been found in TH where in recent years small water bodies dried out and spawn clumps of frogs decreased in size (WELT 2020). The decline in amphibia population also affects white storks who feed from amphibia, especially frogs. In the Spreewald region in Southern BB the result was a decrease in white stork population of 26 % in recent years. However, also other stressors like an increase in agricultural intensity put pressure on the population (WELT 2020).

The best reported changes in insect populations is an increase in bark and jewel beetle population. This is due to the extreme damage the larva living in the bark of trees cause to their host organism (TMIL 2020, MULE n.d., SMEKUL 2020, Forst Brandenburg 2020). Other insects like the dragonfly species *Crocothemis erythraea* and the rose beetle *Oxythyrea funesta* are among the species favoured by recent drought conditions (Süddeutsche Zeitung 2019b).

Ecosystem services such as feed and habitat provision important for wildlife are threatened by drought via the effects on vegetation. However, since these drought impacts are indirect and less obvious, there is less information about the state of wildlife populations, especially

mammals, under drought conditions. On the other hand, drought events increase the probability for sudden ecosystem breakdowns, especially through wildfires, resulting in broad extinction or expulsion of all kinds of animals and plants.

2.5 Drought impacts on human health

2.5.1 Heat stress

The recent drought came with high temperatures during summer, especially in 2018 and 2019. The DWD statistic of heat alerts issued between 2010 and 2020 in the districts of the four federal states BB, SN, ST and TH is shown in Fig. 17. The number of alerts suggests many events with strong heat stress on human health in 2018 and 2019. However, extreme heat stress events defined by perceived temperatures exceeding 38°C are on a low level during both years. This is most probably due to the drought related low level of humidity which drives the perceived temperature.

BB along with the city-state Berlin provides actual data on heat-related mortality (Fig. 18). In the federal states of TH, ST and SN, the provision of such timeseries is lacking, but since the states' demographics are alike with shares of people over 64 years between 24.7 % and 26.7 % (DESTATIS 2021h) and the heatwaves affected the whole area of concern, these data should be representative for the GEB.

High heat-related mortalities were observed in 2018, 2019, and 2020. Even though the summer of 2019 was the warmest summer since 1985 in BB, heat related deaths in 2018 clearly outweighed those in 2019. This is due to a long heatwave with 12 days of average temperatures exceeding 23°C in a row, which is the criterium for the connection of heat and mortality, during 2018 (Statistik BB 2021). In most years, the numbers for Berlin follow the same pattern with slight differences in the amplitude. However, with only about 10% more people older than 64 years in Berlin (DESTATIS 2021h), deaths in 2010 and 2015 exceeded this difference by far. One reason for this is the 0.7 K higher temperature average of the city-state between 1985 and 2020, resulting in an average of 34 % more heat days in Berlin than in BB (Statistik BB 2021).

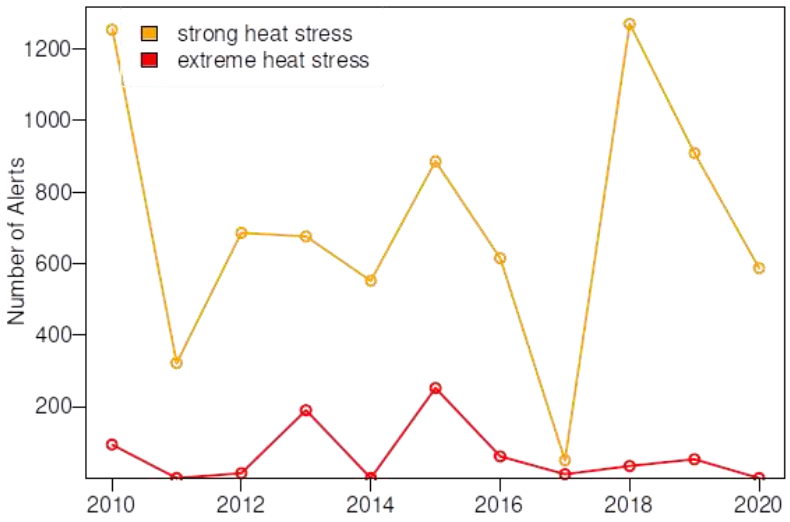

Figure 17: Heat related alerts between 2010 and 2020 in the four federal states BB, SN, ST and TH. Data source: DWD Climate Data Center (CDC): Historical heat warnings in Germany, version 001. URL

https://opendata.dwd.de/climate_environment/health/historical_alerts/heat_warnings/ – Last accessed in September 2021

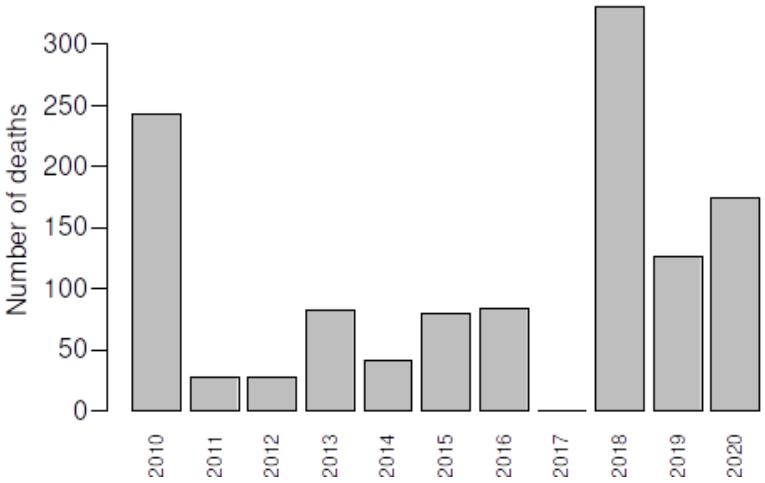

Figure 18: Heat related deaths in BB between 2010 and 2020. Data Source: Amt für Statistik Berlin-Brandenburg (2021).

In ST, excess mortality data suggests about 500 heat-related deaths during the 2016–2020 period. Especially days with high temperatures in the summer of 2018, some exceeding daily average temperatures of 29°C, caused a vast amount of the heat-related deaths in this federal state (Statistik ST 2021).

2.5.2 Air quality

Besides high temperatures, poor air quality is another stressor of human health. Ground-level ozone concentration is driven *inter alia* by weather conditions. High UV radiation levels and nitrogen oxide concentrations trigger chemical reactions producing amplified ozone formations near the surface. Ozone stresses the human respiration system which leads to symptoms like coughing, headache and restricted pulmonary function (UBA 2020).

In BB ozone levels in the 2010–2019 period peaked during the drought years 2018 and 2019. The critical ozone level is regulated in the Federal Imission Control Act (Bundes-Immissionsschutzgesetz) and determined to an average of 120 µg/m³ in an 8-hours period. One target of this act is to minimize the occurrence of the critical level to 25 days on average during three consecutive years. Another long-term goal is not to exceed the critical ozone level at all (LfU 2019). A dataset provided by the German Federal Environmental Agency (UBA 2021) covering ozone measurement stations in the four federal states counts 37 and 24 days exceeding the critical level in 2018 and 2019, respectively, compared to an average of 17 days per year in the 2010–2017 period. The critical 25-day threshold was crossed by 30 % and 40 % of the stations during the 2016–2018 and 2017–2019 periods, respectively. Between 2010 and 2017 only 17 % of the stations exceeded the number of 25 days in a three-year window. However, ozone levels have drastically decreased compared to the first decade of the century when modern catalytic converters on vehicles reducing nitrogen oxide emissions were not as widespread as they are now (UBA 2020).

Regarding the annual values for BB, other air pollutants did not show increased levels during the drought period. However, isolated pollution events as forest fires may not be adequately represented in these time-averages (LfU 2019).

2.5.3 UV radiation

We have requested a representative UV radiation time series at the German Federal Office For Radiation Protection whose monitoring started in 1993, but got no answer in time. As a

replacement, a sunshine duration series provided by the DWD is shown in Fig. 19. Potsdam has been chosen as reference station due to its relatively central position in the GEB. In the respectable observation period 1893[sic!]–2019, May and July of 2018 and June of 2019 were among the five months with the most sunshine. Figure 19 shows the accumulated sunshine duration between May and September of each year between 2010 and 2020. The five months in 2018 contained 1431 hours of sunshine, which is the highest value among all 127 years covered in the dataset. The high UV exposure coming with high radiation levels increases the number of skin cancer diseases making up 290,000 cases per year in Germany. This is particularly important for workers with high shares of outdoor work like construction workers, gardeners and farmers (Hünefeld & Hünefeld 2019).

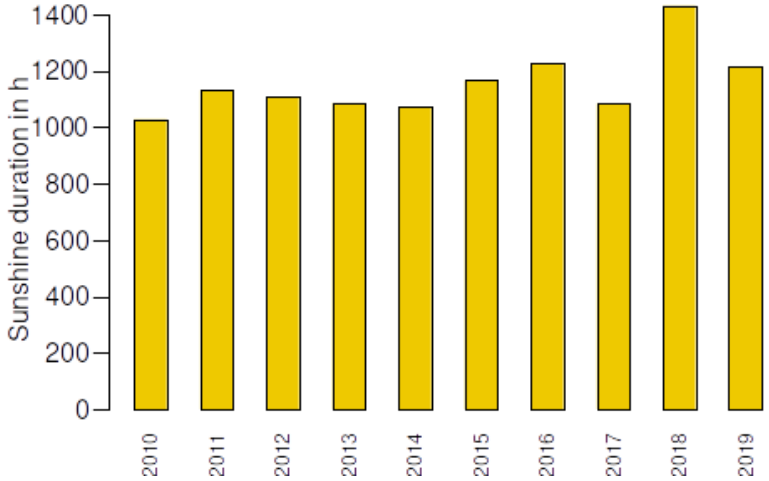

Figure 19: Accumulated sunshine duration during May, June, July, August and September in Potsdam. Data source: German Weather Service (DWD). URL: https://www.dwd.de/DE/leistungen/klimadatendeutschland/klimadatendeutschland.html – Last accessed in September 2021.

3. Impacts in the Boyne basin in Ireland

3.1. Introduction: The Boyne Catchment

The Boyne catchment is located in east Ireland and has an annual average total precipitation of 897mm (1952-2009). The catchment drains a total land area of 2694 km^2. A long term river flow gauging site (1941-present) of good quality is located at Slane Castle in Co. Meath (lat 53.706870^{o}N, long 6.562389^{o}W) and used in this study to represent flows in the catchment. The catchment area to Slane Castle is 2460 km2 and the main channel length is 94 km. There are a number of lakes in the catchment, to the north, the most significant being Lough Ramor and Mullagh lake in Co. Cavan. The catchment can be characterised as being predominantly flat to undulating lowland with elevation ranging between 16 and 338 m (Figure 20). Land-use within the catchment is dominated by agricultural pastures (87 %) with dairy farming being the predominant agricultural enterprise. Other significant land use types in the catchment comprise arable agriculture (~10 %), forestry (~5 %) and bogs (~5 %). The catchment is classified as essentially rural with approximately 1.5 % of the catchment containing urbanised areas. The main towns in the catchment include Drogheda, Navan, Trim, Kells, Virginia, Bailieborough, Athboy, Kinnegad, Edenderry and Enfield. The total population of the catchment is approximately 196,400, with a population density of circa 73 people per km^2. Water supplies in the catchment for human consumption comprise 89 abstractions, including six group water schemes, eight public supplies serving major urban centres and five private supplies.

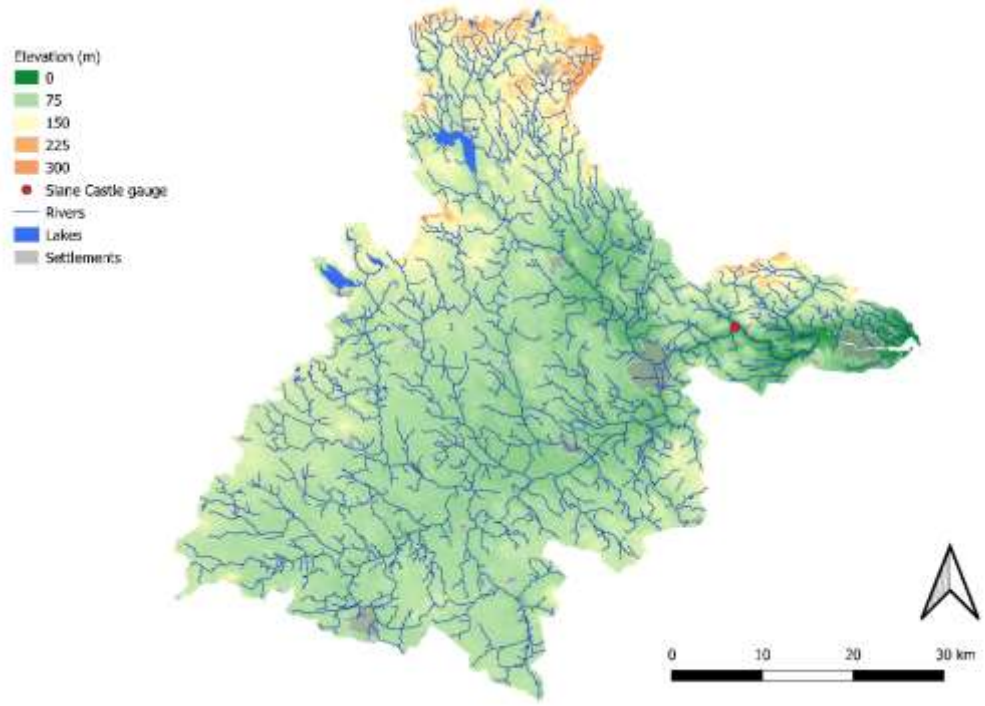

Figure 20: The Boyne catchment in eastern Ireland. The red dot marks the location of the river flow gauge at Slane Castle.

The catchment is underlain by metamorphic rocks in the north and limestone bedrock in the centre and south of the catchment. Extensive sand and gravel areas are found in the upper reaches of the catchment. Geology and soil types show a similar pattern with the southern and central parts of the catchment dominated by grey brown podzolics and gleys with significant peat deposits. In the north of the catchment soils are typically acid brown earths and gleys. More than 35 percent of the catchment is comprised of poorly drained soils, including basin peat and gleys.

Industry in the catchment is dominated by agriculture and traditional activities in the catchment related food processing and meat industries. Over recent decades mining and metal extraction have become important, particularly at Tara Mines, while water pressures are associated with the service sector, electronics and pharmaceutical industries and tourism and recreation activities. The Boyne is an important fishing river nationally, and designated a Salmonid river.

Given the importance of agriculture in the catchment and the presence of poorly drained soils, the catchment has been subject to extensive arterial and field drainage works. Arterial drainage comprises the artificial widening and deepening of main river channels and important tributaries to improve discharge conveyance (O'Kelly, 1955). Following arterial works peak flows have been noted to increase and the time to peak and duration of flood hydrographs to shorten (O' Kelly, 1955; Bree and Cunnane, 1979; Bailey and Bree, 1981). Little is known about the impact of arterial drainage on drought and low flows. The Boyne catchment experienced widespread arterial drainage over the period 1969-1986 (OPW, 2014) with more than 60 % of the river network affected. According to Harrigan et al. (2014) most works were competed between 1977 and 1979 with works on the main channel of the Boyne completed in 1984. Coincident with arterial drainage, the catchment was also subject to extensive field drainage works. This involves the installation of pipes and ditches to remove surplus water for waterlogged agricultural lands, resulting in shorter transmission times of water to river channels (Harrigan et al., 2014). While studies have indicated that field drainage likely increases runoff in winter and spring (Burdon, 1986), little work has been completed on the impacts of field drainage on low flows and droughts. Harrigan et al. (2014) estimate that more than 30 % of the catchment has been subjected to field drainage, however neither exact figures, nor the location of field drainage works are available due to a lack of records on implementation.

3.2. Meteorological and Hydrological Data

A monthly catchment average precipitation series was developed for the period 1950-2019. Data from individual stations within the catchment were derived from Met Éireann for the post 1940 period. Hawkins et al. (2021) succeeded in transcribing monthly data from the '10-year rainfall books' held in the UK Met Office. This dataset contains pre-1940 precipitation data for the UK and Ireland. We extracted available stations for the Boyne catchment and together with available historical data from the Island of Ireland precipitation network developed by Noone et al. (2016), we were able to extend the catchment precipitation series to 1850. The derived annual series was evaluated for breaks to identify any inhomogeneities in the series given changing measurement practice and changing number of stations through time. No significant breaks (0.05 level) were identified (Figure 21).

No long-term temperature series is available within the catchment. We therefore use monthly mean temperature for Dublin Airport for the period of available records. To extend the temperature data back to 1850 we followed the procedure used by O'Connor et al. (2020) whereby gridded monthly mean temperature data from Casty et al. (2007) was extracted for grids overlying the catchment and bias corrected using quantile mapping to available observations. The Oudin method (Oudin et al., 2005) was then used to derive PET estimates from available temperature records.

Daily discharge data for the Boyne catchment at Slane Castle are available from the Office of Public Works for the period 1941 to present. Missing data within the series (<2%) were unfilled. Monthly mean discharge (cubic metres per second) was derived from the available daily data.

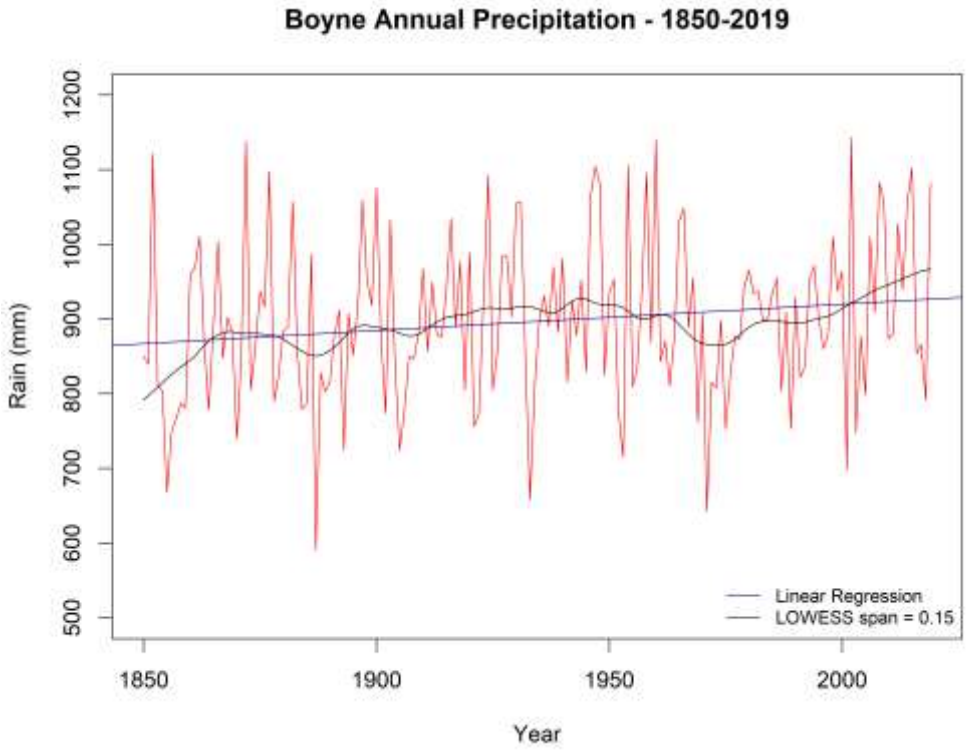

Figure 21. Annual precipitation series for the Boyne catchment for the period 1850-2019.

3.3 Hydrological Modelling

We employ a simple conceptual hydrological model to both i) extend monthly river flows to 1850, concurrent with available meteorological data, and ii) to reconstruct river flows in latter part of the record to examine the possible impacts of arterial and field drainage on drought events. To this end we use the GR2M monthly water balance model (Mouelhi et al., 2006), available via the airGR R hydrological modelling package (Coron et al., 2017). The monthly flow model contains two reservoirs representing a soil store and routing reservoir governed by two parameters: the production store capacity and groundwater exchange coefficient and has been used for flow reconstruction in Irish catchments (O'Connor et al., 2020). The model was calibrated (1942-1959) and validated (1960-1969) during the pre-drainage record and used to both extend and reconstruct river flows. Given the focus on low flows calibration and evaluation was undertaken using the Log Nash Suthcliffe (NS) objective function. Ten thousand parameter sets were sampled from a uniform distribution representing the range of plausible values for each parameter. Those sets with a LogNS score >0.8 during the validation period were retained for deriving extended and reconstructed flows. We base our subsequent analysis on the median simulated flows from retained parameter sets.

3.4 Standardised Drought Indices

We employ widely used standardised drought indices to evaluate and identify droughts in the catchment. Specifically, we use the Standardised Precipitation Index (McKee et al., 1993), the Standardised Precipitation Evapotranspiration Index (SPEI) (Vicente-Serrano et al., 2010) and the Standardised Riverflow/Runoff Index (SRI) (Barker et al., 2016) derived for accumulation periods ranging from 1 to 24 months. For each index values between 0.99 and -0.99 are considered near normal, -1.00 to -1.49 is moderate drought, -1.50 to -1.99 is severe drought and less than -2.0 is extreme drought (WMO, 2012). Both SPI and SPEI are fitted using a

gamma distribution, while SSI is fitted using the Tweedie distribution, following O'Connor et al. (2021). While we typically use the full series as the reference period for fitting distributions, it should be noted that the post drainage period is used as reference period when evaluating the impact of arterial and field drainage on standardised drought metrics.

Drought events are identified and extracted as follows for each accumulation period. Drought start is defined as the month in which standardised values fall below -1.00, and end when they return to positive values. Drought duration is defined as the number of months from start to termination. Drought severity is defined by accumulated deficit, calculated as the sum of deficits during the drought event. We also derive a mean deficit, by dividing accumulated deficits for each event by their duration (months).

3.5 Trend Analysis

To evaluate changes in standardised indices and the drought events though time we examine trends using the modified Mann Kendall test (Yue and Wang, 2004) that employs variance correction to address serial correlation. Trends were evaluated at the 0.05 significance level with a MK Z statistic >1.96 indicating a significant positive trend and a score <-1.96 indicating a significant negative trend. Trend magnitude was evaluated using the non-parametric Sen's slope estimate.

3.6. Historical Droughts in Boyne Catchment

Data rescue activities resulted in the development of a continuous monthly precipitation series for the Boyne catchment for the period 1850-2019. Figure 21 shows the annual total precipitation series. Over the 169-year period there is an increasing trend in annual precipitation significant at the 0.05 level. No significant break points were detected in the annual series using the Pettit change point test.

To investigate historical droughts in the catchment we extracted the standardised precipitation index (SPI) at 3-, 6- and 12-month accumulation periods from the newly derived catchment series. Figure 22 shows the resultant SPI series with the thresholds for severe and extreme drought also noted. Of note is the fact that despite the impacts felt in the catchment, the 2018 drought is unremarkable in the SPI-3 and SPI-12 series, being frequently exceeded in the historical record. Only in the SPI-6 series does the 2018 event register as an extreme drought (minimum SPI < -2.0).

Using the threshold of -1.00 to indicate the onset of a drought event we identify 136 individual events using SPI-3, 83 events for SPI-6 and 42 for SPI-12. Table 3 ranks the top 10 drought events for SPI-3, 6 and 12 in terms of their severity using both the accumulated deficit and the mean deficit identified for each event. Notably the recent 2018 drought does not feature in the top 10 events for any accumulation period. For accumulated deficits the 1887 drought, which commenced in March 1887 and terminated in April 1888 is the most severe SPI-3 drought in the series. The event also ranks highly for SPI-6 and SPI-12. For both SPI-6 and SPI-12 the drought which commenced in 1854 is the most severe by accumulated deficits in the entire series. Of note across all accumulation periods is that the most recent drought to feature in the top 10, occurred in the early 1970s, which the majority of the major events occur prior to the 1940s. This indicates the value of our long-term record for understanding historical drought in the catchment and the lack of severe drought in the catchment. It also highlights the vulnerability to drought given the impacts of the 2018 drought, which does not feature as an extreme event in our data.

3.7 Trends in droughts

Trends in drought were investigated in a number of ways. First, we assessed the SPI series for evidence of change in seasonal and annual droughts. Results are presented in Figure 23 and Table 3. We find an increasing trend (less drought) in winter droughts (February SPI-3)

significant at the 0.10 level. No evidence of change was found for spring droughts (May SPI-3). In summer (August SPI-3) we find a decreasing trend (more drought) significant at the 0.10 level. We find an increasing trend (less drought) in autumn (November SPI-3) significant at the 0.05 level. Annual (December SPI-12) and winter half year (WHY: March SPI-6) drought show increasing trends (less drought), both significant at the 0.05 level. No evidence for trend was found in the summer half year series (September SPI-6) These findings are consistent with Vicente-Serrano et al. (2021) who find evidence for decreasing winter and increasing summer drought for Ireland over the same time period. In summary, no trends or trends towards less drought are evident for all but summer months. In summer however, there is evidence of a trend towards more droughts.

In addition, we also tested for trends in the characteristics of drought events identified from SPI-3, 6 and 12 series. Characteristics examined include the duration, accumulated deficits and mean deficits of events. Most tests revealed no significant trends. The only significant trend (0.05 level) found was an increasing trend in accumulated deficits (less severe droughts) from the SPI-3 series (MKZs 2.02; p = 0.04). The time series of accumulated deficits for each of the 136 SPI-3 derived events is shown in Figure 24.

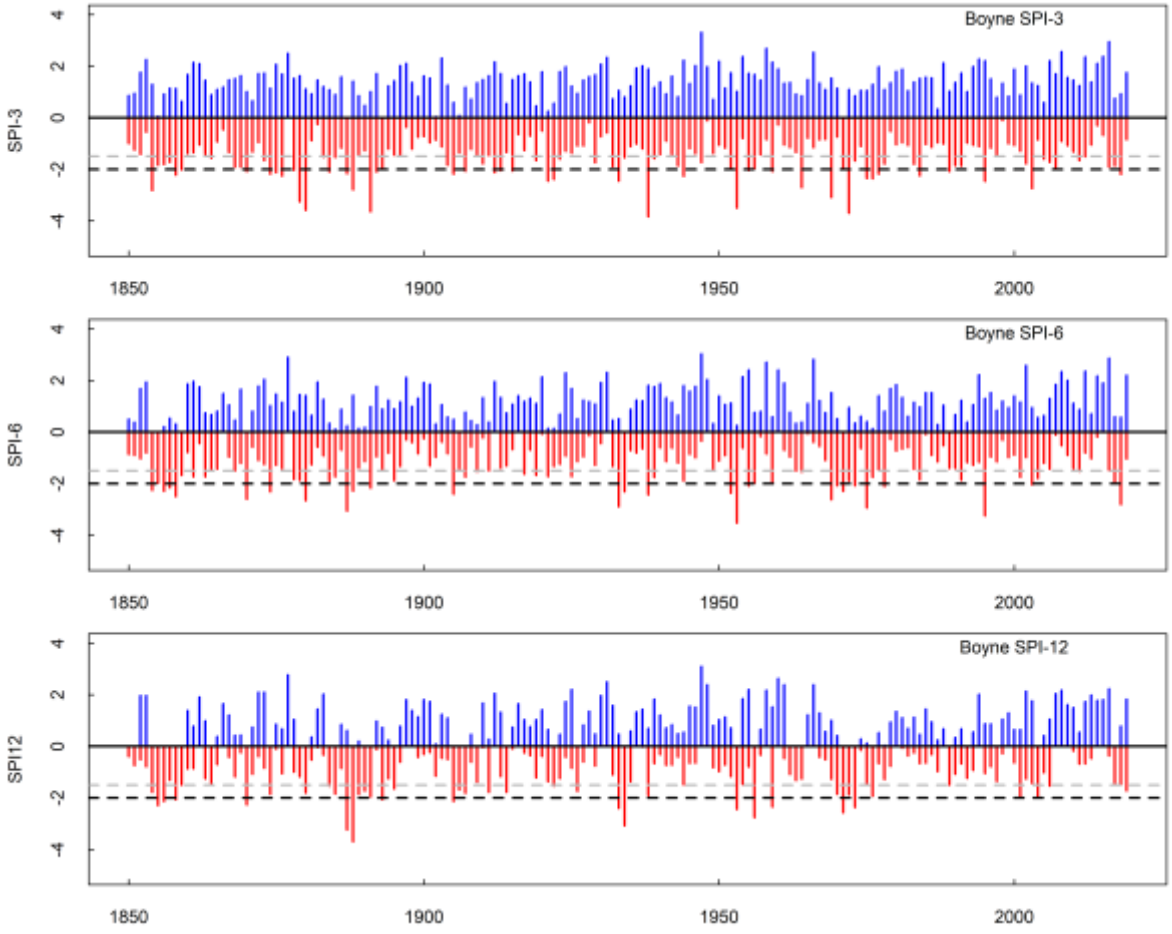

Figure 22 Standardised Precipitation Index (SPI) series of 3-, 6- and 12 month accumulation periods for the Boyne catchment from 1850 to 2019.

3.8 Arterial drainage

As indicated above arterial drainage works have been extensive in the Boyne catchment. While the impacts of drainage on high flows are well understood, little research has investigated the impact of such interventions on droughts. Therefore, we sought to reconstruct monthly river

flows for the gauging station at Slane Castle to create an artificial series representing the catchment without drainage. By deriving and comparing Standardised Streamflow indices of various accumulations (SSI-3, 6, 12) for the observed and reconstructed series we aim to provide a first investigation of the impacts of drainage on drought in the catchment.

The GR2M model was calibrated and validated in the pre-drainage record, before being used to reconstruct the post drainage record and extend river flow estimates back to 1850, concurrent with available precipitation records. The NSE values derived from the Log of flows with a performance >0.8 were identified during calibration and retained for simulation during validation and the reconstruction period (post-drainage). Results are shown in Figure 25. It is evident that for verification (black dots) similar performance levels are obtained by the model, while there is a decrease in performance during the post drainage period (grey dots).

Table 3 Top 10 drought events for each accumulation period (SPI-3, 6 and 12). Events are ranked according to accumulated deficit (left) and mean deficit (right) for each drought. Also provided are drought start and end dates in the form of Year/Month.

	Accumulated Deficit			**Mean Deficit**		
	1887/03	1888/04	-21.2	1891/02	1891/05	-2.8
	1933/08	1934/09	-17.3	1879/11	1880/04	-2.2
	1971/02	1972/03	-13.2	1922/11	1923/02	-2.0
	1955/09	1956/08	-13.1	1972/09	1973/01	-2.0
	1953/01	1953/08	-12.7	1953/01	1953/08	-1.8
	1873/12	1874/09	-11.4	1975/04	1975/09	-1.8
	1857/09	1858/04	-11.1	1964/02	1964/04	-1.8
	1879/11	1880/04	-10.9	1947/10	1947/11	-1.7
SPI-3	1995/05	1995/11	-10.4	1995/05	1995/11	-1.7
	1969/08	1970/02	-10.2	1969/08	1970/02	-1.7
	1854/04	1856/09	-29.6	1995/08	1995/12	-2.0
	1887/04	1888/07	-28.7	1887/04	1888/07	-1.9
	1933/08	1934/12	-27.0	1969/10	1970/04	-1.9
	1952/07	1953/11	-21.5	1879/12	1880/07	-1.7
	1905/10	1907/06	-18.5	1905/01	1905/08	-1.7
	1869/08	1871/01	-18.1	1933/08	1934/12	-1.7
	1971/05	1972/05	-16.1	1878/12	1879/06	-1.6
	1972/09	1973/09	-15.5	1857/10	1858/07	-1.6
SPI-6	1857/10	1858/07	-14.5	1874/02	1874/10	-1.6
	1955/10	1956/08	-14.4	1978/08	1978/12	-1.6
	1854/03	1860/06	-93.7	1887/06	1889/02	-1.8
	1905/01	1908/01	-45.1	1933/09	1935/06	-1.8
	1971/09	1974/02	-39.5	1952/12	1954/05	-1.5
	1933/09	1935/06	-38.0	1971/09	1974/02	-1.4
	1887/06	1889/02	-36.3	1959/08	1960/01	-1.3
	1889/06	1892/02	-29.6	1905/01	1908/01	-1.3
	1952/12	1954/05	-26.3	1969/12	1970/11	-1.3
SPI-12	1921/07	1923/10	-23.0	1854/03	1860/06	-1.2
	1975/07	1977/02	-21.8	1874/01	1875/01	-1.2

1884/10	1886/07	-21.4	1870/03	1871/07	-1.2

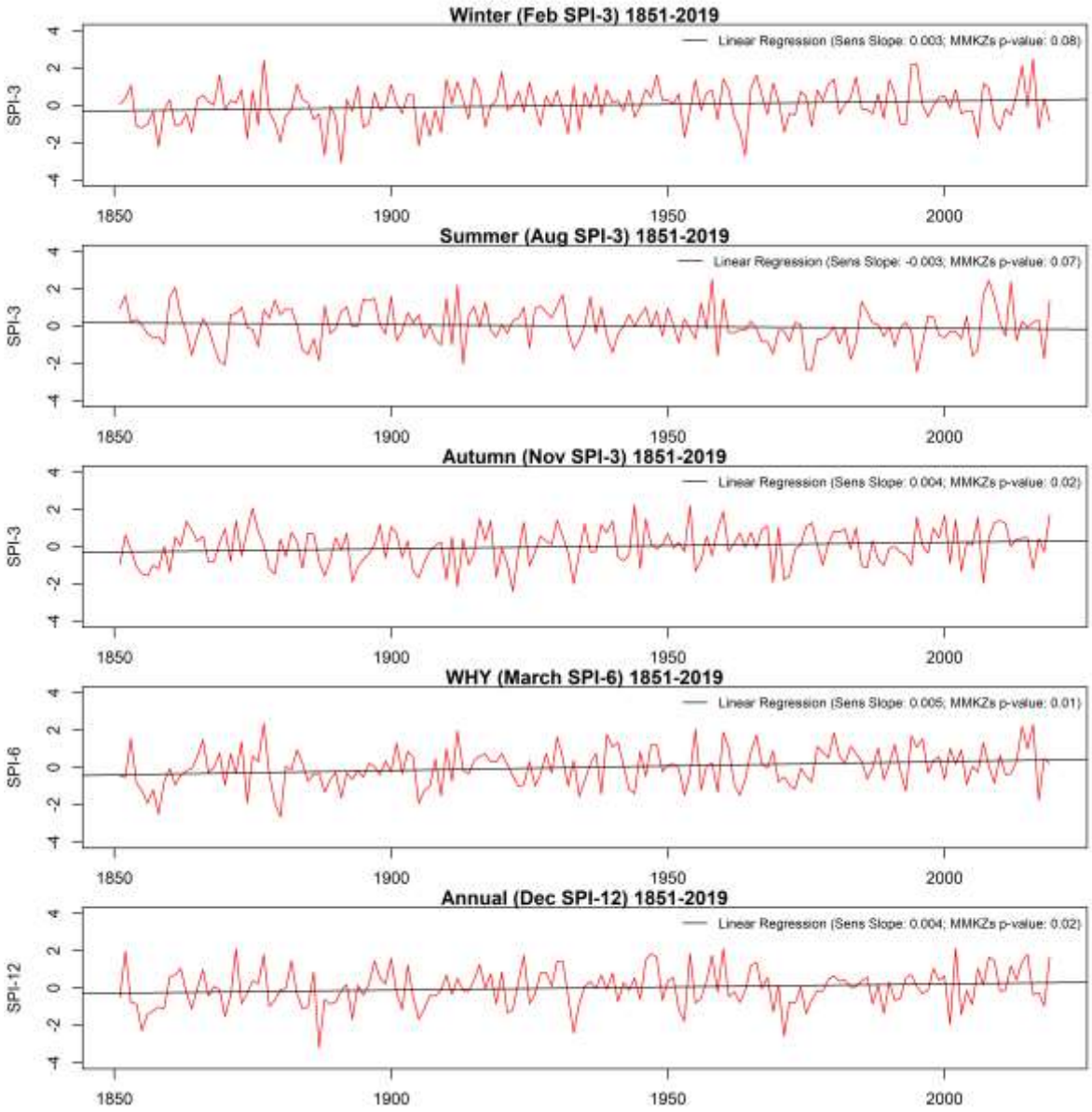

Figure 23 Time series of seasonal and annual SPI series used to evaluate evidence for trend using the Modified Mann-Kendall test. Each plot shows the observed series together with linear regression line, Sen's slope estimate, the Modified Mann-Kendall test statistic and the associated p-value for each test.

This decrease in performance is predominantly due to underestimation of wet months by the model in the post drainage period. Looking at the time series of reconstructed and observed summer mean flows in Figure 26, it is apparent that overall, the model does reasonably well at capturing flows during dry months, with flows during wet summers (e.g. 2009) being considerably underestimated. Figure 6 also points the possible flow data quality issues in summer months in the pre-drainage record, particularly during the 1950s.

Table 4 Results of trend tests for each indicator or seasonal and annual drought. Shown are the Modified Mann-Kendall test statistics (MKZs), the magnitude of trend in standardised units using Sen's slope estimate and the associated p-value of the test on trend magnitude.

Indicator	MKZs	Sen's Slope	p-value
winter (February SPI3)	1.74	0.003	0.08
spring (May SPI3)	0.71	0.001	0.48
summer (August SPI3)	-1.81	-0.003	0.07
autumn (November SPI3)	2.35	0.004	0.02
annual (December SPI12)	2.42	0.004	0.02
WHY (March SPI6)	2.75	0.005	0.01
SHY (September SPI6)	-0.99	-0.001	0.32

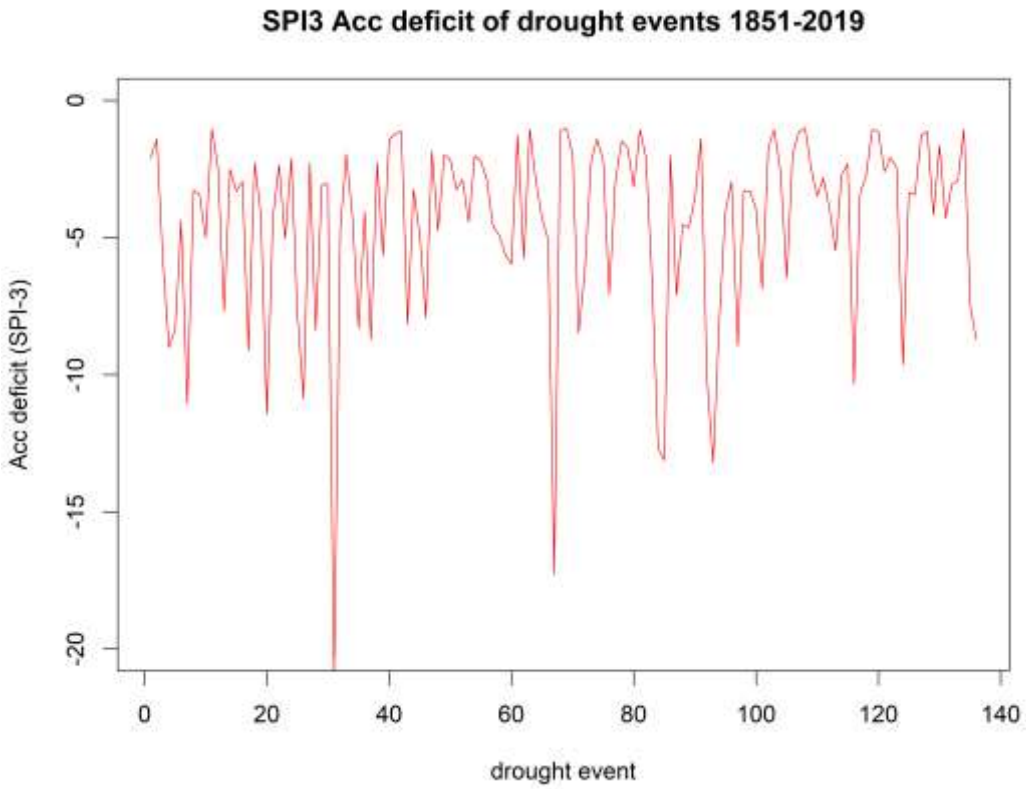

Figure 24 Accumulated deficits for each of the 136 SPI-3 drought events identified in the Boyne catchment over the period 1850-2019.

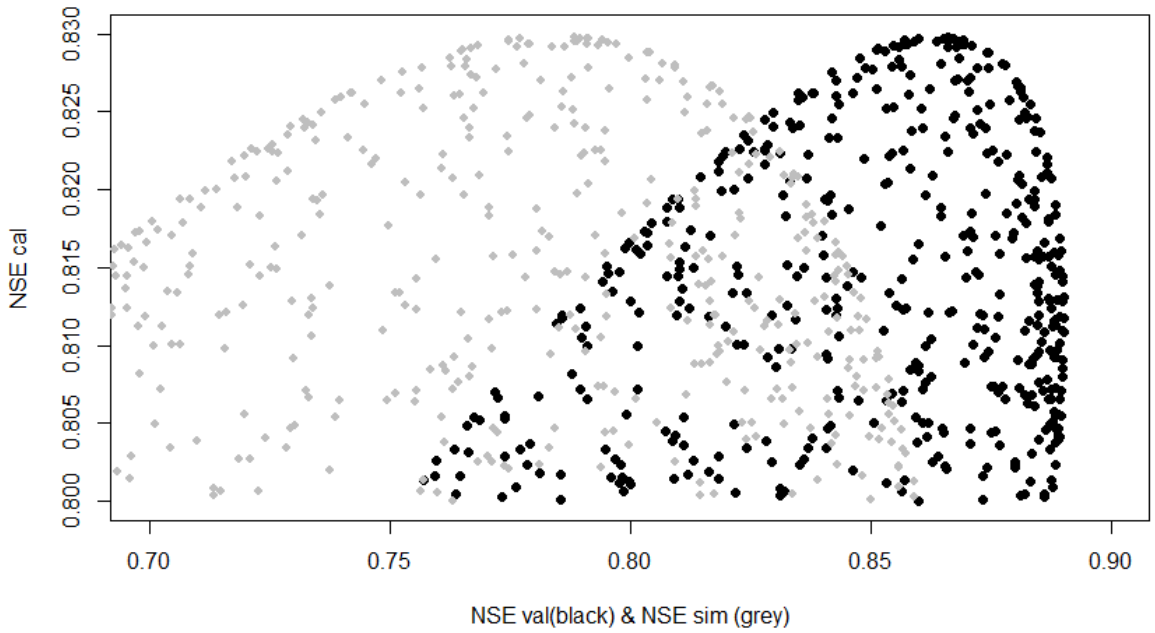

Figure 25 Distribution of behavioural parameters sets (those with logNSE > 0.80 during calibration) for the validation period (pre-drainage; black) and the post drainage record (grey).

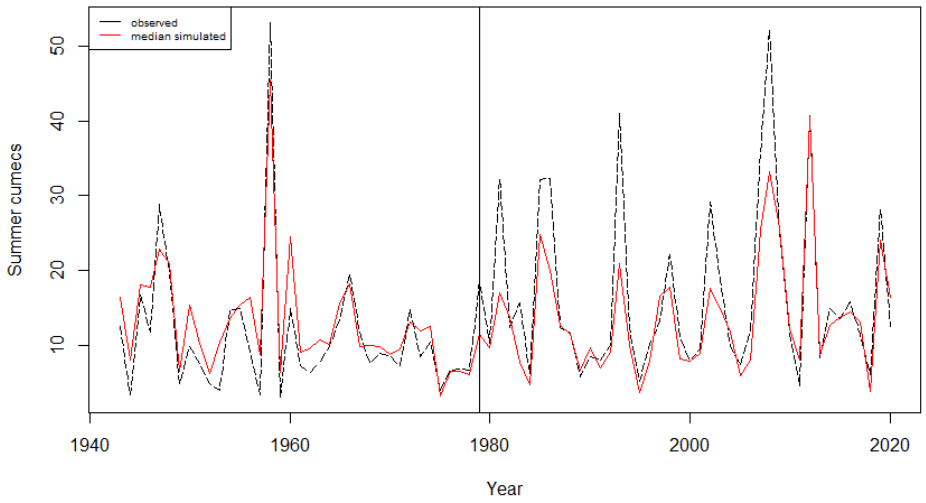

Figure 26 Observed (black) and median reconstructed (red) summer mean flows for the Boyne at Slane Castle for the period 1941-2019. The vertical black line represents the completion of arterial drainage works in the catchment.

To further investigate the impact of drainage on standardised drought indices we derived SRI-1, 3, 6 and 12 from observed and reconstructed flows for the post drainage record (1980-present). Scatter plots of the derived indices are shown in Figure 27. Evident is that at high flow end there is a tendency for reconstructions to underestimate the observations for all accumulation periods. This is consistent with arterial drainage increasing peak flows and flows during wet months (see Harrigan et al., 2015). Notably there is good correspondence between observations and reconstructions at the low end of the distribution, indicating limited impact of arterial drainage of droughts.

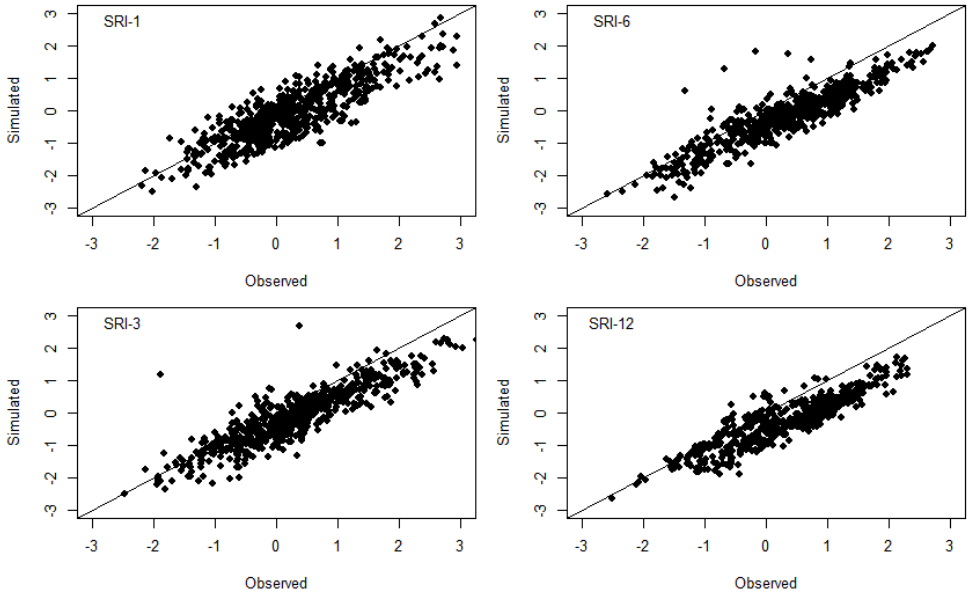

Figure 27 Scatter plots of observed and reconstructed SRI-1, 3, 6 and 12 for observed and reconstructed flows for the post drainage period 1980-2019.

The impact of drainage on the characteristics of drought events was also investigated by identifying drought events for each SRI accumulation period for both observed and modelled flows. The same criteria for identification of drought events as used in the SPI analysis above were implemented. Figure 28 provides an example using SRI-3 events given the greater frequency of such events compared to SRI-12. Both accumulated and mean deficits show no evidence of significance differences in the pre/post drainage record using either observed or modelled flows. These findings again suggest that arterial drainage has limited impacts on the severity of drought events. However, it should be noted that there are fewer droughts in the post drainage record due to natural climate variability also. We assume that our reconstructed flows, driven by observed precipitation adequately captures this.

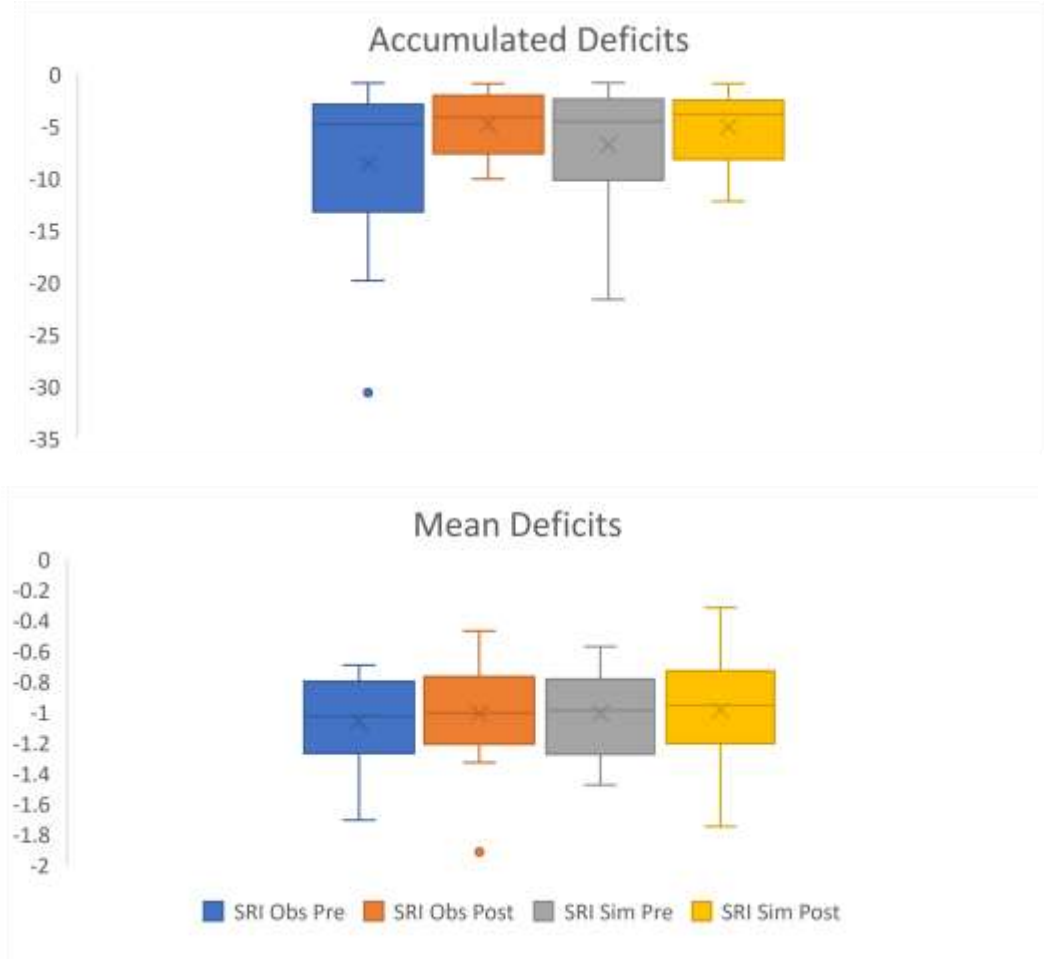

Figure 28 Comparison of SRI-3 mean and accumulated deficits from observed pre (blue) and post (orange) drainage drought events and reconstructed pre (grey) and post (yellow) drainage drought events.

The GR2M model was also used to extend the flow record to 1850, concurrent with available catchment precipitation records. The SRI-3, 6 and 12 series from reconstructed flows for the period 1850-2019 for the Boyne at Slane Castle are presented in Figure 29. The recent 2018 drought is categorised as an extreme drought for all accumulation periods. However the event is not as extreme as others that have occurred in this historical record, particularly for longer accumulation periods (e.g. SRI-12).

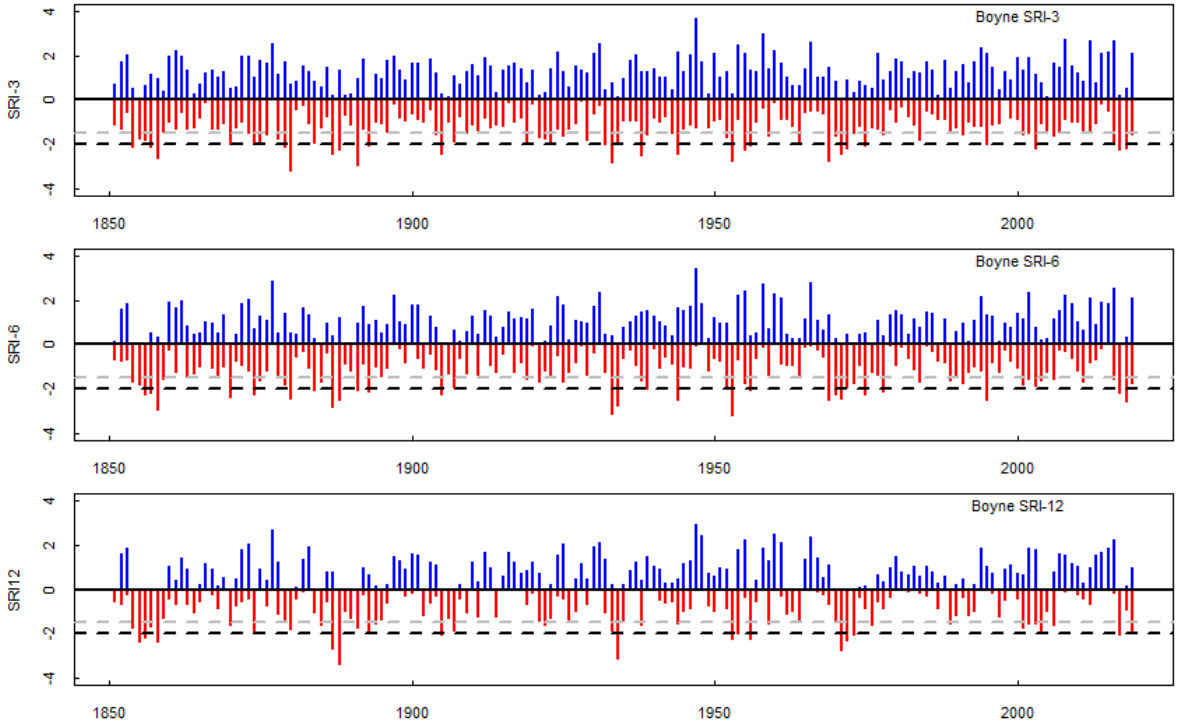

Figure 29 SRI-3, 6 and 12 for reconstructed flows covering the period 1850-2019 for the Boyne at Slane Castle. The grey horizontal line represents the threshold for severe drought (-1.5), while the black horizontal line represents the threshold for extreme drought (-2.0).

3. Impacts in the Aragon basin in Spain

3.1. Study area

With a total area of 2181 km^2, the upper Aragon basin is located in the Central Spanish Pyrenees (Figure 30). The basin is characterized by a strong topographical gradient, with elevations varying from 600 to 2886 m.a.s.l. The Aragón River flows from north to south within a Paleozoic zone, with limestone, shale, and clay formations. It also crosses the Inner Sierras (limestone and sandstone), the flysch sector, and the Inner Depression (marls) before changing its direction westward. Climatologically, the basin receives an annual rainfall totals exceeding 1500 mm in the northernmost sector, declining to 800 mm in the Inner Depression. Apart from summertime, rainfall is distributed all over the year, albeit with higher intensities during spring and autumn. The mean annual air temperature is 10 °C. Snow cover appears in the period from December to April, especially at sites located above 1500 m.a.s.l (López-Moreno and García-Ruiz, 2004; López-Moreno et al., 2020). Long-term annual mean runoff is 915 hm^3, with a peak occurring mainly during springtime. This corresponds to the annual peak of rainfall and melting of the snowpack. With a capacity of 446.8 hm^3, Yesa reservoir, located at the basin outlet, is one of the largest reservoirs in the Pyrenees, providing water resources for irrigation purposes to the Bardenas region (81,000 has), located 80 km to the South of the basin (López-Moreno et al., 2004). This irrigated area is located in the central portions of the Ebro basin, where annual rainfall is generally below 300 mm, with a strong interannual variability and high rates of reference evapotranspiration (> 1300 mm/year) (Tomas-Burguera et al., 2019). The main crops in the Bardenas irrigated area are winter cereals (barley and wheat), which are harvested in June, and summer corn, harvested in September-October.

Vegetation cover in the upper Aragon basin is characterized by the dominance of conifers (*Pinus* sylvestris L*., Pinus uncinata* Ram., *Abies alba* Mill., *Pinus nigra* J.F. Arn.) and hardwood species (*Fagus sylvatica* L*., Quercus faginea* Lam.), while shrubs dominate the understory (e.g., *Buxus sempervirens* L.) or are distributed over the sunfaced slopes and in areas of poor soil (García-Ruiz et al., 2015). Natural vegetation has been strongly impacted by human activities. Historically, cultivated areas were located below 1600 m a.s.l., in the valley bottoms, perched flats and steep, south-facing hillslopes, which were managed even under shifting agriculture (García-Ruiz et al., 2015). Above 1600 m a.s.l. the basin is dominated by pastures generated during the middle ages to maintain big transhumant sheep folks, since the natural treeline was depressed by anthropogenic disturbances. During the 20th century, most cultivated fields were abandoned, except in the valley bottoms, and as consequence, the basin has been affected by a large natural revegetation process (Lasanta-Martínez et al., 2005; Lasanta and Vicente-Serrano, 2007) accentuated by the reforestation of some slopes by coniferous forests during the 1950s and 1960s (Ortigosa et al., 1990). Crops are dominant in the Inner depression and they are characterized by winter cereals: barley and wheat. Land cover changes have had an important impact on hydrological processes, and water production severely decreased over the last decades in the basin as a consequence of increased evapotranspiration (Beguería et al., 2003; López-Moreno et al., 2011).

3.2. Climatic dataset

The precipitation and reference evapotranspiration data for the basin were extracted from a gridded climatic dataset developed by Vicente-Serrano et al. (2017c) for the whole of Spain. This dataset includes information on a wide array of climatic variables (e.g. precipitation, maximum and minimum air temperature, relative humidity, sunshine duration, and wind speed) at high spatial (1.21 km^2) and temporal (weekly) resolution. This dataset was developed using the most complete register of observed climate records provided by the Spanish Meteorological Agency (AEMET), including meteorological stations located at different elevations. In particular, in the upper Aragon basin there are more than 50 meteorological

stations from a range of 500 to 1750 m, although it varies among variables (more available for precipitation than for temperature). The dataset showed good performance in capturing drought characteristics (e.g. severity, spatial extent) in earlier studies over Spain (e.g. Domínguez-Castro et al., 2019; Noguera et al., 2020).

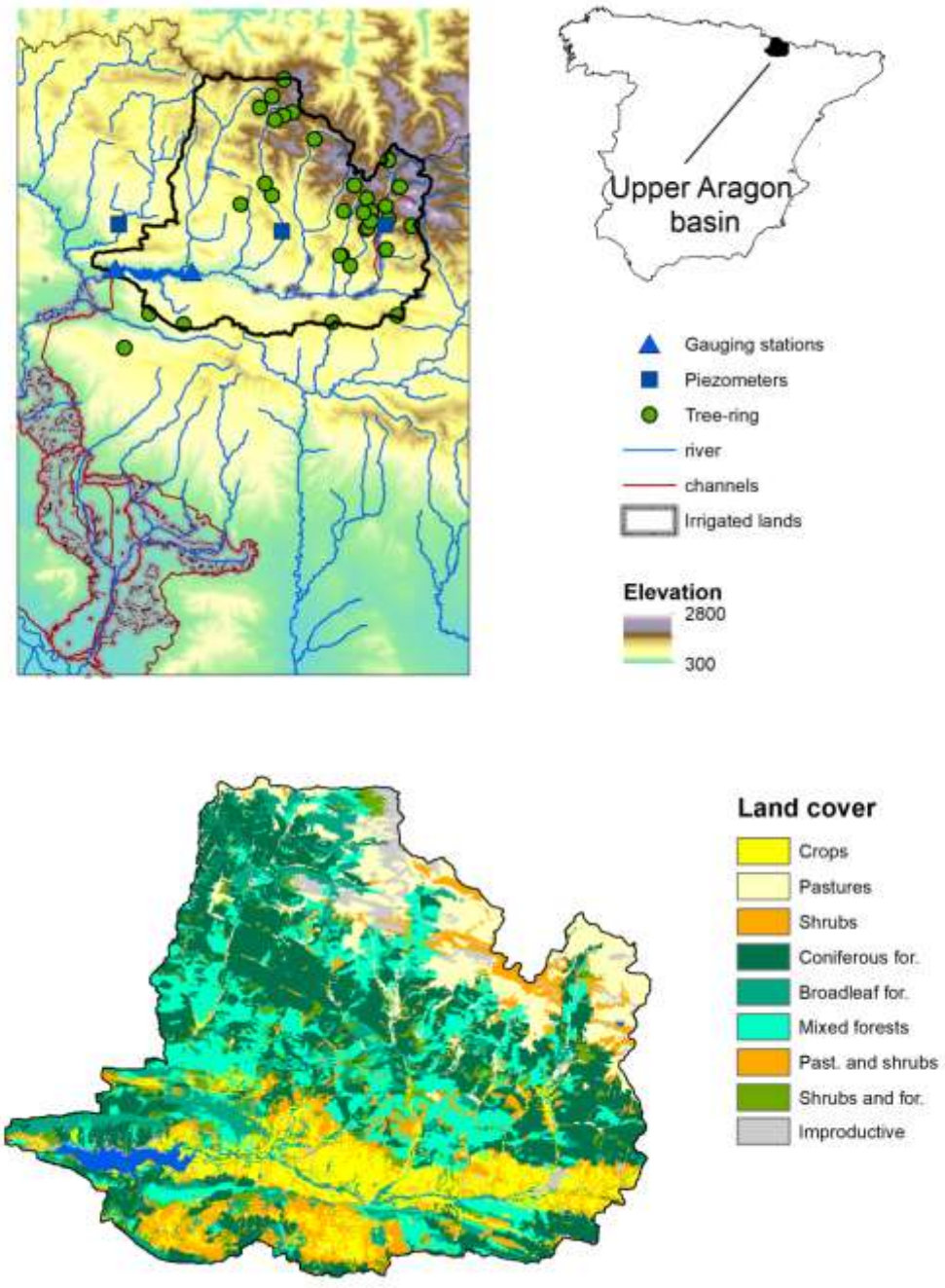

Figure 30: Location of the study domain and the spatial distribution of hydrological stations, sites with piezometric data and tree-ring sampling sites (upper panels); and the main land cover (LC) types in ths study area (lower panels). As illustrated, the Bardenas irrigation channel transports water from the upper Aragón basin to the Irrigated lands of Bardenas in the South.

3.3. Hydrological dataset:

Data on surface flows and storage levels for the Yesa reservoir were obtained from the Ebro Basin Management Agency (*Confederación Hidrográfica del Ebro;* http://www.chebro.es/) This also includes data on monthly inflows into the reservoir and releases downstream (i.e. to the Aragón River and the Bardenas channel). Yesa water inflow is directly influenced by the climatic conditions since there is not other regulation upstream), while all other hydrological variables (Yesa storage, Bardenas channel and the Aragón flows downstream Yesa) are dependent to water management practices. Also, data about the piezometric levels at four gauging stations in the basin were provided by the Spanish Ministry for the Ecological Transition (https://sig.mapama.gob.es/redes-seguimiento) for the period 1992 to 2017 (Figure 1). These data were employed to assess the response of groundwater levels to climatic droughts. Given considerable amount of missing values and data gaps in the piezometric data before 2002, we only employ data for the period 2002-2017 to assess the links between piezometric levels and climate droughts in the basin. We also employ monthly snow depth data for highly elevated sites (above 1500 m.a.s.l). Data were obtained for the months between December and April for the period 1958-2017. A description of this dataset is outlined in López-Moreno et al. (2020).

3.4. Tree-ring data:

Tree-ring width data were collected from six representative tree species in the basin: *A. alba, P. sylvestris, P. uncinata, P. nigra, F. sylvatica* and *Q. faginea*. Data from 37 sites with forest growth were used in this work. Overall, the tree-ring data were processed by means of standard dendrochronological protocols (Fritts, 1976). Specifically, at least 10-15 dominant trees located in undisturbed stands of each species were selected and cored at 1.3 m using increment borers. This procedure aimed to obtain 2–3 cores per tree in each forest. Cores were air dried, carefully sanded and ring series were visually cross-dated. Tree-ring width was measured to at least the nearest 0.01 mm using binocular microscopes and different measuring device systems (i.e. Lintab, RinnTech, Heidelberg, Germany; Velmex Inc., Bloomfirld, NY, USA). In order to check the accuracy of visual cross-dating and measurements, we used the COFECHA program (Holmes, 1983). Each individual tree-ring width series was detrended by fitting negative exponential curves. Then, the residuals were computed through dividing the observed values by the fitted ones. Autoregressive modelling was used to remove the first-order autocorrelation from the individual, detrended tree-ring width series. Finally, the detrended individual series of tree-ring width indices (hereafter TRWi) were averaged for each forest and species by computing the bi-weight robust means. These procedures were carried out using the ARSTAN software (Cook, 1985). Herein, the mean site-level chronology represents the average growth series of the variable number of trees associated with the same species and the same forest stand. A detailed description of the sampling procedure and data processing is documented in recent studies (e.g. Gazol et al., 2018; Peña-Gallardo et al., 2018; Vicente-Serrano et al., 2020a).

3.5. Vegetation activity

Vegetation activity was quantified by means of two-band Enhanced Vegetation Index (EVI2) from the Moderate Resolution Imaging Spectroradiometer (MODIS) satellite sensor for the period 2000-2020. EVI2 is more robust against the three-band EVI, which is sensitive to atmospheric disturbances caused by the blue band (Jiang et al., 2008). While EVI2 is an indicator of the photosynthetic activity, it can also be seen as a proxy of other vegetation parameters (e.g. the leaf area index, vegetation coverage, vegetation primary productivity and carbon uptake) (Huete et al., 2002; Wang et al., 2005, Sjöström et al., 2011). The MODIS reflectance data used for calculating EVI2 were from the MCD43A4 product, retrieved from the

NASA repository (https://modis.gsfc.nasa.gov/data/dataprod/mod13.php) at a grid interval of 500 m and averaged to a temporal frequency of 16-days. Curve fitting was applied to the 16-day composite data to extract comparable monthly values using the TIMESAT software package (Jönsson and Eklundh 2004). Typically, the use of EVI2 data is advantageous in areas with pasture and shrub lands, where samples of forest growth are unavailable. Nonetheless, these data can also be used in forest areas to determine the different impacts of drought, given that vegetation responds differently to drought in forest areas (Gazol et al., 2018; Peña-Gallardo et al., 2018). We also make use of satellite data available at more detailed spatial scales by computing the EVI2 using Sentinel-2 data at 10 m spatial resolution for the period 2017-2019. Sentinel-2 data were obtained from the European Space Agency (https://sentinel.esa.int/web/sentinel/sentinel-data-access) at a spatial resolution of 10 meters and a daily temporal resolution. Curve fitting was applied to Sentinel-2 pixel values using a robust method (Jönsson et al., 2018; Cai et al., 2017) to generate comparable monthly values of EVI2 for each image pixel.

3.6. Vegetation phenology

As vegetation can be impacted by drought at different phenological phases (Reynolds et al., 1999; Sah et al., 2020; Wang et al., 2020), we employed a set of phenological metrics to assess ways in which drought can influence vegetation dynamics. These metrics included the start date, end date, length of season (duration), amplitude (peak vegetation index value minus the off-season base level value) and integral (seasonal sum of the vegetation index values) of the growing season corresponding to each year for the period between 2001 and 2019. The start and end dates represent the location of the growing season in time whereas the amplitude and integrals relate to vegetation production during the growing season. All metrics were retrieved from the EVI2 data using the TIMESAT software (Jönsson and Eklundh, 2004), after applying a function fitting procedure to obtain the different phenological parameters. TIMESAT-based phenology has been widely validated in different regions of the world with a high agreement between phenological ground observations and TIMESAT calculations using satellite data (Peng et al., 2017; Tan et al., 2011).

3.7. Land cover data

A land cover (LC) map developed by the Spanish Ministry of Agriculture (https://www.mapa.gob.es/es/cartografia-y-sig/publicaciones/agricultura/mac_2000_2009.aspx) was used to determine possible differential impacts of drought on vegetation activity and annual phenology in the dominant land cover types of the upper Aragón basin. Although this map was updated in 2010, it remains representative of the current dominant land cover classes in the basin.

3.8. Methods

To characterize climatic drought severity, we used the standardized precipitation evapotranspiration index (SPEI) (Vicente-Serrano et al., 2010). This is one of the well-established drought indices, which has been widely used for drought quantification over the past decade. The SPEI is computed as the difference between precipitation and reference evapotranspiration, accounting for the possible role of atmospheric evaporative demand (AED) in drought severity. Accordingly, it has been widely used for drought analysis and impact monitoring in different regions worldwide (e.g. Bachmair et al., 2018, 2016, 2015; Peña-Gallardo et al., 2018; Peña-Gallardo et al., 2018; Scaini et al., 2015). Herein, SPEI was computed at different timescales ranging from 1- to 48-month timescales. This is simply

because the response of different systems to drought is strongly determined by the time scale at which drought is quantified. This dependency has already been evident in different studies, including natural ecosystems (e.g. Pasho et al., 2011; Vicente-Serrano et al., 2013), hydrology (e.g. Barker et al., 2016; Lorenzo-Lacruz et al., 2017, 2013; Peña-Gallardo et al., 2019), and crop yields (e.g. Peña-Gallardo et al., 2018). We computed a regional series of the SPEI for the whole basin using a simple arithmetic average of the available precipitation and reference evapotranspiration data. In the same manner, a regional series of the SPEI was also calculated for the Bardenas irrigation area

Hydrological drought was quantified by means of the Standardized Streamflow Index (SSI) (Vicente-Serrano et al., 2012). The SSI was computed using data of monthly inflows, streamflow releases, and reservoir storages within the basin for the period 1962-2019. Similar to SPEI, SSI values are expressed in standardized units, with a zero-average and one-standard deviation, enabling direct comparison between streamflow systems with different magnitudes and seasonal regimes. For this purpose, monthly series of the raw hydrological data are fitted to a distribution probability. Given the strong differences in the distribution of the monthly streamflow series, the distribution that shows the best fit with each one of the monthly series is selected. The SSI is always calculated at the time scale of one month. Irrigation from the Bardenas channel was not operative at full capacity until 1970 so standardization and subsequent analysis were based on the period between 1970 and 2020.

The same standardization approach was implemented for data of snow depth. Nevertheless, as the records of piezometric levels were not sufficiently long to allow a fit to a probability distribution, the average and standard deviation of the monthly series were used, assuming a normal distribution. For tree-ring data, the standardized mean series were obtained for each forest and species. The detrended tree-ring series (with a range between 0 and 1) followed a normal distribution so they were also standardized considering the mean and standard deviation of each series. Following this approach the series of all of these variables had the same units (z-units) and they were perfectly comparable, spatially and seasonally, independently of the different magnitude and seasonality of each variable.

We employed the Pearson's r correlations to assess the links between the series of SPEI and those of the different available datasets (e.g. flows, tree-ring growth, phenology metrics, crop yields). Correlations were computed for all SPEI timescales (i.e. 1- to 48-month) and were calculated for each one of the 12 monthly series of the year. No lagged correlations were calculated. Herein, it should be noted that drought severity was computed using different SPEI thresholds, which represents different probabilities of occurrence. These thresholds included SPEI values of zero (1 in 2 years), -0.84 (1 in 5 years), -1.28 (1 in 10 years) and -1.65 (1 in 20 years). However, this analysis was restricted only to forest growth and hydrological variables, mainly due to the availability of longer timeseries to reliably assess the impacts of drought severity analyzing the anomalies recorded in these variables corresponding to different thressholds of the SPEI.

3.9. Temporal variability of climatic droughts

Figure 31 illustrates the temporal evolution of climatic drought over the Yesa basin using SPEI computed at timescales ranging from 3- to 24-month. Results demonstrate that the basin has witnessed frequent drought events in the period 1961-2020, but with more frequent dry events in recent decades (mostly from the 1980s onwards). The longest and more intense drought events were observed during the 1990s, while wet conditions prevailed in the 1960s and 1970s. Nonetheless, it can be noted that the frequency of drought events varies considerably as a function of SPEI time-scale.

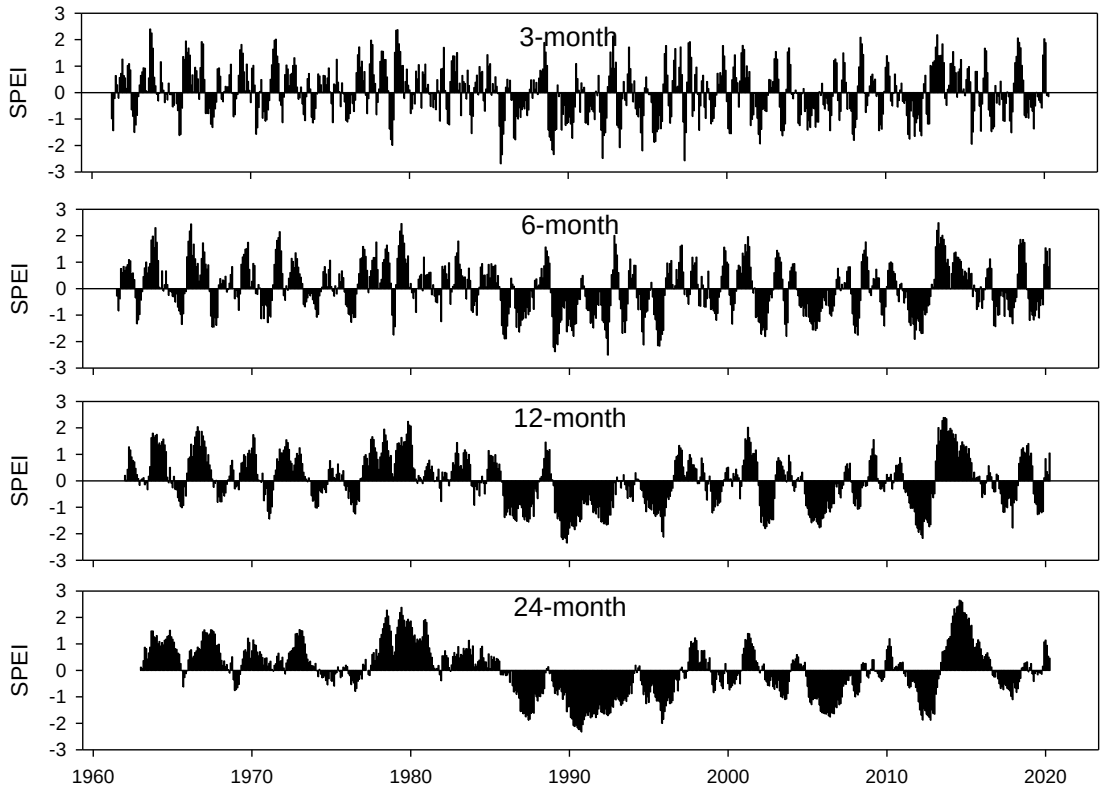

Figure 31: Evolution of climate droughts in the Yesa basin based on SPEI computed at time scales of 3-, 6-, 12- and 24-month.

3.10. Links between meteorological and hydrological droughts

Figure 32 shows the evolution of the SSI between 1962 and 2020, calculated using different hydrological data. Similar to SPEI evolution, the water inflows into the Yesa reservoir showed generally wetter conditions during the 1960s and 1970s, and more severe droughts in the early 1990s and between 2005 and 2020. Relative to SPEI, it seems that hydrological droughts exhibits higher interdecadal variability and a stronger negative trend over the concurrent period of record. A similar pattern was observed for the Yesa reservoir storage. Large important negative anomalies were recorded at the beginning of the 1990s and during the 2000s. A reversed pattern was observed for the water released to Bardenas channel during the 2010s, despite the pre-dominantly negative anomalies in the Yesa reservoir storage. In accordance with other hydrological data, the SSI computed downstream of the Aragón River showed a clear decreasing trend from the 1960s to 2020. Thus, from 1990 negative SSI anomalies are clearly dominant. These negative anomalies are much more accentuated and persistent than those identified from the inflows to the Yesa reservoir.

To further explore links between climatic and hydrological droughts, we computed the correlation between SPEI and SSI. Results demonstrate varying responses of hydrological variables to climate drought, which seem to be strongly related to water management in the basin (Figure 33). As illustrated, the inflows to the Yesa reservoir showed the highest correlation with climatic drought at the 2-month timescale. In contrast, reservoir storages generally exhibited lower correlations with climatic drought. The highest correlations were recorded at the 6-month timescale. Figure 33a reveals that the dependency between climatic drought and both inflows in Yesa reservoir and reservoir storages showed similar patterns at the different timescales, albeit with quite lower correlations with reservoir storages. Figure 33a also shows low correlations between hydrological drought in the Bardenas channel and

climatic drought, with values generally below 0.4. This weak association is evident for all timescales. These general correlations vary considerably on the monthly scale (Figure 33b). Specifically, inflows showed high correlations with SPEI during all months, but with a stronger association in the period from September to May. Reservoir storages exhibited stronger correlations with SPEI from October to February and in July and August. However, this dependency seems to be more sensitive at longer time scales (10-15 months) during summertime. The sensitivity of SSI to SPEI indicated high seasonality downstream of the Yesa reservoir, with higher dependency between December and March and low dependency during summer months. As opposed to other hydrological variables, it seems that hydrological droughts in the Bardenas channel shows weaker response to climatic droughts, irrespective of the season. Exceptionally, in some years (e.g. 1990, 2003 and 2005), the channel flow was strongly constrained by climate drought events (refer to Figure 3). In these three years the reservoir storages were reduced and they were not sufficient to supply the channel at the normal level. This pattern is not identified in all drought events. In 2013 a severe drought event produced low inflows and reservoir storages, but the SSI of the Bardenas channel only recorded small negative anomalies during a few months of the year. On the contrary, the releases to the Aragón river, downstream of Yesa, showed the largest negative values during the 2013 drought.

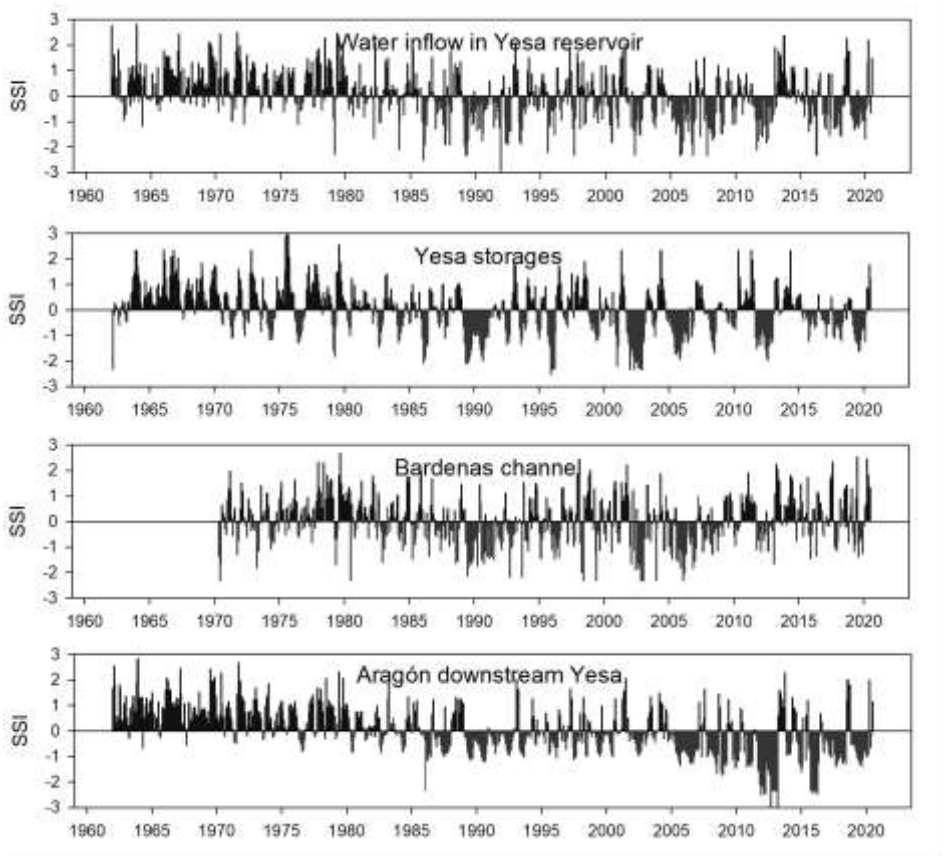

Figure 32: Evolution of hydrological drought, as revealed by SSI, computed for the period 1962-2020. SSI was calculated using water inflows, reservoir storages, Bardenas channel flow and the Aragón River downstream the Yesa reservoir.

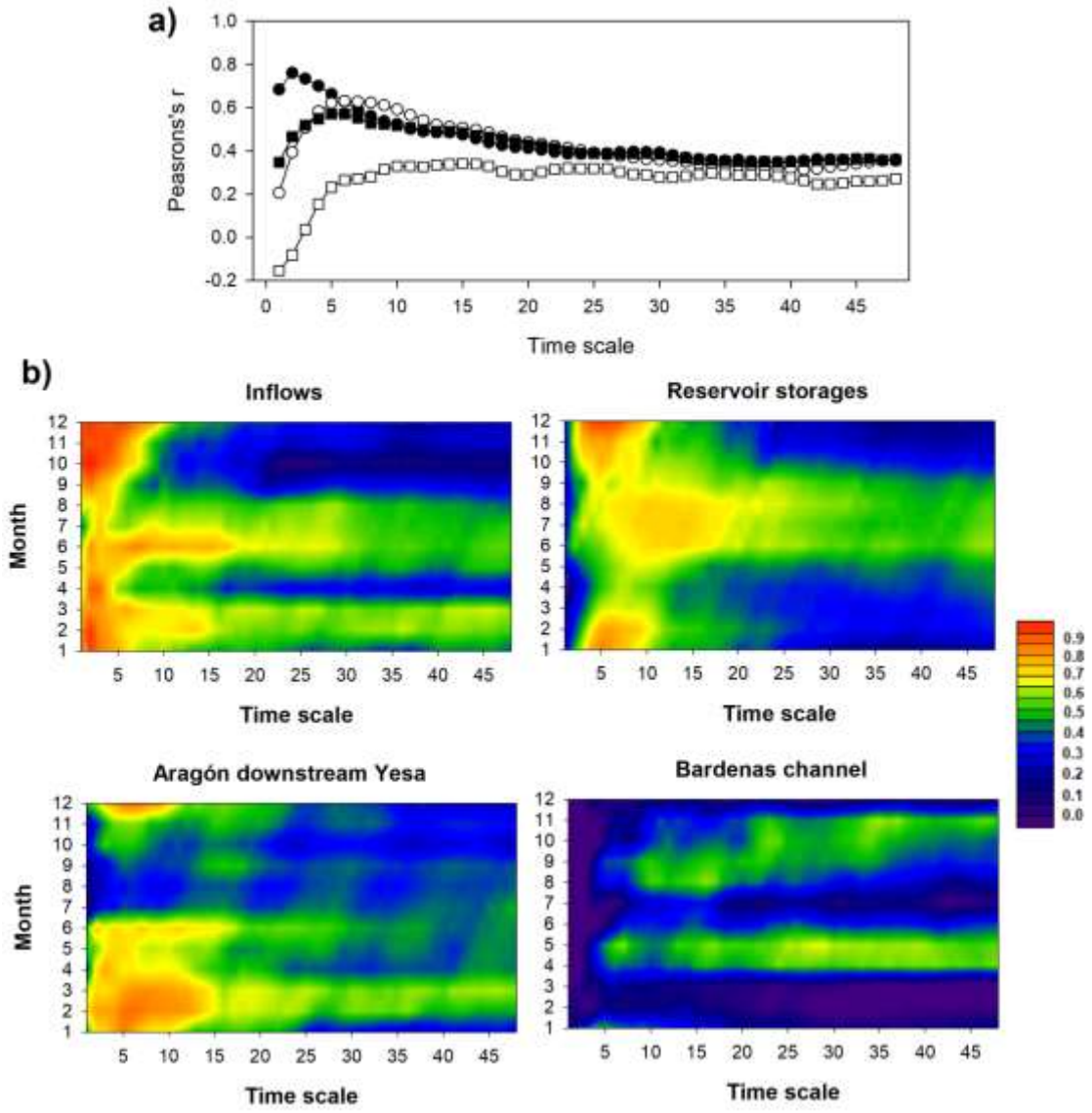

Figure 33: a) Pearson's r correlations between climatic drought (as defined using SPEI at 1- to 48-month timescales) and hydrological drought (as represented using SSI computed for the four hydrological variables). . Black circles: Yesa inflows, White circles: Reservoir storages, Black squares: Releases to the Aragón river downstream Yesa, White squares: Bardenas channel, b) same as panel a, but considering correlations at monthly scale. Significant correlations are set at Pearson's r = +/-0.25 ($p < 0.05$, two-tailed), for inflows, reservoir storages and the Aragón flows downstream Yesa and at Pearson's r = +/-0.27 ($p < 0.05$, two-tailed), for the Bardenas channel.

An inspection of these Figures illustrates that the slightly dry climate conditions between 2015 and 2020 coincided with pre-dominantly negative anomalies of reservoir inflows, positive anomalies in the Bardenas channel, and strongly negative anomalies in the Yesa releases to the Aragón River. This behavior is illustrated in Figure 34, which indicates that severe climate drought conditions, as represented by a return period of one event on average per 20 years, corresponded to negative anomalies in the flow of the Bardenas channel during the warm season (MJJAS). Rather, climatic drought showed relatively less impact on the releases to the Aragón River. Reservoir storages are also constrained by severe drought conditions in summer

months. The situation is different during the cold season (ONDJFMA) since the inflows/outflows to/from the Yesa reservoir are more affected by drought severity than the anomalies in reservoir storages and the flows of the Bardenas channel, which show high spread with drought severity. Figure 34 also shows that hydrological droughts downstream of the Aragon River are more sensitive to drought severity during the warm season, with notable variability in response to mild, moderate and extreme drought events.

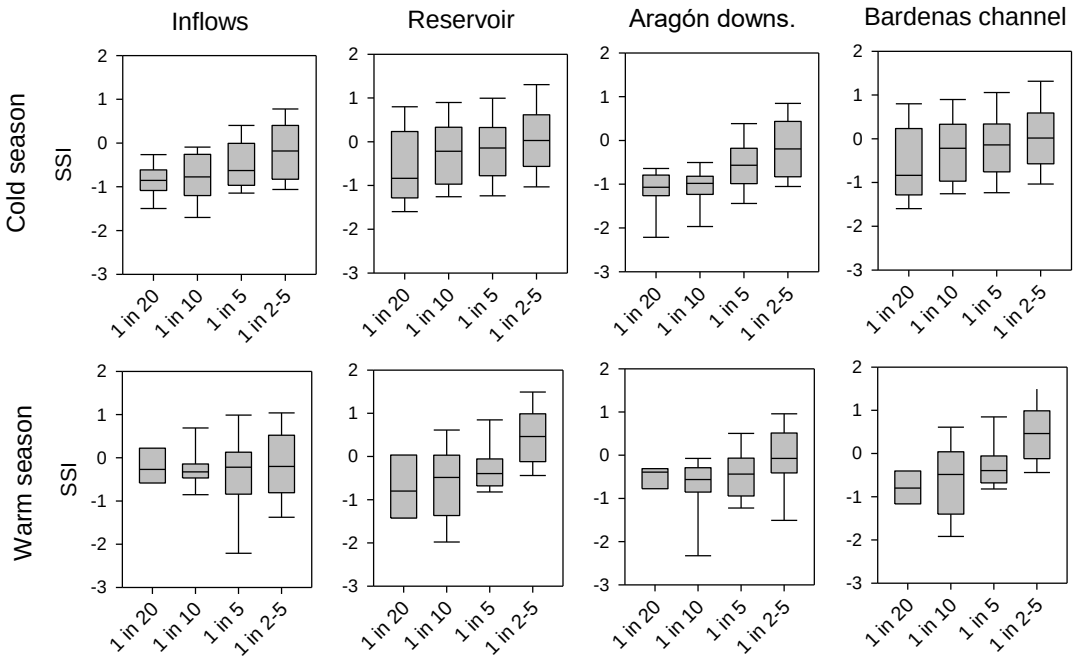

Figure 34: Boxplots showing the values of SSI corresponding to the different climatic drought severities, as represented by return periods. Herein, results are presented only for drought timescales at which the different hydrological variables showed the best correlation (refer to Figure 4). Warm season (MJJAS): Inflows (2-month); Reservoir storages, outflows and Bardenas channel (14-month); Outflows (14-month); Cold season (ONDJFMA): Inflows (2-month); Reservoir storages; outflows and Bardenas channel (8-month. The central solid line indicates the median. The whiskers represent the 10th and the 90th, while the 25th and the 75th are plotted as the vertical lines of the bounding boxes.

To assess the impacts of climatic drought on groundwater, we correlated the piezometric levels across the study domain with SPEI. As illustrated in Figure 35-a, the most anomalous drought events, which were recorded in 2005, 2012 and 2017, corresponded to a notable decline of piezometric levels. Figure 35-b reveals a strong seasonality in the response of groundwater to the climatic drought variability. Specifically, the highest correlations were found for April, May and October, while a weak response was noted during wintertime. Similarly, winter snow depth in the study domain showed a strong interannual variability (Figure 36), which can partly be linked to drought occurrence and severity. Results demonstrate that snow depth between January and April is highly correlated with SPEI at 4-6-month timescales (Figure 37).

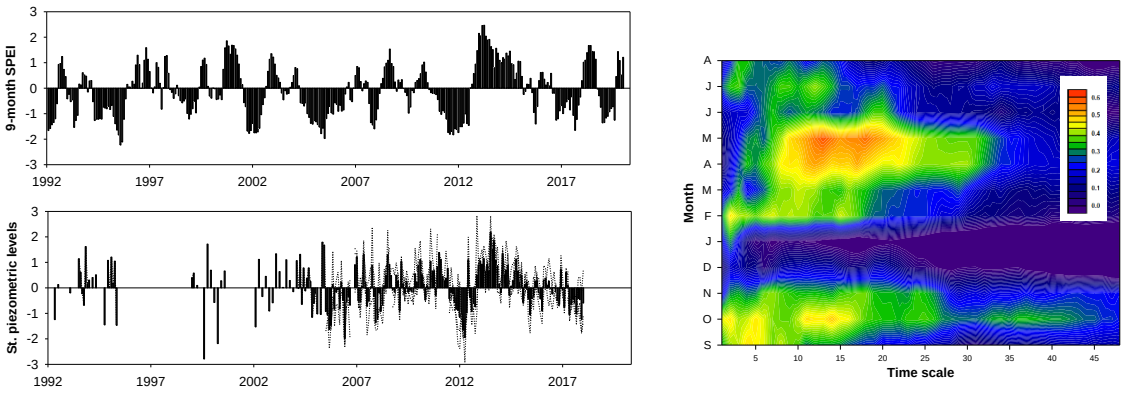

Figure 35: Left: Evolution of both SPEI at 9-month timescale and the standardized piezometric levels. Right: Monthly Pearson's r coefficients calculated between the mean standardized piezometric levels and SPEI at 1- to 48-month timescales.

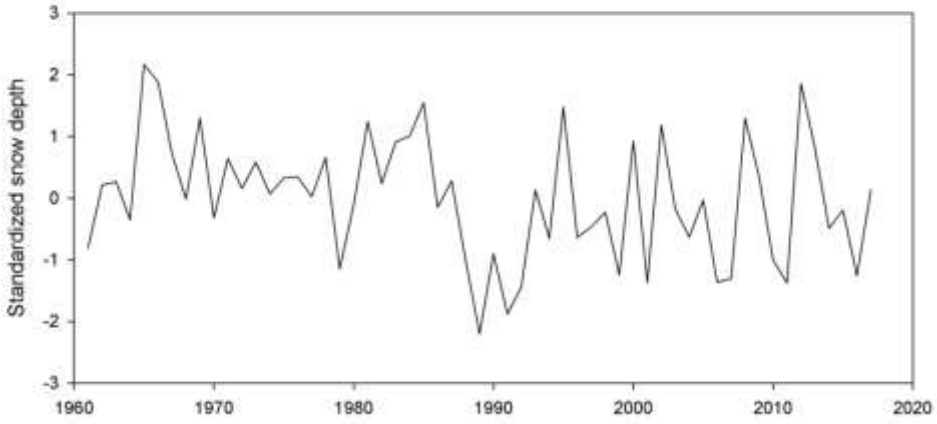

Figure 36: Evolution of the standardized December-April snowpack in the Aragón basin from 1961 to 2017

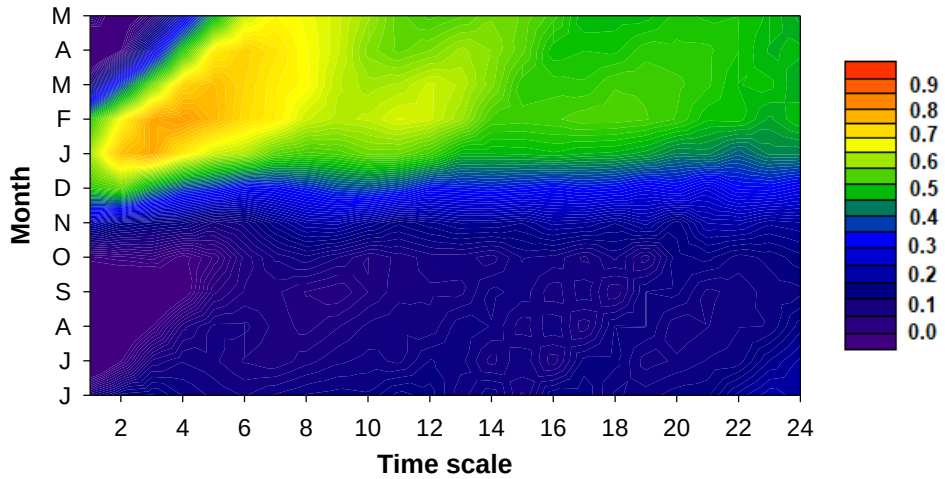

Figure 37: Monthly Pearson's r coefficients calculated between snow depth over the period December-April and SPEI at 1- to 24-month timescales.

3.11. Drought impacts on vegetation activity

Figure 38 depicts correlations between the EVI2, as a proxy of vegetation cover, and SPEI at 1- to 48-month timescales. Results suggest that the correlation is seasonally dependent, with remarkable differences among seasons and land cover types. Notably, vegetation activity in the upper Aragón basin is mostly impacted by climatic drought during summertime, especially at both 2- to 8-month and 20- to 24-month timescales. This dependency was less evident for other periods of the year.

The differences between land cover types were also important (Figure 38). In particular, coniferous forests showed weaker response to drought variability, compared to shrubs and crops that were highly sensitive to SPEI at 2- to 5-month timescales during June and July. Interestingly, results reveal that spring pastures, mainly located in the bottom valleys, were more sensitive to climatic drought than mountainous summer pastures (> 1600 m.a.s.l.). A similar pattern was also found for different forest species. A representative example is *P. sylvestris,* which showed higher sensitivity to climatic drought than *P. uncinata (mainly located* above 1600 m a.s.l.). In the same context, apart from long SPEI timescales during summer, *F. sylvatica* (located in humid sites and N-NW-facing slopes) exhibited low sensitivity to climatic droughts. Figure 38 also indicates that the mixed forest (mostly forests of *Q. faginea* and *P. sylvestris*) showed mixed responses. Figure 40 shows that –regardless of the dominant land cover type- there is a significant association between EVI2 and SPEI over large areas of the basin during summertime. However, a more detailed assessment of this dependency using an improved grid resolution of Sentinel-2 images (from 500 to 10 m) suggests considerable spatial differences over the basin. In particular, it seems that this spatial variability is driven largely by terrain exposure and topographical gradient. This has been evident for the three years investigated using Sentinel-2 images, although drier conditions were found in 2019, compared to 2017 and 2018 (Figure 40).

3.12. Drought impact on forest growth

An assessment of the tree-ring growth variability in the study domain reveals considerable differences among the dominant tree species (Figure 41). This is reflected in the varying responses of these species to climatic drought variability. These differential responses among the forest species are highly coherent with those observed using EVI2 data, albeit with lower correlations. Results demonstrate that tree-ring growth in the forests of the Upper Aragón basin show better association with climatic drought at 3- to 5-month timescales in August, as well as 15-20 month timescales during summer months (Figure 42). Interestingly, the forest types located at low elevations and drier areas (e.g. *P. nigra* and *Q. faginea*) showed stronger dependency on climatic drought than forest species situated in the most humid areas and at high elevation sites (e.g. *A. alba, F. sylvatica* and *P. uncinata*). Rather, *P. sylvestris* indicates an intermediate response between these two groups of species. Overall, regardless of the tree species, it is clearly evident that forest growth is more impacted by climatic drought during summer. Figure 43 summarizes forest growth anomalies in response to drought events of different severities. It is evident that a clear gradient in the negative anomalies of forest growth in response to drought severity exists, with forest growth reducing largely during most severe drought events (i.e. 1 event in 20 years). A comparison between the different tree species reveals that *P. uncinata* is mostly insensitive to drought variability. In contrast, species of more humid habitats (e.g. *A. alba* and *F. sylvatica*) showed less dependency on climatic drought variability. However, even the growth of those species is impacted notably by climatic drought during extreme drought episodes.

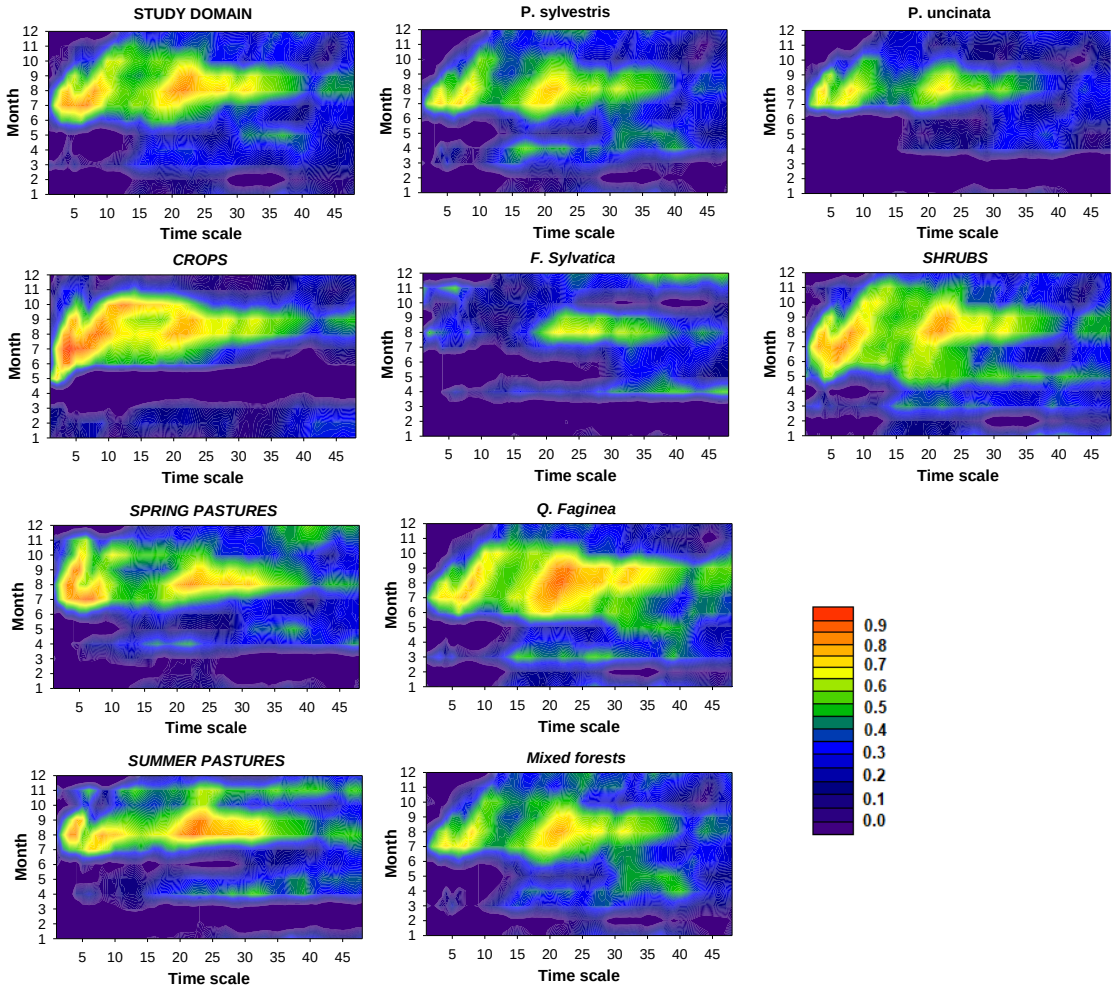

Figure 38: Monthly Pearson's r coefficients between the values of EVI and those of SPEI 1- to 48-month timescales for the dominant land cover types of the upper Aragón basin.

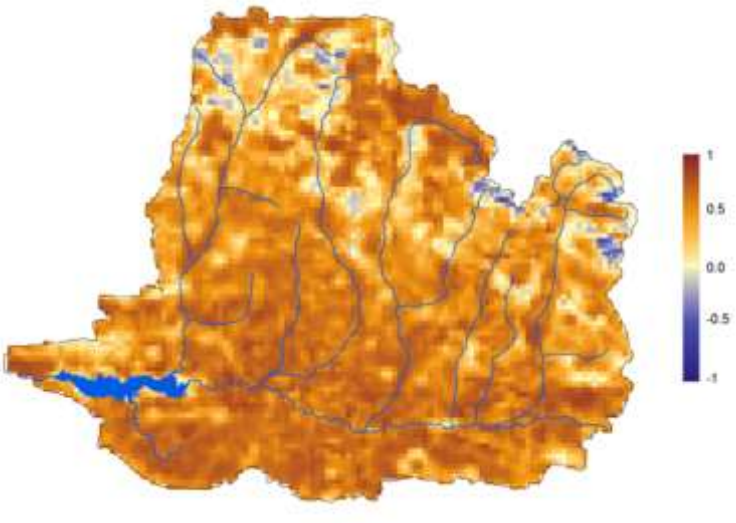

Figure 39: Spatial distribution of the Pearson's r correlations between the SPEI 6-month timescale and the EVI in July.

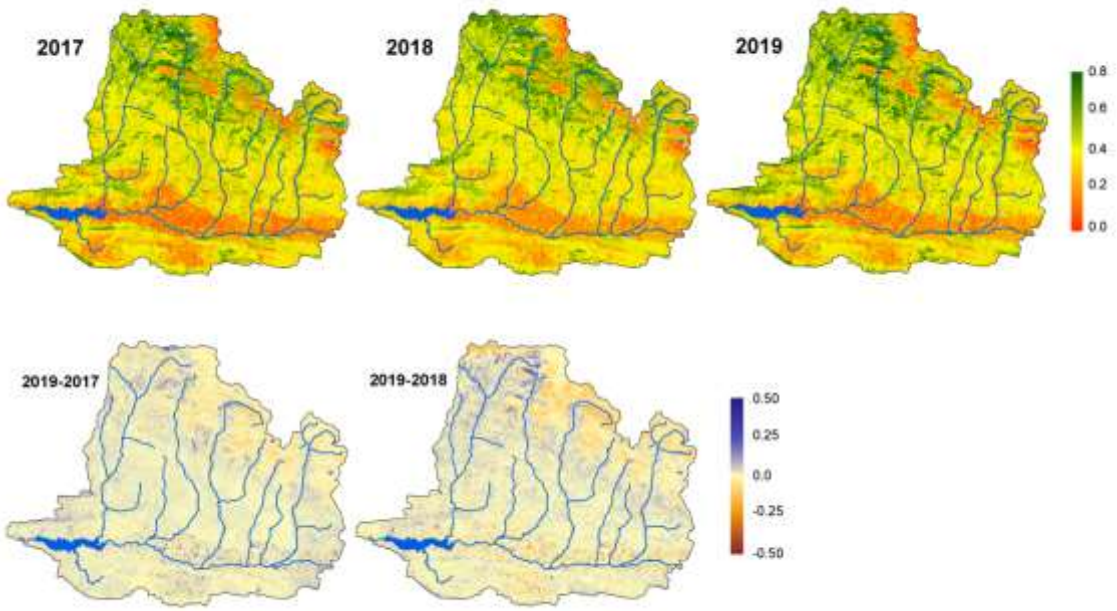

Figure 40: Top: Monthly values of the EVI in July 2017, 2018 and 2019 based on the Sentinel-2 satellite. Bottom: Differences between the EVI values in the years 2019 and 2017, as compared to the differences between 2019 and 2018.

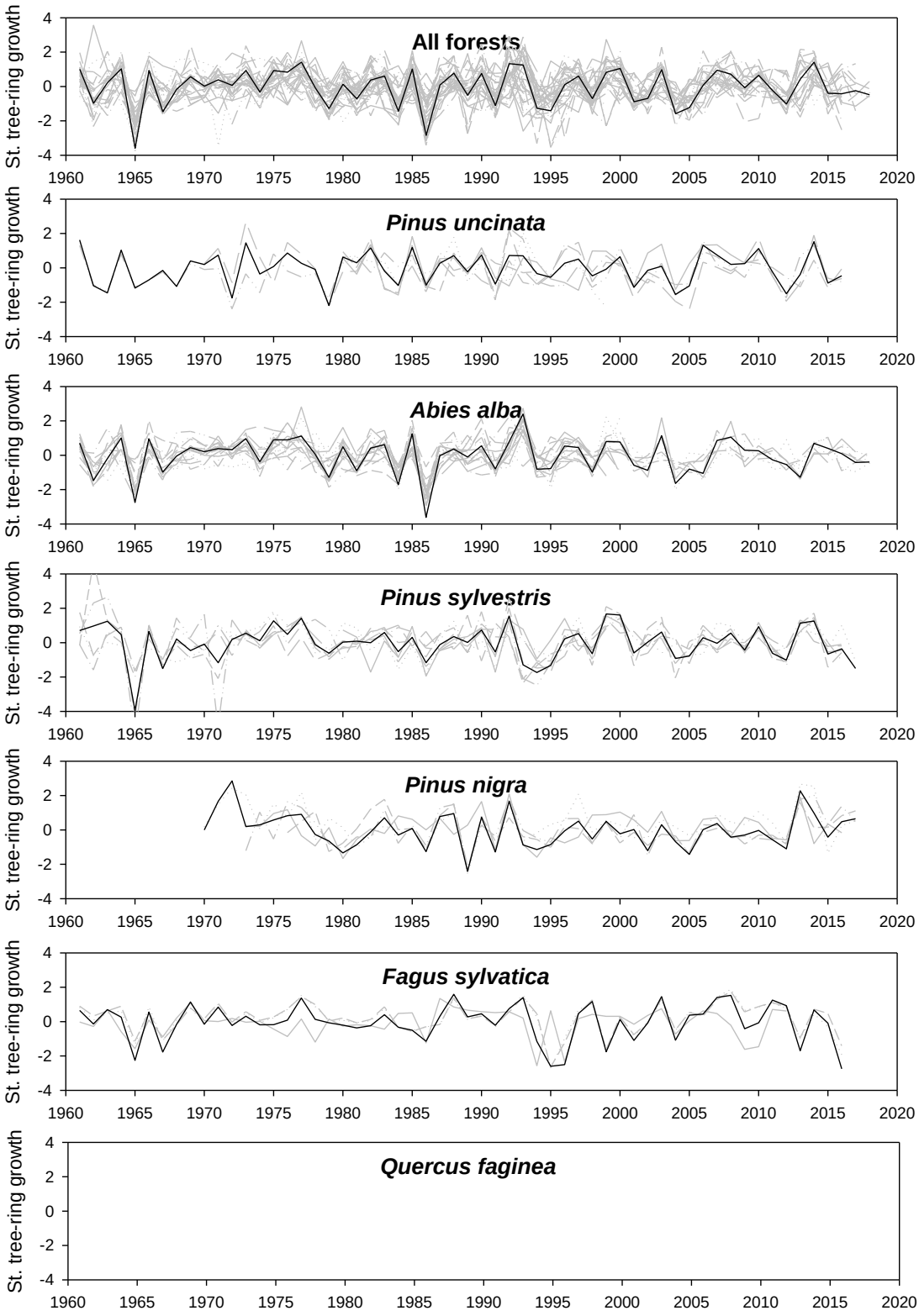

Figure 41: Evolution of the tree-ring series of the different forest species. Gray: the different forest chronologies; and black: the average of the series.

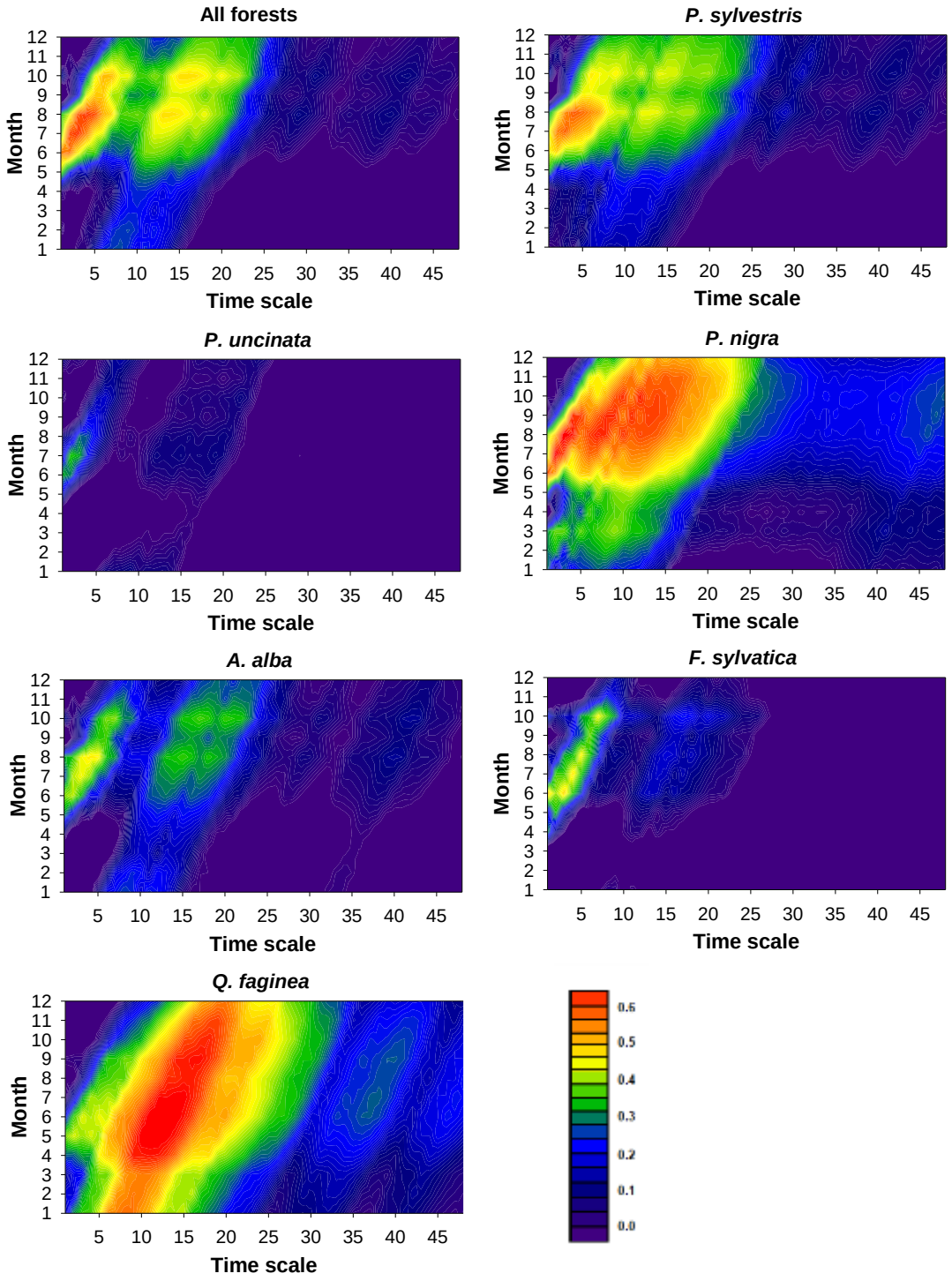

Figure 42: Monthly Pearson's r coefficients between the values of the annual tree-ring growth and those of SPEI 1- to 48-month timescales for the dominant land forest species of the upper Aragón basin.

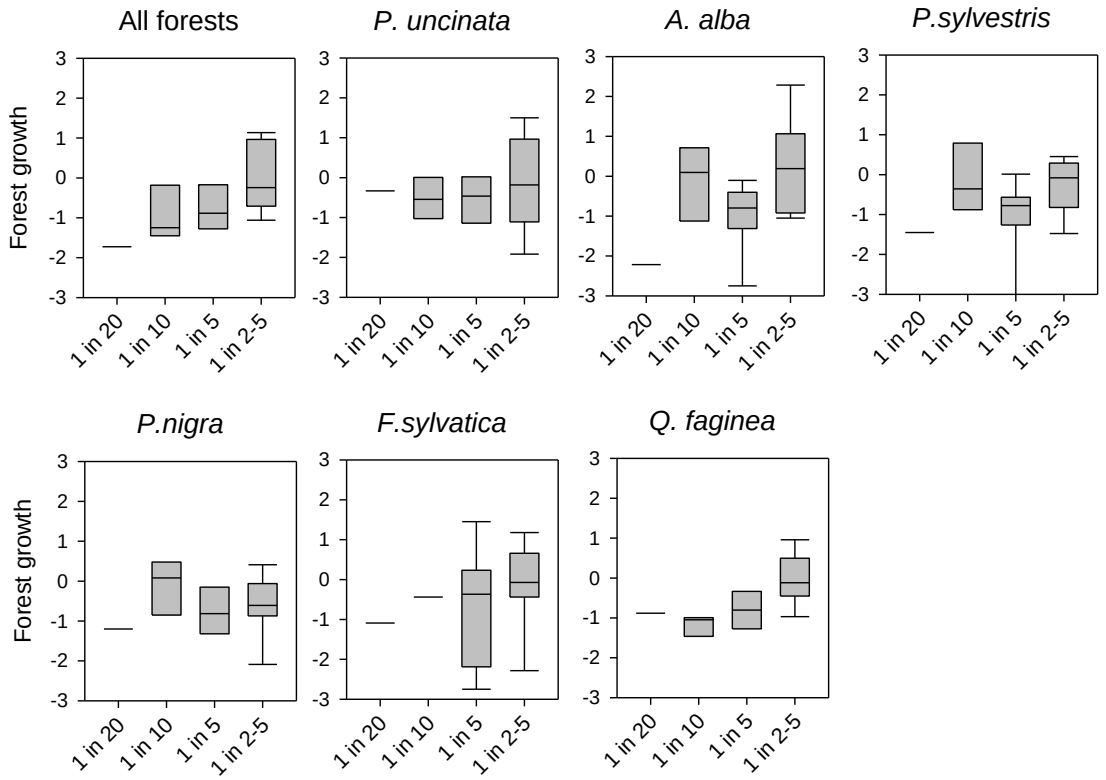

Figure 43: Boxplots showing the standardized values of forest growth, as a function of the different drought severity thresholds (return periods). Herein, results are presented only for monthly SPEI timescales that showed the highest correlation with forest growth, as illustrated in Figure 9. All: 3-month in July; P. uncinata: 2-month in July; A. alba: 4-month in August; P. sylvestris: 4-month in August; P. nigra: 3-month in August; F. sylvatica: 1-month in June; and Q. faginea: 14-month in June. The central solid line indicates the median. The whiskers represent the 10th and the 90th, while the 25th and the 75th are plotted as the vertical lines of the bounding boxes.

3.13. Drought impacts on plant phenology

The effect of drought on plant phenology is clearly visible although less seasonally distinct in as compared to those found for vegetation activity or forest growth. Correlations were found to be significant considering the onset of the growing season, which tends to advance in response to dry events. Notably, the highest correlations were found for the integral of the whole growing season (Figure 44). Nonetheless, this dependency varies considerably over space (Figure 45) and as a function of the different land cover types (Figures 46-50). The integral of the growing season is more sensitive to climatic drought in shrubs and *Q. faginea* forests, which are usually located in low elevated areas. Rather, the onset of the growing season and the total length of the active period seem to be more impacted by drought in areas where summer pastures dominate.

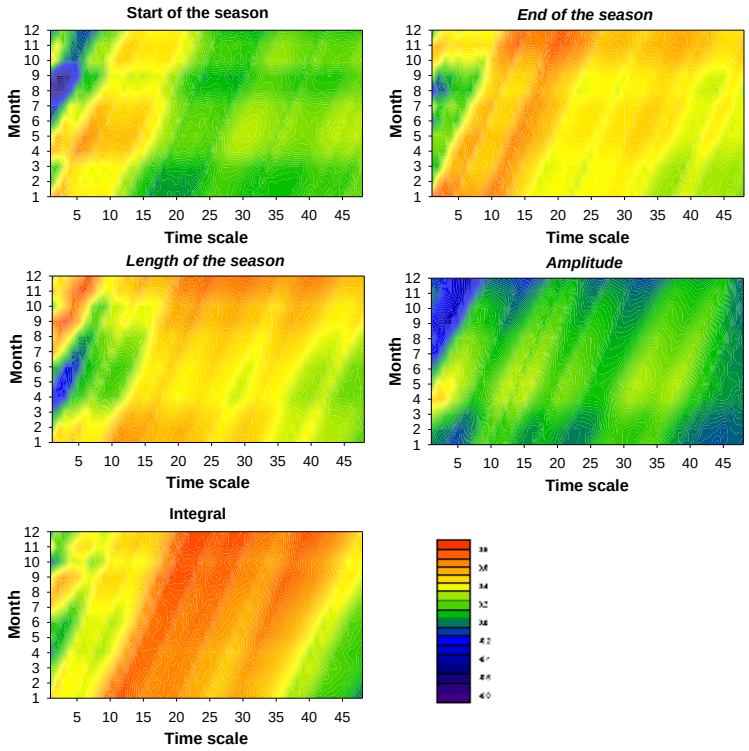

Figure 44: Monthly Pearson's r coefficients between different metrics of plant phenology and SPEI 1- to 48-month timescales averaged for the whole upper Aragón basin.

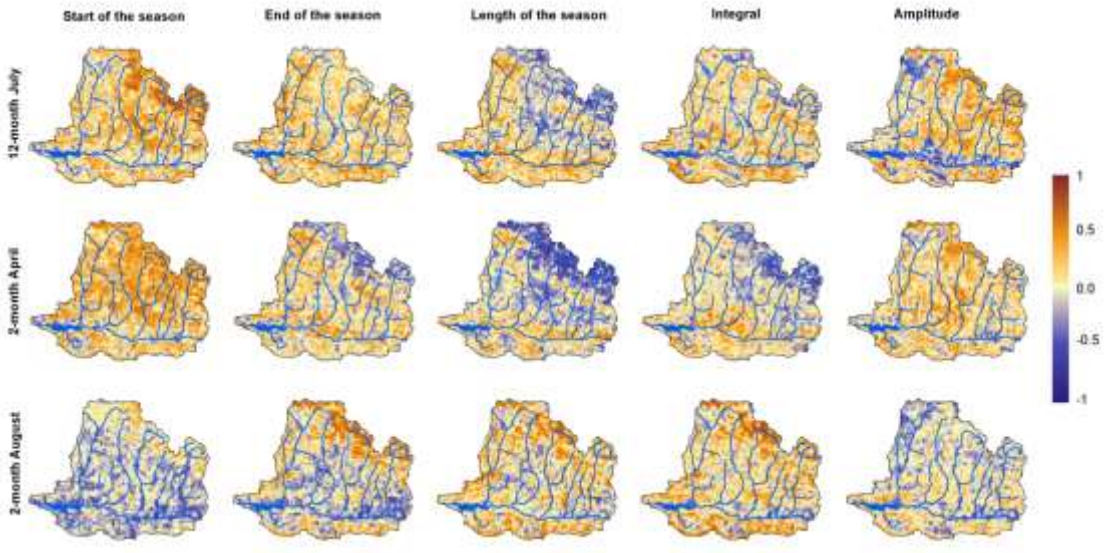

Figure 45: Spatial distribution of the correlation coefficients between the annual values of different metrics of plant phenology and SPEI at selected months and timescales

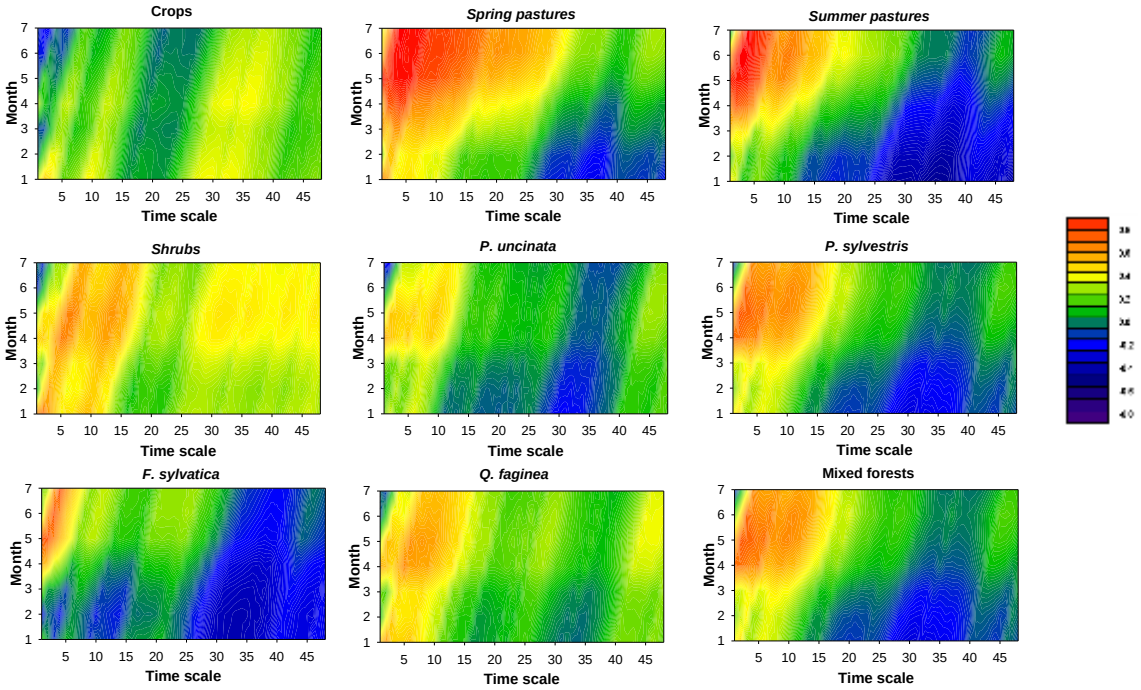

Figure 46: Pearson's r correlations between the monthly series of the SPEI and the date of start of the vegetative season in the main land cover types in the Aragón basin.

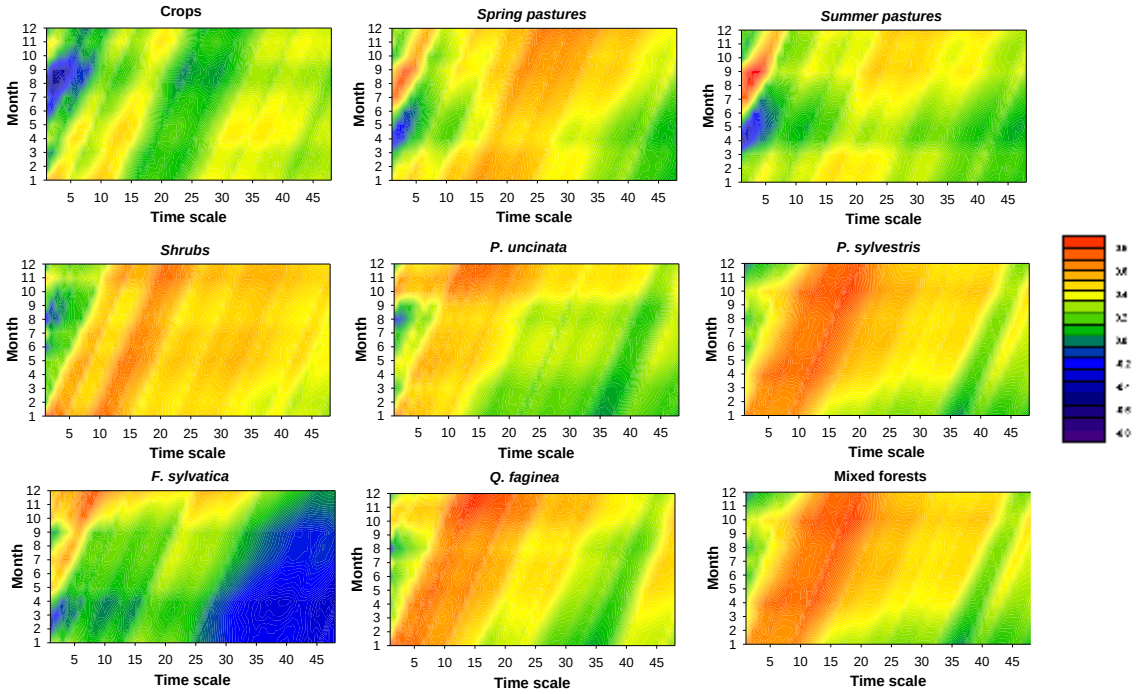

Figure 47: Pearson's r correlations between the monthly series of the SPEI and the date of end of the vegetative season in the main land cover types in the Aragón basin

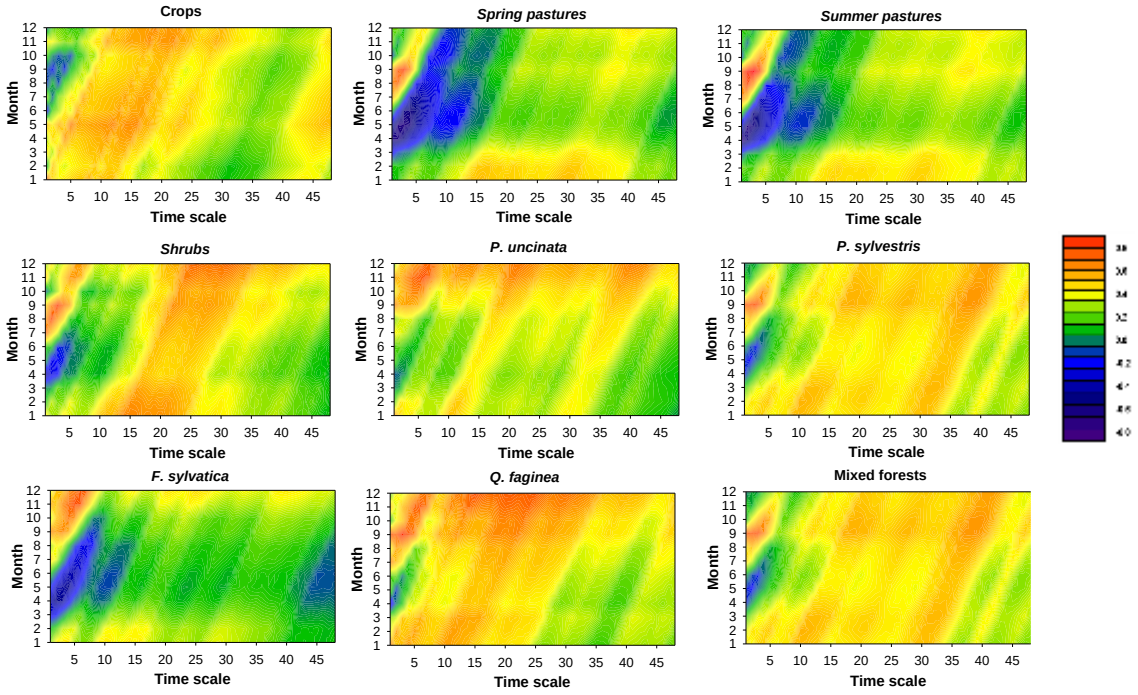

Figure 48: Pearson's r correlations between the monthly series of the SPEI and the length of the vegetative season in the main land cover types in the Aragón basin.

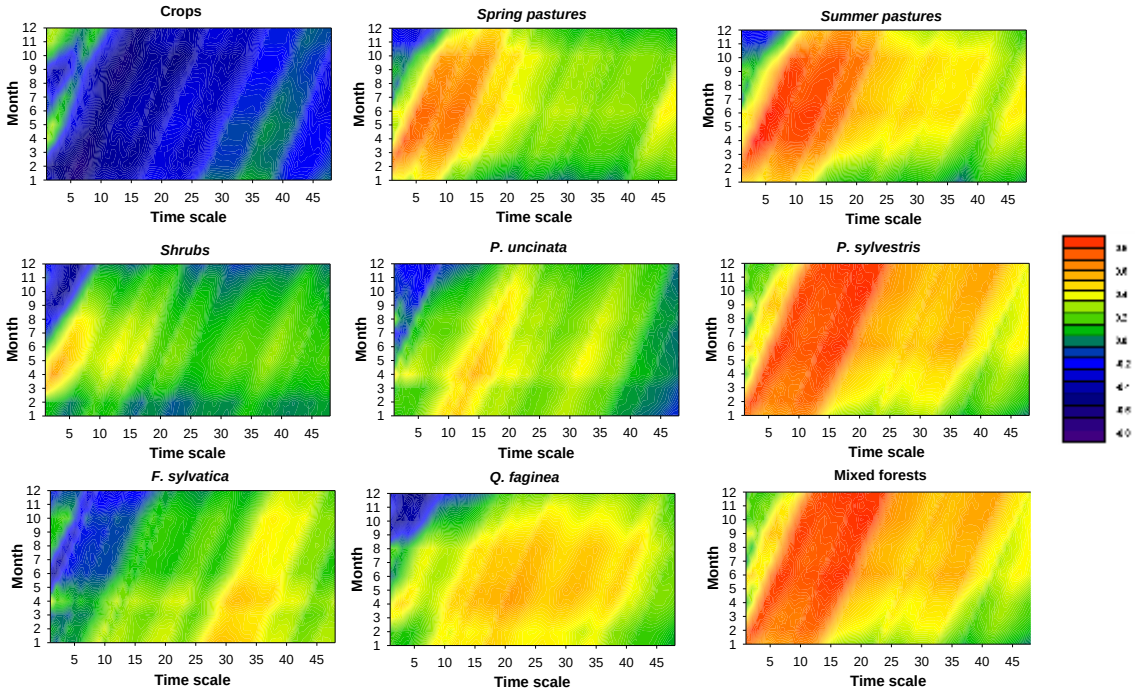

Figure 49: Pearson's r correlations between the monthly series of the SPEI and the amplitude of the vegetative season in the main land cover types in the Aragón basin.

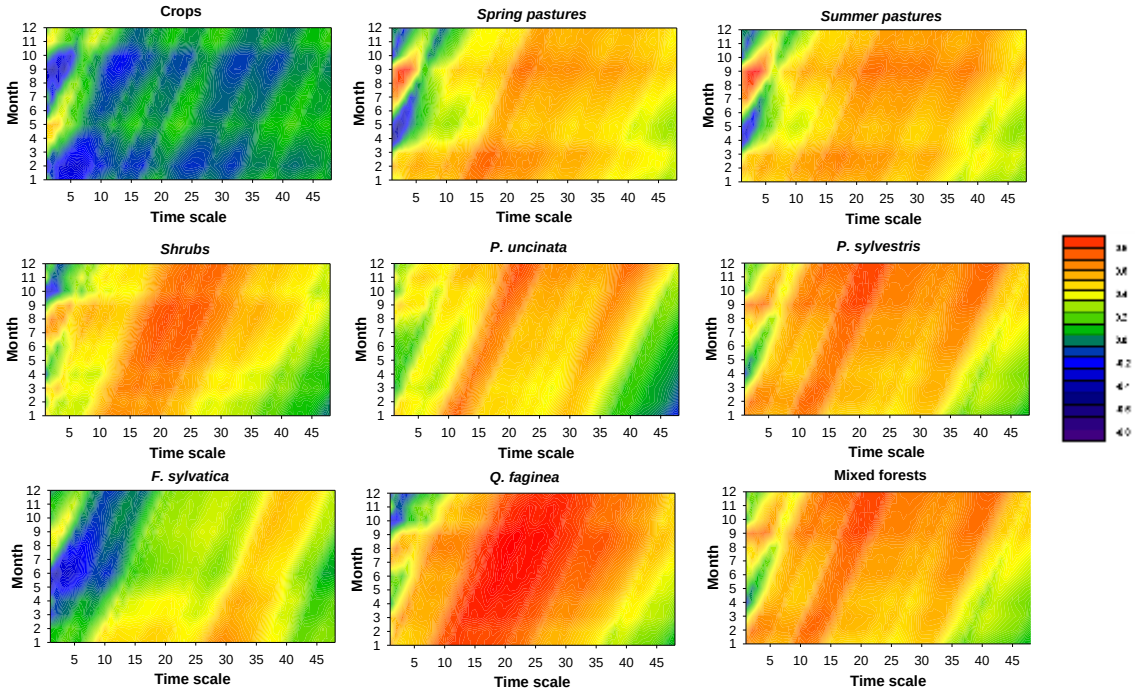

Figure 50: Pearson's r correlations between the monthly series of the SPEI and the integral of the vegetative season in the main land cover types in the Aragón basin.

4. Conclusions

In Germany, the 2018–2019 drought which partly extended into 2020 was the most severe in Central Europe for centuries – probably for more than 2110 years (Büntgen et al. 2021). Hari et al. (2020) ranked the 1949–1950 drought second in a screening of two-year events over the last 250 years, and it seems one has to go back to the first half of the 16th century to find heat and drought of comparable magnitudes in this region (Brázdil et al. 2020, Büntgen et al. 2021, Orth et al. 2016, Wetter et al. 2014). The impacts on natural ecosystems were locally substantial (depletion of water resources, fish kill, withered vegetation, wildfires, outbreak of bark beetles). However, the sector-wise assessment of economic impacts showed significant effects only for the agricultural and forest sectors, the former principally essential as basis for food production, the latter *inter alia* important for biodiversity and climate protection – but even a combination of both with a one-percent contribution to the total gross value added of all economic activities in the GEB practically irrelevant for general welfare.

Overall, this report stresses that drought impacts in the Aragon basin vary considerably among the different hydrological and environmental and agricultural subsystems. These differences can also be further enhanced by the strong diversity of hydrological regimes, forest types and tree species, and land cover types. This complexity makes it difficult to characterize, monitor, and mitigate the adverse impacts of drought in the study domain. This concurs with earlier studies that indicated that the components of the hydrological cycle (e.g. soil moisture, streamflow, groundwater) can respond differently to precipitation deficits (Changnon et al., 2007; McKee et al., 1993). These natural differences in the hydrological response can be one of the main reasons to explain the strong diversity of the multi-sectorial drought impacts in our study domain since we have identified different responses to drought time scales between streamflow and reservoir storages. This strong dependency was confirmed in some earlier studies covering the study basin (e.g. Vicente-Serrano and López-Moreno, 2005).

In the Aragon basin in Spain our results indicate that hydrological drought, represented by SSI using different hydrological variables, is highly correlated with climatic drought using SPEI. This implies that the occurrence of extreme drought events has an important role in explaining water deficits in the basin. As expected, snow cover, streamflow, and groundwater showed a clear response to climatic drought variability in the basin. However, groundwater responded to drought at longer timescales than did streamflow and snow depth. This behavior can simply be seen in the context that groundwater droughts are characterized generally by their slow dynamics and delayed response to climatic drought. This agrees with the findings of Bloomfield et al. (2015), Lorenzo-Lacruz et al. (2017), and Marchant and Bloomfield (2018).

It should be stressed that although water resources are strongly impacted by climatic drought variability in the upper Aragón basin, human management and practices are dominant factors controlling hydrological drought severity downstream. Different studies concluded that human management and water demands strongly alter the response of hydrological droughts to climate variability (e.g. López-Moreno et al., 2009; Tijdeman et al., 2018; Vicente-Serrano et al., 2017; Xu et al., 2019). In the upper Aragón basin, the Yesa reservoir determines considerably the response of hydrological droughts downstream. This is mainly because the Yesa reservoir has an accumulation capacity of almost 446 Hm^3, which reduces the sensitivity of the reservoir storage to high variability of climatic drought severity. Thus, it is expected that the Yesa reservoir will only respond to climatic drought at longer time scales. A different behavior is found for streamflow and snow depth, which respond to climatic drought at shorter timescales, with a seasonally dependent response. The stronger response of reservoir storage anomalies to climatic droughts in the basin during summer months stresses the need

for reliable water management practices to secure water transfers to the irrigated lands of Bardenas, although water releases to the Aragón river downstream Yesa are strongly reduced (López-Moreno et al., 2004).

Reservoir management reduces the sensitivity of the Aragón flows downstream the Yesa reservoir to climatic drought variability. A similar role can also be observed in the flow anomalies recorded in the Bardenas channel. This indicates that the management practices of the Yesa reservoir contribute significantly to the degree of hydrological drought severity downstream since they priorise the water releases to the Bardeas channel. For example, there were minimal effects of the severe drought recorded in 2013 on the flows of the Bardenas channel. However, the Yesa reservoir is important from seasonal perspective. In particular, the reservoir releases to the Aragón River basin responds to climatic drought variability only during winter, given that water demands in the Bardenas area are low and managers release all inflow downstream except the needed amount to progressively fill the reservoir storage capacity. In summer, the response of hydrological droughts downstream to climate variability is minimized because managers of the dam must satisfy the environmental flow assigned to the Aragon river by the Ebro basin authorities (López-Moreno et al., 2004). These alterations in the severity and frequency of hydrological droughts in the downstream reaches have already been identified in other catchments, especially with reservoir management for hydropower (López-Moreno et al., 2009; Morán-Tejeda et al., 2012; Nakayama and Shankman, 2013) and irrigation management (Vicente-Serrano et al., 2017; Zhang et al., 2009). Nevertheless, this study shows that although efforts should be oriented towards reducing the negative anomalies of water transfers to the Bardenas area, the reservoir storages historically witnessed drastic reductions (e.g. 1990, 2003 and 2005), as a consequence of extreme drought events. This situation induced a decline in the necessary channel flows into the basin downstream, with important socioeconomic impacts. This indicates that although hydrological management of the basin can alter the response to climatic droughts, these practices cannot completely mitigate these effects. This is particularly likely during the most extreme dry events, which have consequences in the Aragón river downstream Yesa reservoir and also reduce the water transfers by the Bardenas channel.

We have found a variety of drought impacts on the activity and growth of natural vegetation in the basin. This may be related to the presence of different vegetation types, with various cycles and resistance to water deficits, combined with differences in the average climatic conditions. Different studies discussed the mechanisms and strategies the vegetation adopts to cope with water deficits (e.g. Allen et al., 2010; Chaves et al., 2003; Sperry and Love, 2015; Vose et al., 2016). Thus, local site conditions (topography, soil depth, forest composition and structure, management) and species physiological traits seem to be key factors that determine the resistance and resilience of natural vegetation to drought (Anderegg et al., 2019, 2016; Peguero-Pina et al., 2011). In general, our study found strong impacts of climatic drought on vegetation activity, as revealed by EVI2, and to a lesser extent by tree-ring growth. This finding contradicts previous works in Spain, which suggested greater sensitivity to drought in terms of radial growth than the photosynthetic activity quantified by the Normalized Difference Vegetation Index (NDVI) (e.g. Gazol et al., 2018; Marina Peña-Gallardo et al., 2018). Nevertheless, we must stress that this study employed a different vegetation index i.e., the EVI2. As compared to NDVI, EVI2 is less affected by the possible saturation of the signal under very dense vegetation coverages (Giner et al., 2012; Huete et al., 2002), which could suggest a higher response to drought variability. Moreover, the length of the EVI2 series used in this study is still short and limits comparability with long-term data of tree-ring data (20 vs. 60 years, respectively). Nevertheless, although there are important differences in the response of vegetation types to climatic drought, we found two peaks of response to SPEI from the EVI and the tree-ring growth data: at short time scales but also longer timescales, characteristics of a

two year period in summer. This suggests that drought conditions over the previous year could affect vegetation growth and activity during the following year given the role of nonstructural carbohydrate reserves (Babst et al., 2014a, 2014b; Richardson et al., 2013; Skomarkova et al., 2006).

The forest types located in the drier and warmer locations (e.g. *P. nigra* and *Q. faginea*) showed a stronger response to climatic drought than forests of colder and more humid climates (e.g. *P. uncinata, F. sylvatica,* and *A. alba*). Humid forests are located in areas with water surplus (precipitation-evapotranspiration), which frequently generate runoff. This makes soil moisture almost sufficient for vegetation growth and activity, irrespective of precipitation deficit. In contrast, low elevation forests (e.g. *P. nigra* and *Q. faginea*) tend to receive lower amounts of precipitation, with enhanced atmospheric evaporative demand (Tomas-Burguera et al., 2019). This would explain the higher sensitivity of forest species at low elevations to climatic drought variability. Interestingly, in the upper Aragón basin, humid forest species showed a significant response to severe droughts. Different studies have suggested that resistance and resilience of vegetation types to drought varies strongly as a function of the regional and local climate conditions (e.g. Anderegg et al., 2016; Gazol et al., 2018, 2017; Pasho et al., 2011). Thus, species from wet sites tend to show low correlations with drought variability and accordingly respond to drought at short timescales (Vicente-Serrano et al., 2014, 2013). This behavior was also identified in the upper Aragón basin. Nevertheless, although the forests of *A. alba* and *Q. faginea* are less impacted by climatic drought variability, they show stronger growth reductions than species from more xeric sites (e.g. *P. nigra* Q. faginea) under severe drought events. This can be seen in the context that species from mesic sites are characterized by their low acclimatisation to water deficits and accordingly they will quickly respond to severe water deficits. This mechanism would explain the higher correlations obtained considering SPEI at short timescales. Numerous studies have stressed a severe forest dieback and mortality in the *A. alba* forests over the western Spanish Pyrenees in response to recent drought events (e.g. Camarero et al., 2015, 2011; Peguero-Pina et al., 2007). Conversely, the higher acclimatisation to water deficits would reduce the impact of drought severity on dry forests. Indeed, the drought threshold could play a major role (Slette et al., 2020) and, accordingly, vegetation from xeric sites could also be highly impacted in the presence of severe drought events.

All these processes and feedbacks stress that drought impacts on natural vegetation can be complex even over a small basin like the study domain. The important vegetation changes recorded in the basin over recent decades, as a consequence of the abandonment of traditional agricultural and livestock activities (García-Ruiz et al., 2015), can also be a source of uncertainty when assessing drought impacts on vegetation. With the exception of mature forests, which cover a small percentage of the total surface of the basin, the majority of the areas of dominant natural vegetation have been affected by different types of vegetation changes. The remaining shrubs have been colonized by conifers (e.g. *P. sylvestris*) (Vicente-Serrano et al., 2006), but there are also advances of oaks in previously colonized *P. sylvestris* forests. Finally, as a consequence of livestock abandonment in summer pastures located above 1600 m.a.s.l., they have been colonized by shrubs and *P. uncinata* (García-Ruiz et al., 2015). All these processes and the results forest encroachement would alter the sensitivity of vegetation to drought and the response to the most extreme drought events.
The response to drought of start and end of season dates, as measured by EVI, was weaker than for other vegetation variables. It should be stressed that it is very difficult to estimate these parameters with high accuracy since the precision in the data is limited by clouds and other disturbances, and phenological shifts are normally only in the order of fractions of a day per year. It also reflects the fact that the Aragon basin is located in a humid and cold region where temperature is the most important limiting factor to vegetation seasonality. In a recent

study at northern European latitudes with predominantly cold climate, start of season showed very low sensitivity to change in precipitation (Jin et al. 2019). On the other hand, the integral of the growing season is an aggregated variable that is less noise sensitive and also more directly related to total net primary production. Natural cycles of vegetation are mostly driven by temperature behavior. For this reason, it is expected that variables like the onset, duration and end of the season show weak relationship with drought variability in the basin. As expected, the integral of the growing season is more linked to drought variability, as this variable is highly dependent on the total net primary production (Carlson and Ripley, 1997) and total vegetation biomass (Cihlar et al., 1991; Nicholson et al., 1990; Tucker and Sellers, 1986). Nevertheless, it is also important to note the important differences found between vegetation types. In any case, longer periods with data availability would be necessary to obtain more robust conclusions on this issue.

This report has also extended available precipitation records for the Boyne catchment to cover the period 1850-2019, providing a detailed view of drought conditions over nearly 170 years in the catchment. We have also employed hydrological models to evaluate the impacts of arterial drainage on drought metrics in the catchment and to extend river flow records to a period concurrent with precipitation observations. Our historical analysis indicates the frequent occurrence of drought in the Boyne catchment and provides a catalogue of drought events derived from the standardised precipitation index and the standardised runoff index. We find limited evidence that arterial drainage impacted drought in the Boyne. We also find evidence for trends in SPI series and drought events themselves, dominated by increasing trends in SPI in winter and decreasing trends for SPI-3 in summer (ie. more drought in summer) over the period of record. We also find an increasing trend in accumulated deficits of SPI-3 droughts, indicating decreasing severity.

In summary, drought variability and severity can have serious hydrological, environmental, and agricultural impacts on both natural and human environments. This multifaceted character of drought can induce strong spatial and temporal complexity when assessing drought impacts. This work identified – for the first time- the complex multisectorial impacts of climatic droughts in different basins of Europe. The impacts of climatic droughts are found to be complex, with different responses not only as a function of hydrological subsystems, vegetation metrics and vegetation types, but also seasonally, over different drought time-scales, and water resources management policies. All these interactive processes and feedbacks make it a challenge to determine and monitor the diverse implications of climatic droughts, especially with the lack of real-time impact data. For this reason, governmental authorities should build their early-warning drought monitoring systems using a variety of climate-based drought indices (Svoboda et al., 2002; Trnka et al., 2020, 2009). However, we stress that the response to climatic droughts can also be strongly diverse, which makes it necessary to comprehensively assess the utility of these drought metrics in terms of real drought impacts before establishing the appropriate drought mitigation strategies. Otherwise, we may misinterpret drought severity in particular systems.

References

Allen, M.R., O.P. Dube, W. Solecki, F. Aragón-Durand, W. Cramer, S. Humphreys, M. Kainuma, J. Kala, N. Mahowald, Y. Mulugetta, R. Perez, M. Wairiu, and K. Zickfeld (2018) Framing and Context. Chapter 1 in: Masson-Delmotte, V., P. Zhai, H.-O. Pörtner, D. Roberts, J. Skea, P.R. Shukla, A. Pirani, W. Moufouma-Okia, C. Péan, R. Pidcock, S. Connors, J.B.R. Matthews, Y. Chen, X. Zhou, M.I. Gomis, E. Lonnoy, T. Maycock, M. Tignor, and T. Waterfield (eds.) Global Warming of 1.5°C. An IPCC Special Report on the impacts of global warming of 1.5°C above pre-industrial levels and related global greenhouse gas emission pathways, in the context of strengthening the global response to the threat of climate change, sustainable development, and efforts to eradicate poverty. Intergovernmental Panel on Climate Change, Geneva. URL https://www.ipcc.ch/site/assets/uploads/sites/2/2019/05/SR15_Chapter1_Low_Res.pdf – Last accessed in May 2021.

Allen, C.D., Breshears, D.D., McDowell, N.G., 2015. On underestimation of global vulnerability to tree mortality and forest die-off from hotter drought in the Anthropocene. Ecosphere 6. https://doi.org/10.1890/ES15-00203.1

Allen, C.D., Macalady, A.K., Chenchouni, H., Bachelet, D., McDowell, N., Vennetier, M., Kitzberger, T., Rigling, A., Breshears, D.D., Hogg, E.H. (T. ., Gonzalez, P., Fensham, R., Zhang, Z., Castro, J., Demidova, N., Lim, J.-H., Allard, G., Running, S.W., Semerci, A., Cobb, N., 2010. A global overview of drought and heat-induced tree mortality reveals emerging climate change risks for forests. For. Ecol. Manage. 259, 660–684. https://doi.org/10.1016/j.foreco.2009.09.001

Anderegg, W.R.L., Klein, T., Bartlett, M., Sack, L., Pellegrini, A.F.A., Choat, B., Jansen, S., 2016. Meta-analysis reveals that hydraulic traits explain cross-species patterns of drought-induced tree mortality across the globe. Proc. Natl. Acad. Sci. U. S. A. 113, 5024–5029. https://doi.org/10.1073/pnas.1525678113

Anderegg, W.R.L., Konings, A.G., Trugman, A.T., Yu, K., Bowling, D.R., Gabbitas, R., Karp, D.S., Pacala, S., Sperry, J.S., Sulman, B.N., Zenes, N., 2018. Hydraulic diversity of forests regulates ecosystem resilience during drought. Nature 561, 538–541. https://doi.org/10.1038/s41586-018-0539-7

Anderegg, W.R.L., Trugman, A.T., Bowling, D.R., Salvucci, G., Tuttle, S.E., 2019. Plant functional traits and climate influence drought intensification and land–atmosphere feedbacks. Proc. Natl. Acad. Sci. U. S. A. 116, 14071–14076. https://doi.org/10.1073/pnas.1904747116

Arzac, A., García-Cervigón, A.I., Vicente-Serrano, S.M., Loidi, J., Olano, J.M., 2016. Phenological shifts in climatic response of secondary growth allow Juniperus sabina L. to cope with altitudinal and temporal climate variability. Agric. For. Meteorol. 217. https://doi.org/10.1016/j.agrformet.2015.11.011

Babst, F., Bouriaud, O., Alexander, R., Trouet, V., Frank, D., 2014a. Toward consistent measurements of carbon accumulation: A multi-site assessment of biomass and basal area increment across Europe. Dendrochronologia 32, 153–161. https://doi.org/10.1016/j.dendro.2014.01.002

Babst, F., Bouriaud, O., Papale, D., Gielen, B., Janssens, I.A., Nikinmaa, E., Ibrom, A., Wu, J., Bernhofer, C., Köstner, B., Grünwald, T., Seufert, G., Ciais, P., Frank, D., 2014b. Above-ground woody carbon sequestration measured from tree rings is coherent with net ecosystem productivity at five eddy-covariance sites. New Phytol. 201, 1289–1303. https://doi.org/10.1111/nph.12589

Bachmair, S., Kohn, I., Stahl, K., 2015. Exploring the link between drought indicators and impacts. Nat. Hazards Earth Syst. Sci. 15, 1381–1397. https://doi.org/10.5194/nhess-15-1381-2015

Bachmair, S., Svensson, C., Hannaford, J., Barker, L.J., Stahl, K., 2016. A quantitative analysis to objectively appraise drought indicators and model drought impacts. Hydrol. Earth Syst. Sci. 20, 2589–2609. https://doi.org/10.5194/hess-20-2589-2016

Bachmair, S., Tanguy, M., Hannaford, J., Stahl, K., 2018. How well do meteorological indicators represent agricultural and forest drought across Europe? Environ. Res. Lett. 13. https://doi.org/10.1088/1748-9326/aaafda

Bailey, A. D. and Bree, T. (1981) Effect of improved land drainage on river flow, in: Flood Studies Report – five Years on, Thomas Telford, London, 131–142.

Barker, L.J., Hannaford, J., Chiverton, A. and Svensson, C. (2016) From meteorological to hydrological drought using standardised indicators. *Hydrology and Earth System Sciences*, *20*(6), pp.2483-2505.

Beguería, S., López-Moreno, J.I., Lorente, A., Seeger, M., García-Ruiz, J.M., 2003. Assessing the effect of climate oscillations and land-use changes on streamflow in the Central Spanish Pyrenees. Ambio 32, 283–286. https://doi.org/10.1579/0044-7447-32.4.283

Beguería, S., S. M. Vicente-Serrano, F. Reig, B. Latorre (2014) Standardized precipitation evapotranspiration index (SPEI) revisited: parameter fitting, evapotranspiration models, tools, datasets and drought monitoring. International Journal of Climatology 34 (10) 3001–3023. doi:10.1002/joc.3887

Beguería, S., S. M. Vicente-Serrano (2017) Package 'SPEI' – Calculation of the Standardised Precipitation-Evapotranspiration Index. R software package, version 1.7. URL: https://CRAN.R-project.org/package=SPEI – Last accessed in May 2021.

Bloomfield, J.P., Marchant, B.P., 2013. Analysis of groundwater drought building on the standardised precipitation index approach. Hydrol. Earth Syst. Sci. 17, 4769–4787. https://doi.org/10.5194/hess-17-4769-2013

Bloomfield, J.P., Marchant, B.P., Bricker, S.H., Morgan, R.B., 2015. Regional analysis of groundwater droughts using hydrograph classification. Hydrol. Earth Syst. Sci. 19, 4327–4344. https://doi.org/10.5194/hess-19-4327-2015

Brázdil, R., P. Dobrovolný, M. Bauch, C. Camenisch, A. Kiss, O. Kotyza, P. Oliński, L. Řezníčková (2020) Central Europe, 1531–1540 CE: The driest summer decade of the past five centuries? Climate of the Past 16 (6) 2125–2151. doi:10.5194/cp-16-2125-2020

Bree, T. and Cunnane, C. (1979) Evaluating the effects of arterial drainage on river flood discharges, Annexe 1, Office of the Public Works, Dublin, Ireland.

Büntgen, U., O. Urban, P. J. Krusic, M. Rybníček, T. Kolář, T. Kyncl, A. Ač, E. Koňasová, J. Čáslavský, J. Esper, S. Wagner, M. Saurer, W. Tegel, P. Dobrovolný, P. Cherubini, F. Reinig, M. Trnka (2021) Recent European drought extremes beyond Common Era background variability. Nature Geoscience 14 (4) 190–196+12 pp. doi:10.1038/s41561-021-00698-0

Burdon, D. J. (1986) Hydrogeological Aspects of Agricultural Drainage in Ireland, Environ. Geol. Water S., 9, 41–65.

Camarero, J.J., Bigler, C., Linares, J.C., Gil-Pelegrín, E., 2011. Synergistic effects of past historical logging and drought on the decline of Pyrenean silver fir forests. For. Ecol. Manage. 262, 759–769. https://doi.org/10.1016/j.foreco.2011.05.009

Camarero, J.J., Gazol, A., Sangüesa-Barreda, G., Oliva, J., Vicente-Serrano, S.M., 2015. To die or not to die: Early warnings of tree dieback in response to a severe drought. J. Ecol. 103. https://doi.org/10.1111/1365-2745.12295

Carlson, T.N., Ripley, D.A., 1997. On the relation between NDVI, fractional vegetation cover, and leaf area index. Remote Sens. Environ. 62, 241–252. https://doi.org/10.1016/S0034-4257(97)00104-1

Casty, C., Raible, C., Stocker, T.F., Wanner, H. and Luterbacher, J. (2007) A European pattern climatology 1766–2000. *Climate Dynamics*, 29, 791–805.

Changnon, S., E. Easterling, W., Changnon, S.A., Easterling, W.E., 2007. Measuring Drought Impacts: The Illinois Case. JAWRA J. Am. Water Resour. Assoc. 25, 27–42. https://doi.org/10.1111/j.1752-1688.1989.tb05663.x

Chaves, M.M., Maroco, J.P., Pereira, J.S., 2003. Understanding plant responses to drought - From genes to the whole plant. Funct. Plant Biol. 30, 239–264. https://doi.org/10.1071/FP02076

Cihlar, J., St.-Laurent, L., Dyer, J.A., 1991. Relation between the normalized difference vegetation index and ecological variables. Remote Sens. Environ. 35, 279–298. https://doi.org/10.1016/0034-4257(91)90018-2

Copernicus (2020) CORINE Land Cover (CLC) 2018, version v.2020_20u1, downloaded in March 2021. Source: Copernicus Land Monitoring Service, part of the European Earth monitoring programme (GMES). URL: https://land.copernicus.eu/pan-european/corine-land-cover/clc2018

Coron, L., Thirel, G., Delaigue, O., Perrin, C. and Andréassian, V. (2017) The suite of lumped GR hydrological models in an R package. *Environmental Modelling & Software*, 94, 166–171.

Dalla Costa, L., Gianquinto, G., 2002. Water stress and watertable depth influence yield, water use efficiency, and nitrogen recovery in bell pepper: Lysimeter studies. Aust. J. Agric. Res. 53, 201–210. https://doi.org/10.1071/AR00133

DESTATIS (2019b) Öffentliche Wasserversorgung und öffentliche Abwasserentsorgung. Fachserie 19 Reihe 2.1.1., 78+22 pp. Statistisches Bundesamt, Wiesbaden. URL https://www.destatis.de/DE/Themen/Gesellschaft-Umwelt/Umwelt/Wasserwirtschaft/Publikationen/Downloads-Wasserwirtschaft/wasser-oeffentlich-2190211169004.pdf – last accessed in June 2021.

DESTATIS (2021h) Bevölkerung und Erwerbstätigkeit Bevölkerungsfortschreibung auf Grundlage des Zensus 2011. Fachserie 1, Reihe 1.3 – 2019. Statistisches Bundesamt, Wiesbaden. URL https://www.destatis.de/DE/Themen/Gesellschaft-Umwelt/Bevoelkerung/Bevoelkerungsstand/Publikationen/Downloads-Bevoelkerungsstand/bevoelkerungsfortschreibung-2010130197004.pdf – Last accessed in September 2021.

Dietrich, O., J. Steidl, D. Pavlik (2012) The impact of global change on the water balance of large wetlands in the Elbe Lowland. Regional Environmental Change 12 (4) 701–713. doi: 10.1007/s10113-012-0286-5.

Domínguez-Castro, F., Vicente-Serrano, S.M., Tomás-Burguera, M., Peña-Gallardo, M., Beguería, S., El Kenawy, A., Luna, Y., Morata, A., 2019. High spatial resolution climatology of drought events for Spain: 1961–2014. Int. J. Climatol.

DWD-CDC (2021a) DWD Climate Data Center (CDC): Grids of monthly averaged daily air temperature (2m) over Germany, version v1.0. ASCII files. Deutscher Wetterdienst, Wiesbaden. URL: https://opendata.dwd.de/climate_environment/CDC/grids_germany/monthly/air_temperature_mean/ – last accessed in May 2021.

DWD-CDC (2021b) DWD Climate Data Center (CDC): Grids of monthly total precipitation over Germany, version v1.0. ASCII files. Deutscher Wetterdienst, Wiesbaden. URL: https://opendata.dwd.de/climate_environment/CDC/grids_germany/monthly/precipitation/ – last accessed in May 2021.

DWD-CDC (2021c) DWD Climate Data Center (CDC): Grids of monthly total sunshine duration over Germany, version v1.0. ASCII files. Deutscher Wetterdienst, Wiesbaden. URL: https://opendata.dwd.de/climate_environment/CDC/grids_germany/monthly/sunshine_duration/ – last accessed in May 2021.

FGG Elbe (2015) Aktualisierung des Bewirtschaftungsplans nach § 83 WHG bzw. Artikel 13 der Richtlinie 2000/60/EG für den deutschen Teil der Flussgebietseinheit Elbe für den Zeitraum von 2016 bis 2021. Flussgebietsgemeinschaft Elbe, Magdeburg, xvii + 240 pp.

URL: https://www.fgg-elbe.de/berichte/aktualisierung-nach-art-13.html – Last accessed in March 2021.

Folland, C.K., Hannaford, J., Bloomfield, J.P., Kendon, M., Svensson, C., Marchant, B.P., Prior, J., Wallace, E., 2015. Multi-annual droughts in the English Lowlands: A review of their characteristics and climate drivers in the winter half-year. Hydrol. Earth Syst. Sci. 19, 2353–2375. https://doi.org/10.5194/hess-19-2353-2015

Fritts, H.C., 1976. Tree Rings Clim.

Forst Brandenburg (2020) Waldzustandsbericht 2020 des Landes Brandenburg. Ministerium für Landwirtschaft, Umwelt und Klimaschutz des Landes Brandenburg, Landesbetrieb Forst Brandenburg, Eberswalde, 38 pp. URL https://mluk.brandenburg.de/sixcms/media.php/9/Waldzustandsbericht-BB-2020.pdf – Last accessed in September 2021.

García-Ruiz, J.M., López-Moreno, J.I., Lasanta, T., Vicente-Serrano, S.M., González-Sampériz, P., Valero-Garcés, B.L., Sanjuán, Y., Beguería, S., Nadal-Romero, E., Lana-Renault, N., Gómez-Villar, A., 2015. Geo-ecological effects of global change in the Central Spanish Pyrenees: A review at different spatial and temporal scales [Los efectos geoecológicos del cambio global en el pirineo central español: Una revisión a distintas escalas espaciales y temporales. Pirineos 170. https://doi.org/10.3989/Pirineos.2015.170005

Gazol, A., Camarero, J.J., Anderegg, W.R.L., Vicente-Serrano, S.M., 2017. Impacts of droughts on the growth resilience of Northern Hemisphere forests. Glob. Ecol. Biogeogr. 26. https://doi.org/10.1111/geb.12526

Gazol, A., Camarero, J.J., Vicente-Serrano, S.M., Sánchez-Salguero, R., Gutiérrez, E., de Luis, M., Sangüesa-Barreda, G., Novak, K., Rozas, V., Tíscar, P.A., Linares, J.C., Martín-Hernández, N., Martínez del Castillo, E., Ribas, M., García-González, I., Silla, F., Camisón, A., Génova, M., Olano, J.M., Longares, L.A., Hevia, A., Tomás-Burguera, M., Galván, J.D., 2018. Forest resilience to drought varies across biomes. Glob. Chang. Biol. 24. https://doi.org/10.1111/gcb.14082

Giner, C., Martínez, B., Gilabert, M.A., Alcaraz-Segura, D., 2012. Trends in vegetation greenness and gross primary production in Spain (2000-2009) | Tendencias en el verdor de la vegetación y en la producción primaria bruta de las áreas forestales en la España peninsular (2000-2009). Rev. Teledetec. 51–64.

Grünewald, U. (2001) Water resources management in river catchments influenced by lignite mining. Ecological Engineering 17 (2–3) 143–152. doi:10.1016/S0925-8574(00)00154-3

Grünewald, U. (2010) Wasserbilanzen der Region Berlin–Brandenburg. Diskussionspapier 7, Berlin-Brandenburgische Akademie der Wissenschaften, Interdisziplinäre Arbeitsgruppe »Globaler Wandel – Regionale Entwicklung«, Berlin, 57 pp. URL https://edoc.bbaw.de/files/278/diskussionspapier_7_gruenewald_online.pdf – last accessed in June 2021.

Hari, V., O. Rakovec, Y. Markonis, M. Hanel, R. Kumar (2020) Increased future occurrences of the exceptional 2018–2019 Central European drought under global warming. Nature Scientific Reports 10, 12207 (10 pp). doi:10.1038/s41598-020-68872-9

Harrigan, S., Murphy, C., Hall, J., Wilby, R.L. and Sweeney, J. (2014) Attribution of detected changes in streamflow using multiple working hypotheses. *Hydrology and Earth System Sciences*, *18*(5), pp.1935-1952.

Hawkins, E., Burt, S., McCarthy, M., Murphy, C., Ross, C., Baldock, M., Brazier, J., Hersee, G., Huntly, J., Meats, R., O'Grady, J., Scrimgeour, I., Silk, T. (2021) Millions of historical monthly rainfall observations taken in the UK and Ireland rescued by citizen scientists. Geoscience Data Journal. Under Review.

Hayes, M., M. Svoboda, N. Wall and M. Widhalm (2011) The Lincoln Declaration on Drought Indices: Universal Meteorological Drought Index Recommended. Bulletin of the American Meteorological Society, 92 (4) 485–488. doi:10.1175/2010BAMS3103.1

Heim, R.R., 2002. A Review of Twentieth-Century Drought Indices Used in the United States. Bull. Am. Meteorol. Soc. 83, 1149–1165. https://doi.org/10.1175/1520-0477(2002)083<1149:AROTDI>2.3.CO;2

Heklau, H., G. Jetschke, H. Bruelheide, G. Seidler, S. Haider (2019) Species-specific responses of wood growth to flooding and climate in floodplain forests in Central Germany. iForest - Biogeosciences and Forestry 12 (3) 226–236. doi:10.3832/ifor2845-012

Hoymann, J., J. Dekkers, E. Koomen (2016) Szenarien zur Siedlungsflächenentwicklung. In: Wechsung, F., V. Hartje, S. Kaden, M. Venohr, B. Hansjürgens, P. Gräfe (eds) Die Elbe im globalen Wandel – Eine integrative Betrachtung. Vol. 9 in series Konzepte für die nachhaltige Entwicklung einer Flusslandschaft. Chapter 2.6, pp 135–175. Schweizerbart Science Publishers, Stuttgart, Germany. ISBN 978-3-510-65306-5.

Huete, A., Didan, K., Miura, T., Rodriguez, E.P., Gao, X., Ferreira, L.G., 2002. Overview of the radiometric and biophysical performance of the MODIS vegetation indices. Remote Sens. Environ. 83, 195–213. https://doi.org/10.1016/S0034-4257(02)00096-2

Humphries, P. and Baldwin, D. S. (2003) Drought and aquatic ecosystems: an introduction. Freshwater Biology 48 (7) 1141–1146. doi:10.1046/j.1365-2427.2003.01092.x

Hünefeld, L., A. Hünefeld (2019) Arbeiten im Freien – Beschäftigte vor UV-Strahlung schützen: BIBB/BAuA-Faktenblatt 29. doi:10.21934/baua:fakten20190628.

Kim, W., Iizumi, T., Nishimori, M., 2019. Global Patterns of Crop Production Losses Associated with Droughts from 1983 to 2009. J. Appl. Meteorol. Climatol. 58, 1233–1244. https://doi.org/10.1175/JAMC-D-18-0174.1

Koch, H., S. Vögele, M. Kaltofen, M. Grossmann, U. Grünewald (2014) Security of Water Supply and Electricity Production: Aspects of Integrated Management. Water Resources Management 28 (6) 1767–1780. doi:10.1007/s11269-014-0589-z

Lasanta-Martínez, T., Vicente-Serrano, S.M., Cuadrat-Prats, J.M., 2005. Mountain Mediterranean landscape evolution caused by the abandonment of traditional primary activities: A study of the Spanish Central Pyrenees. Appl. Geogr. 25. https://doi.org/10.1016/j.apgeog.2004.11.001

Lasanta, T., Vicente-Serrano, S.M., 2007. Cambios en la cubierta vegetal en el pirineo aragonés en los últimos 50 años. Pirineos.

LfU (2019) Luftqualität in Brandenburg – Jahresbericht 2019. Landesamt für Umwelt Brandenburg. Ministerium für Landwirtschaft, Umwelt und Klimaschutz (MLUK), Potsdam. URL https://lfu.brandenburg.de/sixcms/media.php/9/Luftqualitaet_BB_2019.pdf – Last accessed in September 2021.

Liu, W.T., Kogan, F.N., 1996. Monitoring regional drought using the vegetation condition index. Int. J. Remote Sens. 17, 2761–2782. https://doi.org/10.1080/01431169608949106

Lloyd-Hughes, B., 2014. The impracticality of a universal drought definition. Theor. Appl. Climatol. 117, 607–611. https://doi.org/10.1007/s00704-013-1025-7

López-Moreno, J.I., Beguería, S., García-Ruiz, J.M., 2004. The management of a large Mediterranean reservoir: Storage regimens of the Yesa Reservoir, Upper Aragon River basin, Central Spanish Pyrenees. Environ. Manage. 34, 508–515. https://doi.org/10.1007/s00267-003-0249-1

López-Moreno, J.I., García-Ruiz, J.M., 2004. Influence of snow accumulation and snowmelt on streamflow in the central Spanish Pyrenees | Influence de l'accumulation et de la fonte de la neige sur les écoulements dans les Pyrénées centrales espagnoles. Hydrol. Sci. J. 49, 787–802.

López-Moreno, J.I., Soubeyroux, J.M., Gascoin, S., Alonso-Gonzalez, E., Durán-Gómez, N., Lafaysse, M., Vernay, M., Carmagnola, C., Morin, S., 2020. Long-term trends (1958–2017) in snow cover duration and depth in the Pyrenees. Int. J. Climatol. n/a. https://doi.org/10.1002/joc.6571

López-Moreno, J.I., Vicente-Serrano, S.M., Begueria, S., Garcia-Ruiz, J.M., Portela, M.M., Almeida, A.B., 2009. Dam effects on droughts magnitude and duration in a transboundary basin: The lower river tagus, pain and Portugal. Water Resour. Res. 45. https://doi.org/10.1029/2008WR007198

López-Moreno, J.I., Vicente-Serrano, S.M., Moran-Tejeda, E., Zabalza, J., Lorenzo-Lacruz, J., García-Ruiz, J.M., 2011. Impact of climate evolution and land use changes on water yield in the ebro basin. Hydrol. Earth Syst. Sci. 15. https://doi.org/10.5194/hess-15-311-2011

López-Moreno, J.I., Vicente-Serrano, S.M., Zabalza, J., Beguería, S., Lorenzo-Lacruz, J., Azorin-Molina, C., Morán-Tejeda, E., 2013. Hydrological response to climate variability at different time scales: A study in the Ebro basin. J. Hydrol. 477, 175–188. https://doi.org/10.1016/j.jhydrol.2012.11.028

Löpmeier, F.-J. (1993) Agrarmeteorologisches Modell zur Berechnung der aktuellen Verdunstung (AMBAV). Beiträge zur Agrarmeteorologie 1983 (7). Deutscher Wetterdienst, Zentrale Agrarmeteorologische Forschungsstelle Braunschweig, 55+22 pp.

Löpmeier, F.-J. (1994) Berechnung der Bodenfeuchte und Verdunstung mittels agrarmeteorologischer Modelle. Zeitschrift für Bewässerungswirtschaft 29 (2) 157–167.

Löpmeier, F.-J. (n.d.) Agrarmeteorologisches Modell zur Berechnung der aktuellen Verdunstung (AMBAV). DWD Climate Data Center (CDC), online PDF document, 39 pp. URL https://opendata.dwd.de/climate_environment/CDC/derived_germany/soil/daily/recent/AMBAV.pdf – Last accessed in June 2021.

Lorenzo-Lacruz, J., Garcia, C., Morán-Tejeda, E., 2017. Groundwater level responses to precipitation variability in Mediterranean insular aquifers. J. Hydrol. 552, 516–531. https://doi.org/10.1016/J.JHYDROL.2017.07.011

Lorenzo-Lacruz, J., Vicente-Serrano, S.M., González-Hidalgo, J.C., López-Moreno, J.I., Cortesi, N., 2013. Hydrological drought response to meteorological drought in the Iberian Peninsula. Clim. Res. 58. https://doi.org/10.3354/cr01177

Ludewig, K., D. W. Donath, B. Zelle, R. L. Eckstein, E. Mosner, A. Otte, K. Jensen (2015) Effects of Reduced Summer Precipitation on Productivity and Forage Quality of Floodplain Meadows at the Elbe and the Rhine River. PLOS ONE, 10 (5) e0124140. doi:10.1371/journal.pone.0124140

Maltby, E., M. C. Acreman (2011) Ecosystem services of wetlands: pathfinder for a new paradigm. Hydrological Sciences Journal 56 (8) 1341–1359. doi:10.1080/02626667.2011.631014.

Marchant, B.P., Bloomfield, J.P., 2018. Spatio-temporal modelling of the status of groundwater droughts. J. Hydrol. 564, 397–413. https://doi.org/10.1016/j.jhydrol.2018.07.009

Maretzke, S., J. Hoymann, C. Schlömer, A. Stelzer (2021) Raumordnungsprognose 2040 – Bevölkerungsprognose: Ergebnisse und Methodik. BBSR-Analysen KOMPAKT 03/2021, 24 pp. Bundesinstitut für Bau-, Stadt- und Raumforschung im Bundesamt für Bauwesen und Raumordnung, Bonn, Germany. ISBN 978-3-87994-626-6. URL: https://www.bbsr.bund.de/BBSR/DE/veroeffentlichungen/analysen-kompakt/2021/ak-03-2021-dl.pdf – Last accessed in March 2021.

McKee, T. B., N. J. Doesken and J. Kleist (1993) The relationship of drought frequency and duration to time scale. In: Proceedings of the Eighth Conference on Applied Climatology, Anaheim, California,17–22 January 1993. Boston, American Meteorological Society, 179–184. URL https://www.droughtmanagement.info/literature/AMS_Relationship_Drought_Frequency_Duration_Time_Scales_1993.pdf – Last accessed in September 2021.

Mishra, A.K., Singh, V.P., 2010. A review of drought concepts. J. Hydrol. 391, 202–216. https://doi.org/10.1016/j.jhydrol.2010.07.012

Möllers, F. (no date a) Jahresbericht 2018. Anglerverband Niedersachsen e.V., Hannover, 48 pp. URL https://av-nds.de/wp-content/uploads/2021/04/2018_AVN-Geschaeftsbericht_WEB.pdf – Last accessed in September 2021.

Möllers, F. (no date b) Jahresbericht 2019. Anglerverband Niedersachsen e.V., Hannover, 68 pp. URL https://av-nds.de/wp-content/uploads/2021/04/2019_AVN_Geschaeftsbericht_WEB.pdf – Last accessed in eptember 2021.

Morán-Tejeda, E., Lorenzo-Lacruz, J., López-Moreno, J.I., Ceballos-Barbancho, A., Zabalza, J., Vicente-Serrano, S.M., 2012. Reservoir Management in the Duero Basin (Spain): Impact on River Regimes and the Response to Environmental Change. Water Resour. Manag. 26. https://doi.org/10.1007/s11269-012-0004-6

Mosley, L. M. (2015) Drought impacts on the water quality of freshwater systems; review and integration. Earth-Science Reviews 140, 203–214. doi:10.1016/j.earscirev.2014.11.010.

Mouelhi, S., Michel, C., Perrin, C. and Andréassian, V. (2006) Stepwise development of a two-parameter monthly water balance model. *Journal of Hydrology*, 318(1–4), 200–214.

Mukherjee, S., Mishra, A., Trenberth, K.E., 2018. Climate Change and Drought: a Perspective on Drought Indices. Curr. Clim. Chang. Reports 4, 145–163. https://doi.org/10.1007/s40641-018-0098-x

MULE (2021) Internationaler Tag der Feuchtgebiete: Renaturierung der Flutrinnen an der Elbe im Oberluch Roßlau. Web page, Ministerium für Umwelt, Landwirtschaft und Energie, Magdeburg, 1st February 2021. URL https://mule.sachsen-anhalt.de/newsarchiv/artikel-detail/news/internationaler-tag-der-feuchtgebiete-renaturierung-der-flutrinnen-an-der-elbe-im-oberluch-rosslau/ – Last accessed in July 2021.

MULE (n.d.) Waldzustandsbericht Sachsen-Anhalt 2020. Ministerium für Umwelt, Landwirtschaft und Energie Sachsen-Anhalt (MULE), Magdeburg, 40 pp. URL https://mule.sachsen-anhalt.de/fileadmin/Bibliothek/Politik_und_Verwaltung/MLU/MLU/03_Landwirtschaft/Forst/Waldschutz/201203_NFO_WZB-Sachsen-Anhalt-2020_BF_NEU_klein.pdf – Last accessed in September 2021

Nakayama, T., Shankman, D., 2013. Impact of the Three-Gorges Dam and water transfer project on Changjiang floods. Glob. Planet. Change 100, 38–50. https://doi.org/10.1016/j.gloplacha.2012.10.004

Nicholson, S.E., Davenport, M.L., Malo, A.R., 1990. A comparison of the vegetation response to rainfall in the Sahel and East Africa, using normalized difference vegetation index from NOAA AVHRR. Clim. Change 17, 209–241. https://doi.org/10.1007/BF00138369

Noguera, I., Domínguez-Castro, F., Vicente-Serrano, S.M., 2020. Characteristics and trends of flash droughts in Spain, 1961-2018. Ann. N. Y. Acad. Sci. https://doi.org/10.1111/nyas.14365

Noone, S., Broderick, C., Duffy, C., Matthews, T., Wilby, R.L. and Murphy, C. (2017) A 250-year drought catalogue for the Island of Ireland (1765–2015). *International Journal of Climatology*, *37*, pp.239-254.

Noone, S., Murphy, C., Coll, J., Matthews, T., Mullan, D., Wilby, R.L. and Walsh, S. (2016) Homogenization and analysis of an expanded long-term monthly rainfall network for the Island of Ireland (1850–2010). *International Journal of Climatology*, *36*(8), pp.2837-2853.

O'Connor, P., Murphy, C., Matthews, T. and Wilby, R.L. (2021) Reconstructed monthly river flows for Irish catchments 1766–2016. *Geoscience Data Journal*, *8*(1), pp.34-54.

O'Kelly, J. J. (1955) The employment of Unit Hydrographs to determine the flows of Irish arterial drainage channels, Proc. Inst. Civil Eng., 4, 365–412.

Orth, R., M. M. Vogel, J. Luterbacher, C. Pfister, S. I. Seneviratne (2016) Did European temperatures in 1540 exceed present-day records? Environmental Research Letters 11, 114021 (10 pp). doi:10.1088/1748-9326/11/11/114021

Ortigosa, L.M., Garcia-Ruiz, J.M., Gil-Pelegrin, E., 1990. Land reclamation by reforestation in the Central Pyrenees. Mt. Res. & Dev. 10, 281–288. https://doi.org/10.2307/3673607

Pasho, E., Camarero, J.J., de Luis, M., Vicente-Serrano, S.M., 2011. Impacts of drought at different time scales on forest growth across a wide climatic gradient in north-eastern Spain. Agric. For. Meteorol. 151. https://doi.org/10.1016/j.agrformet.2011.07.018

Peguero-Pina, J.J., Sancho-Knapik, D., Cochard, H., Barredo, G., Villarroya, D., Gil-Pelegrin, E., 2011. Hydraulic traits are associated with the distribution range of two closely related Mediterranean firs, Abies alba Mill. and Abies pinsapo Boiss. Tree Physiol. 31, 1067–1075. https://doi.org/10.1093/treephys/tpr092

Peña-Gallardo, M, SM, V.-S., Domínguez-Castro, F., Quiring, S., Svoboda, M., Beguería, S., Hannaford, J., 2018. Effectiveness of drought indices in identifying impacts on major crops across the USA . Clim. Res. 75, 221–240.

Peña-Gallardo, Marina, Vicente-Serrano, S.M., Camarero, J.J., Gazol, A., Sánchez-Salguero, R., Domínguez-Castro, F., El Kenawy, A., Beguería-Portugés, S., Gutiérrez, E., de Luis, M., Sangüesa-Barreda, G., Novak, K., Rozas, V., Tíscar, P.A., Linares, J.C., del Castillo, E., Ribas Matamoros, M., García-González, I., Silla, F., Camisón, Á., Génova, M., Olano, J.M., Longares, L.A., Hevia, A., Galván, J.D., 2018. Drought Sensitiveness on Forest Growth in Peninsular Spain and the Balearic Islands. Forests 9.

Peña-Gallardo, M, Vicente-Serrano, S.M., Dom\'\inguez-Castro, F., Beguer\'\ia, S., 2019. The impact of drought on the productivity of two rainfed crops in Spain. Nat. Hazards Earth Syst. Sci. 19, 1215–1234. https://doi.org/10.5194/nhess-19-1215-2019

Peña-Gallardo, M., Vicente-Serrano, S.M., Hannaford, J., Lorenzo-Lacruz, J., Svoboda, M., Domínguez-Castro, F., Maneta, M., Tomas-Burguera, M., Kenawy, A.E., 2019. Complex influences of meteorological drought time-scales on hydrological droughts in natural basins of the contiguous Unites States. J. Hydrol. 568. https://doi.org/10.1016/j.jhydrol.2018.11.026

Peng, D., Wu, C., Li, C., Zhang, X., Liu, Z., Ye, H., Luo, S., Liu, X., Hu, Y., Fang, B., 2017. Spring green-up phenology products derived from MODIS NDVI and EVI: Intercomparison, interpretation and validation using National Phenology Network and AmeriFlux observations. Ecol. Indic. 77, 323–336. https://doi.org/10.1016/j.ecolind.2017.02.024

Rangecroft, S., Van Loon, A.F., Coxon, G., Breña-Naranjo, J.A., Van Ogtrop, F., Van Lanen, H.A.J., 2018. Using paired catchments to quantify the human influence on hydrological droughts. Hydrol. Earth Syst. Sci. Discuss. 1–23. https://doi.org/10.5194/hess-2018-215

Reinermann, S., U. Gessner, S. Asam, C. Kuenzer, S. Dech (2019) The Effect of Droughts on Vegetation Condition in Germany: An Analysis Based on Two Decades of Satellite Earth Observation Time Series and Crop Yield Statistics. Remote Sensing 11 (15) 1783, 21 pp. doi:10.3390/rs11151783

Restaino, C.M., Peterson, D.L., Littell, J., 2016. Increased water deficit decreases Douglas fir growth throughout western US forests. Proc. Natl. Acad. Sci. U. S. A. 113, 9557–9562. https://doi.org/10.1073/pnas.1602384113

Reynolds, J.F., Virginia, R.A., Kemp, P.R., De Soyza, A.G., Tremmel, D.C., 1999. Impact of drought on desert shrubs: Effects of seasonality and degree of resource island development. Ecol. Monogr.

Richardson, A.D., Carbone, M.S., Keenan, T.F., Czimczik, C.I., Hollinger, D.Y., Murakami, P., Schaberg, P.G., Xu, X., 2013. Seasonal dynamics and age of stemwood nonstructural carbohydrates in temperate forest trees. New Phytol. 197, 850–861. https://doi.org/10.1111/nph.12042

Sah, R.P., Chakraborty, M., Prasad, K., Pandit, M., Tudu, V.K., Chakravarty, M.K., Narayan, S.C., Rana, M., Moharana, D., 2020. Impact of water deficit stress in maize: Phenology and yield components. Sci. Rep.

Sánchez-Salguero, R., Camarero, J.J., Dobbertin, M., Fernández-Cancio, T., Vilà-Cabrera, A., Manzanedo, R.D., Zavala, M.A., Navarro-Cerrillo, R.M., 2013. Contrasting vulnerability and resilience to drought-induced decline of densely planted vs. natural rear-edge Pinus nigra forests. For. Ecol. Manage. 310, 956–967. https://doi.org/10.1016/j.foreco.2013.09.050

Scaini, A., Sánchez, N., Vicente-Serrano, S.M., Martínez-Fernández, J., 2015. SMOS-derived soil moisture anomalies and drought indices: A comparative analysis using in situ measurements. Hydrol. Process. 29. https://doi.org/10.1002/hyp.10150

Sena, A., Barcellos, C., Freitas, C., Corvalan, C., 2014. Managing the health impacts of drought in Brazil. Int. J. Environ. Res. Public Health 11, 10737–10751. https://doi.org/10.3390/ijerph111010737

Simon, M., V. Bekele, B. Kulasová, C. Maul, R. Oppermann, P. Řehák (2005) Die Elbe und ihr Einzugsgebiet – Ein geographisch-hydrologischer und wasserwirtschaftlicher Überblick. Internationale Kommission zum Schutz der Elbe, Magdeburg, 258 pp. URL: https://www.ikse-mkol.org/fileadmin/media/user_upload/D/06_Publikationen/07_Verschiedenes/2005_IKSE-Elbe-und-ihr-Einzugsgebiet.pdf – last accessed in March 2021.

Skomarkova, M.V., Vaganov, E.A., Mund, M., Knohl, A., Linke, P., Boerner, A., Schulze, E.-D., 2006. Inter-annual and seasonal variability of radial growth, wood density and carbon isotope ratios in tree rings of beech (Fagus sylvatica) growing in Germany and Italy. Trees - Struct. Funct. 20, 571–586. https://doi.org/10.1007/s00468-006-0072-4

SMEKUL (2020) Waldzustandsbericht 2020. Sächsisches Staatsministerium für Energie, Klimaschutz, Umwelt und Landwirtschaft (SMEKUL), Dresden, 64 pp. URL https://publikationen.sachsen.de/bdb/artikel/36806 – Last accessed in September 2021.

Slette, I.J., Post, A.K., Awad, M., Even, T., Punzalan, A., Williams, S., Smith, M.D., Knapp, A.K., 2019. How ecologists define drought, and why we should do better. Glob. Chang. Biol. 25, 3193–3200. https://doi.org/10.1111/gcb.14747

Slette, I.J., Smith, M.D., Knapp, A.K., Vicente-Serrano, S.M., Camarero, J.J., Beguería, S., 2020. Standardized metrics are key for assessing drought severity. Glob. Chang. Biol. 26, e1–e3. https://doi.org/10.1111/gcb.14899

Sperry, J.S., Love, D.M., 2015. What plant hydraulics can tell us about responses to climate-change droughts. New Phytol. 207, 14–27. https://doi.org/10.1111/nph.13354

Stanke, C., Kerac, M., Prudhomme, C., Medlock, J., Murray, V., 2013. Health effects of drought: a systematic review of the evidence. PLoS Curr. 5. https://doi.org/10.1371/currents.dis.7a2cee9e980f91ad7697b570bcc4b004

Statistik BB (2021) Hitzebedingte Sterblichkeit in Berlin und Brandenburg, Heft 1/2021. URL https://download.statistik-berlin-brandenburg.de/4c241e5c83eedf6b/d9ec6a993297/hz_202101-06.pdf – Last accessed in September 2021.

Statistik ST (2021) Übersterblichkeit an Hitzetagen. Press release 260/2021. Statistisches Landesamt Sachsen-Anhalt, Halle (Saale). URL https://statistik.sachsen-anhalt.de/fileadmin/Bibliothek/Landesaemter/StaLa/startseite/Daten_und_Veroeffentlichungen/Pressemitteilungen/2021/h_August/260-Hitzesterblichkeit.pdf – Last accessed in September 2021.

Süddeutsche Zeitung (2019b) Andauerende Trockenheit setzt Amphibien und Pflanzen zu. Online news, .27th July 2019, 08:34. URL https://www.sueddeutsche.de/wissen/natur-dresden-andauerende-trockenheit-setzt-amphibien-und-pflanzen-zu-dpa.urn-newsml-dpa-com-20090101-190727-99-230619 – Last accessed in September 2021.

Svoboda, M., LeComte, D., Hayes, M., Heim, R., Gleason, K., Angel, J., Rippey, B., Tinker, R., Palecki, M., Stooksbury, D., Miskus, D., Stephens, S., 2002. The drought monitor. Bull. Am. Meteorol. Soc. 83, 1181–1190. https://doi.org/10.1175/1520-0477(2002)083<1181:TDM>2.3.CO;2

SVZ (2020) Trockenheit: Frosch, Lurch und Molch fehlt Wasser. Online news, Schweriner Volkszeitung, 23rd May 2020, 05:00. URL https://www.svz.de/regionales/brandenburg/frosch-lurch-und-molch-fehlt-wasser-id28410542.html – Last accessed in September 2021.

Tan, B., Gao, F., Tan, B., Gao, F., Wolfe, R.E., Pedelty, J.A., Nightingale, J., Morisette, J.T., Ederer, G.A., Nightingale, J., 2011. An Enhanced TIMESAT Algorithm for Estimating Vegetation Phenology Metrics From MODIS Data. IEEE J. Sel. Top. Appl. Earth Obs. Remote Sens. 4, 361–371. https://doi.org/10.1109/JSTARS.2010.2075916

Tijdeman, E., Bachmair, S., Stahl, K., 2016. Controls on hydrologic drought duration in near-natural streamflow in Europe and the USA. Hydrol. Earth Syst. Sci. 20, 4043–4059. https://doi.org/10.5194/hess-20-4043-2016

Tijdeman, E., Hannaford, J., Stahl, K., 2018. Human influences on streamflow drought characteristics in England and Wales. Hydrol. Earth Syst. Sci. 22, 1051–1064. https://doi.org/10.5194/hess-22-1051-2018

TMIL (2020) Waldzustandsbericht 2020 – Forstliches Umweltmonitoring in Thüringen. Thüringer Ministerium für Infrastruktur und Landwirtschaft (TMIL), Erfurt, 30 pp. URL https://infrastruktur-landwirtschaft.thueringen.de/fileadmin/Forst_und_Jagd/Forstwirtschaft/20_11_20_WaldzustandsberichtWeb.pdf – Last accessed in September 2021

Tomas-Burguera, M., M Vicente-Serrano, S., Beguería, S., Reig, F., Latorre, B., 2019. Reference crop evapotranspiration database in Spain (1961-2014). Earth Syst. Sci. Data 11, 1917–1930. https://doi.org/10.5194/essd-11-1917-2019

La Tribune (2019) Canicule et refroidissement des centrales nucléaires : le pire est à venir. Online news, 2nd July 2019, 10:31. URL https://www.latribune.fr/entreprises-finance/industrie/energie-environnement/canicule-et-refroidissement-des-centrales-nucleaires-le-pire-est-a-venir-822302.html

Trnka, M., Dubrovský, M., Svoboda, M., Semerádová, D., Hayes, M., Žalud, Z., Wilhite, D., 2009. Developing a regional drought climatology for the Czech Republic. Int. J. Climatol.

Trnka, M., Hlavinka, P., Možný, M., Semerádová, D., Štěpánek, P., Balek, J., Bartošová, L., Zahradníček, P., Bláhová, M., Skalák, P., Farda, A., Hayes, M., Svoboda, M., Wagner, W., Eitzinger, J., Fischer, M., Žalud, Z., 2020. Czech Drought Monitor System for monitoring and forecasting agricultural drought and drought impacts. Int. J. Climatol. n/a. https://doi.org/10.1002/joc.6557

Tucker, C.J., Sellers, P.J., 1986. Satellite remote sensing of primary production. Int. J. Remote Sens. 7, 1395–1416. https://doi.org/10.1080/01431168608948944

UBA (2020) Ozonsituation in Deutschland - Wissensstand, Forschungsbedarf und Empfehlungen. Dokumentation des Workshops „Was sind Gründe für die Ozonbelastung in Deutschland?“. Umweltbundesamt (UBA), Dessau-Roßlau. URL https://www.umweltbundesamt.de/sites/default/files/medien/479/publikationen/dokumentation_02-2020_uba-iass_ozon-workshop_fin.pdf – Last accessed in September 2021.

UBA (2021) Aktuelle Luftdaten – Jahresbilanzen, Stand: 06.09.2021. Umweltbundesamt (UBA), Dessau-Roßlau. URL https://www.umweltbundesamt.de/daten/luft/luftdaten/jahresbilanzen/eJxrWpScv9B4UWXqEiMDIwMAML8Fsw== – Last accessed in September 2021.

Van Lanen, H.A.J., Wanders, N., Tallaksen, L.M., Van Loon, A.F., 2013. Hydrological drought across the world: Impact of climate and physical catchment structure. Hydrol. Earth Syst. Sci. 17, 1715–1732. https://doi.org/10.5194/hess-17-1715-2013

Van Loon, A.F., 2015. Hydrological drought explained. Wiley Interdiscip. Rev. Water 2, 359–392. https://doi.org/10.1002/wat2.1085

Vicente-Serrano, S. M., S. Beguería, J. I. López-Moreno (2010) A Multiscalar Drought Index Sensitive to Global Warming: The Standardized Precipitation Evapotranspiration Index. Journal of Climate 23 (7) 1696–1718. doi:10.1175/2009JCLI2909.1

Vicente-Serrano, S. M., J. I López-Moreno, S. Beguería, J. Lorenzo-Lacruz, C. Azorin-Molina, E. Morán-Tejeda (2012) Accurate Computation of a Streamflow Drought Index. Journal of Hydrologic Engineering 17 (2) 318–332. doi:10.1061/(ASCE)HE.1943-5584.0000433

Vicente-Serrano, S.M., Domínguez-Castro, F., Murphy, C., Hannaford, J., Reig, F., Peña-Angulo, D., Tramblay, Y., Trigo, R.M., Mac Donald, N., Luna, M.Y. and Mc Carthy, M. (2021) Long-term variability and trends in meteorological droughts in Western Europe (1851–2018). *International journal of climatology*, *41*, pp.E690-E717.

Vicente-Serrano, S.M., 2016. Foreword: Drought complexity and assessment under climate change conditions. Cuad. Investig. Geogr. 42. https://doi.org/10.18172/cig.2961

Vicente-Serrano, S.M., Beguería, S., Lasanta, T., 2006. Spatial diversity of vegetal activity in abandoned fields of the central Spanish Pyrenees: Analysis of the processes of succession by means of Landsat imagery (1984-2001). Pirineos.

Vicente-Serrano, S.M., Camarero, J.J., Azorin-Molina, C., 2014. Diverse responses of forest growth to drought time-scales in the Northern Hemisphere. Glob. Ecol. Biogeogr. 23. https://doi.org/10.1111/geb.12183

Vicente-Serrano, S.M., Gouveia, C., Camarero, J.J., Beguería, S., Trigo, R., López-Moreno, J.I., Azorín-Molina, C., Pasho, E., Lorenzo-Lacruz, J., Revuelto, J., Morán-Tejeda, E., Sanchez-Lorenzo, A., 2013. Response of vegetation to drought time-scales across global land biomes. Proc. Natl. Acad. Sci. U. S. A. 110, 52–7. https://doi.org/10.1073/pnas.1207068110

Vicente-Serrano, S.M., López-Moreno, J.I., 2005. Hydrological response to different time scales of climatological drought: An evaluation of the Standardized Precipitation Index in a mountainous Mediterranean basin. Hydrol. Earth Syst. Sci. 9. https://doi.org/10.5194/hess-9-523-2005

Vicente-Serrano, S M, Martín-Hernández, N., Reig, F., Azorin-Molina, C., Zabalza, J., Beguería, S., Domínguez-Castro, F., El Kenawy, A., Peña-Gallardo, M., Noguera, I., García, M., 2020b. Vegetation greening in Spain detected from long term data (1981–2015). Int. J. Remote Sens. 41, 1709–1740. https://doi.org/10.1080/01431161.2019.1674460

Vicente-Serrano, S.M., Quiring, S., Peña-Gallardo, M., Domínguez-castro, F., Yuan, S., 2020. A review of environmental droughts: Increased risk under global warming? Earth Sci. Rev.

Vicente-Serrano, S M, Zabalza-Martínez, J., Borràs, G., López-Moreno, J.I., Pla, E., Pascual, D., Savé, R., Biel, C., Funes, I., Azorin-Molina, C., Sanchez-Lorenzo, A., Martín-Hernández, N., Peña-Gallardo, M., Alonso-González, E., Tomas-Burguera, M., El Kenawy, A., 2017. Extreme hydrological events and the influence of reservoirs in a highly regulated river basin of northeastern Spain. J. Hydrol. Reg. Stud. 12, 13–32. https://doi.org/10.1016/j.ejrh.2017.01.004

Vicente-Serrano, S.M., Zabalza-Martínez, J., Borràs, G., López-Moreno, J.I., Pla, E., Pascual, D., Savé, R., Biel, C., Funes, I., Martín-Hernández, N., Peña-Gallardo, M., Beguería, S., Tomas-Burguera, M., 2017. Effect of reservoirs on streamflow and river regimes in a heavily regulated river basin of Northeast Spain. Catena 149. https://doi.org/10.1016/j.catena.2016.03.042

Vose, J.M., Miniat, C.F., Luce, C.H., Asbjornsen, H., Caldwell, P.V., Campbell, J.L., Grant, G.E., Isaak, D.J., Loheide, S.P., Sun, G., 2016. Ecohydrological implications of drought for forests in the United States. For. Ecol. Manage. 380, 335–345. https://doi.org/10.1016/j.foreco.2016.03.025

Wang, H., Vicente-serrano, S.M., Tao, F., Zhang, X., Wang, P., Zhang, C., Chen, Y., Zhu, D., Kenawy, A.E., 2016. Monitoring winter wheat drought threat in Northern China using multiple climate-based drought indices and soil moisture during 2000–2013. Agric. For. Meteorol. 228–229. https://doi.org/10.1016/j.agrformet.2016.06.004

Wang, J., Yang, D., Detto, M., Nelson, B.W., Chen, M., Guan, K., Wu, S., Yan, Z., Wu, J., 2020. Multi-scale integration of satellite remote sensing improves characterization of dry-season green-up in an Amazon tropical evergreen forest. Remote Sens. Environ.

Webber, H., Ewert, F., Olesen, J.E., Müller, C., Fronzek, S., Ruane, A.C., Bourgault, M., Martre, P., Ababaei, B., Bindi, M., Ferrise, R., Finger, R., Fodor, N., Gabaldón-Leal, C., Gaiser, T., Jabloun, M., Kersebaum, K.-C., Lizaso, J.I., Lorite, I.J., Manceau, L., Moriondo, M., Nendel, C., Rodríguez, A., Ruiz-Ramos, M., Semenov, M.A., Siebert, S., Stella, T., Stratonovitch, P., Trombi, G., Wallach, D., 2018. Diverging importance of drought stress for maize and winter wheat in Europe. Nat. Commun. 9, 4249. https://doi.org/10.1038/s41467-018-06525-2

WELT (2020) April zu trocken: Stress für Pflanzen und Amphibien. Online news, 18th April 2020. URL https://www.welt.de/regionales/thueringen/article207338895/April-zu-trocken-Stress-fuer-Pflanzen-und-Amphibien.html – Last accessed in July 2021.

Wetter, O., C. Pfister, J. P. Werner, E. Zorita, S. Wagner, S. I. Seneviratne, J. Herget, U. Grünewald, J. Luterbacher, M.-J. Alcoforado, M. Barriendos, U. Bieber, R. Brázdil, K. H. Burmeister, C. Camenisch, A. Contino, P. Dobrovolný, R. Glaser, I. Himmelsbach, A. Kiss, O. Kotyza, T. Labbé, D. Limanówka, L. Litzenburger, Ø. Nordl, K. Pribyl, D. Retsö, D. Riemann, C. Rohr, W. Siegfried, J. Söderberg, J.-L. Spring (2014) The year-long unprecedented European heat and drought of 1540 – a worst case. Climatic Change 125 (8) 349–363. doi:10.1007/s10584-014-1184-2 – Erratum: Climatic Change 125 (8) 365–367. doi:10.1007/s10584-014-1193-1

Wild, M. (2014) Global Dimming and Brightening. In: Freedman B. (ed.) Global Environmental Change. Handbook of Global Environmental Pollution, vol 1, pp. 39–47. Springer, Dordrecht. doi:10.1007/978-94-007-5784-4_2739–47

Wild, M., S. Wacker, S. Yang, A. Sanchez-Lorenzo (2021) Evidence for Clear-Sky Dimming and Brightening in Central Europe. Geophysical Research Letters 48 (6) e2020GL092216 (9 pp). doi:10.1029/2020GL092216

Wilhite, D.A., 2005. Drought. Encycl. Earth Sci. Ser. 338–341. https://doi.org/10.1007/1-4020-3266-8_70

Wilhite, D.A., Pulwarty, R.S., 2017. Drought as Hazard: Understanding the Natural and Social Context, in: Drought and Water Crises: Integrating Science, Management, and Policy. pp. 3–22.

Wilhite, D.A., Svoboda, M.D., Hayes, M.J., 2007. Understanding the complex impacts of drought: A key to enhancing drought mitigation and preparedness. Water Resour. Manag. 21, 763–774. https://doi.org/10.1007/s11269-006-9076-5

Wirth, C., R. A. Engelmann, N. Haack, H. Hartmann, R. Richter, F. Schnabel, M. Scholz, C. Seele-Dilbat (2021) Naturschutz und Klimawandel im Leipziger Auwald: Ein Biodiversitätshotspot an der Belastungsgrenze. Biologie in unserer Zeit 51 (1) 55–65. doi:10.11576/biuz-4107

WMO (2012) World Meteorological Organization, 2012: Standardized Precipitation Index User Guide (M. Svoboda, M. Hayes and D. Wood). (WMO-No. 1090), Geneva. ISBN 978-92-63-11091-6. URL https://www.droughtmanagement.info/literature/WMO_standardized_precipitation_index_user_guide_en_2012.pdf – last accessed in May 2021.

WMO & GWP (2016) World Meteorological Organization (WMO) and Global Water Partnership (GWP): Handbook of Drought Indicators and Indices (M. Svoboda and B.A. Fuchs). Integrated Drought Management Programme (IDMP), Integrated Drought Management Tools and Guidelines Series 2. Geneva. ISBN 978-92-63-11173-9. URL

https://public.wmo.int/en/resources/library/handbook-of-drought-indicators-and-indices – last accessed in May 2021.

Xu, Y., Zhang, X., Wang, X., Hao, Z., Singh, V.P., Hao, F., 2019. Propagation from meteorological drought to hydrological drought under the impact of human activities: A case study in northern China. J. Hydrol. 579. https://doi.org/10.1016/j.jhydrol.2019.124147

Yue, S. and Wang, C. (2004) The Mann-Kendall test modified by effective sample size to detect trend in serially correlated hydrological series. *Water resources management*, *18*(3), pp.201-218.

Zhang, L., Xiao, J., Zhou, Y., Zheng, Y., Li, J., Xiao, H., 2016. Drought events and their effects on vegetation productivity in China. Ecosphere 7. https://doi.org/10.1002/ecs2.1591

Zhang, R., Chen, X., Zhang, Z., Shi, P., 2014. Evolution of hydrological drought under the regulation of two reservoirs in the headwater basin of the Huaihe River, China. Stoch. Environ. Res. Risk Assess. 29, 487–499. https://doi.org/10.1007/s00477-014-0987-z

Zhang, X., Zhang, L., Zhao, J., Rustomji, P., Hairsine, P., 2009. Responses of streamflow to changes in climate and land use/cover in the Loess Plateau, China. Water Resour. Res. 45. https://doi.org/10.1029/2007WR006711

Zink, M., L. Samaniego, R. Kumar, S. Thober, J. Mai, D. Schäfer, A. Marx (2016) The German drought monitor. Environmental Research Letters 11 (7) 074002, 9pp. doi:10.1088/1748-9326/11/7/074002